ABSTRACT

EXPERIMENTAL AND NUMERICAL INVESTIGATION OF ABRASIVE WATERJET POLISHING TECHNOLOGY

by
Fenggang Li

The objective of this investigation is the development of the abrasive waterjet (AWJ) based polishing technology. The result of the investigation will assist the implementation of AWJ polishing for manufacturing processes and procedures.

Experimental exploration of AWJ polishing involving processing of difficult-machine materials such as Alumina ceramic and stainless steel. Surface improvement due to this processing is evaluated by measuring the roughness of the generated surfaces and examining the microhardness and micro-topography of the surfaces using Scanning Electronic Microscopy (SEM). The surface roughness of 0.3 micron was obtained at samples of ceramic and metal alloys at a reasonable rate using 500-mesh garnet. No surface defects are induced.

The effect of various process variables on the topography of surfaces generated during AWJ polishing was evaluated. It is shown that the particles dimension and jet impact angle are two critical parameters controlling the process. The former determines the feasibility of AWJ polishing, and the later limits the extent of improvement in the surface topography. The force exerted on the sample surface is measured at various impingement angles. And, the effects of the tangential and normal component of the force on the surface topography is evaluated. The abrasive particles which constitute a

machining tool in the AWJ polishing are collected after mixing and after impact, and analyzed using Laser Scanning Sizer and SEM. The acquired data reveal the details of the mechanism of AWJ polishing processes.

Numerical simulation of the motion of particles prior and after the impingement are conducted. Numerical solutions of the differential equations as applied to the two-phase turbulent jet flow are obtained using FIDAP package. The numerical prediction of jet velocity and force exerted on the target surface comply with the experimental results. The simulation of particles trajectories reveals existence of five distinctive patterns of particles motion which determine the surface topography.

This work pioneers the use of AWJ as a polishing tool. and identifies the principal features of AWJ polishing and its use of computational packages for evaluation of the behavior of ultrahigh speed two-phase flows.

EXPERIMENTAL AND NUMERICAL INVESTIGATION OF ABRASIVE WATERJET POLISHING TECHNOLOGY

by
Fenggang Li

A Dissertation
Submitted to the Faculty of the
New Jersey Institute of Technology
in Partial Fulfillment of the requirement for the Degree of
Doctor of Philosophy

Department of Mechanical Engineering

May 1996

APPROVAL PAGE

EXPERIMENTAL AND NUMERICAL INVESTIGATION OF ABRASIVE WATERJET POLISHING TECHNOLOGY

Fenggang Li

Dr. Ernest S. Geskin, Dissertation Advisor — Date
Professor of Mechanical Engineering
of the Department of Mechanical Engineering, NJIT

Dr. Rong Chen, Committee Member — Date
Professor of Mechanical Engineering and Graduate Advisor
of the Department of Mechanical Engineering, NJIT

Dr. Roland A. Levy, Committee Member — Date
Professor of Physics and Director of Materials Science and Engineering Program
of the Department of Physics, NJIT

Dr. Avraham Harnoy, Committee Member — Date
Professor of Mechanical Engineering
of the Department of Mechanical Engineering, NJIT

Dr. Nouri Levy, Committee Member — Date
Associate Professor of Mechanical Engineering
of the Department of Mechanical Engineering, NJIT

BIOGRAPHICAL SKETCH

Author: Fenggang Li

Degree: Doctor of Philosophy

Date: May 1996

Undergraduate and Graduate Education:

- Doctor of Philosophy in Mechanical Engineering,
  New Jersey Institute of Technology, Newark, NJ, 1996

- Master of Science in Materials Science & Engineering,
  Shanghai Jiao Tong University, Shanghai, P. R. China, 1985

- Bachelor of Science in Materials Science & Engineering,
  Shanghai Jiao Tong University, Shanghai, P. R. China, 1985

Major: Mechanical Engineering

Presentations and Publications:

Li, F., Geskin, E. S. and Tismenetskiy, L., 1996. "Feasibility Study of Abrasive Waterjet Polishing", 13th International Conference on Jet Cutting Technology, Oct., Sardinia, Italy.

Li, F., Geskin, E. S. and Tismenetskiy, L., 1996. "Development of Icejet Machining Technology", 13th International Conference on Jet Cutting Technology, Oct., Sardinia, Italy.

Meng, P., Geskin, E. S., Leu, M. C., Li, F. and Tismenetskiy, L., 1996. "An Analitical and Experimental Study of Cleaning with Moving Waterjets", ASME Journal of Manufacturing Science and Engineering.

Geskin, E. S., Meng, P., Leu, M. C., Tismenetskiy, L. and Li, F., 1996. "Waterjet Based Precision Cleaning Technology", Proceeding of Precision Cleaning.

Li, F., Geskin, E. S. and Tismenetskiy, L., 1995. "Development of Ice Jet Machining Technology", Proceedings of 8th American Water Jet Conference, pp. 671-680, August, Houston.

BIOGRAPHICAL SKETCH
(Continued)

Geskin E. S., Tismenetskiy, L., Bakhromi, E. and Li, F., 1995. "Investigation of Ice Jet Machining", Proceedings of the 1995 NSF Design and Manufacturing Grantees Conference, San Diego.

Geskin E. S., Tismenetskiy, L., Bakhromi, E. and Li, F., 1995. "Investigation of Ice Jet Machining", International Symposium for Electromachining, Lausanne, Switzerland.

Singh, P. J., Geskin, E. S, Li, F., Meng, P. and Mehiman, S., 1994. "Relative Performance of Abrasives in Abrasive Waterjet Cutting", 12th International Conference on Jet Cutting Technology, France.

Li, F., Yang, Z. R. and Mao, X. W., 1986, "Study of Growth characteristics of Short Fatigue Cracks in High and Low Strength steels". Acta Metallurgical Sinica, Vol.23, No.3, pp.211-216.

This dissertation is dedicated to
my family

ACKNOWLEDGMENT

The author wishes to express his sincere gratitude to his advisor, Dr. E. S. Geskin, for his remarkable guidance, constant supervision, friendship, and moral support throughout this research. A special appreciation is extended to Dr. R. Levy, Dr. D. Raghu and Dr. R. Chen for their remarkable help and advice. This thesis could not be completed without their support.

Special thanks to Dr. R. Chen , Dr. N. Levy, Dr. A. Harnoy and Dr. R. Levy for serving as members of the committee, having kindly read through the original manuscript, and providing many valuable suggestions. Additionally, sincere thanks to Dr. L. Tismenetskiy and Mr. P. Meng for their timely help and suggestions in this study.

Also Thanks to Mr. R. Kolatac (Vibra Screw Incorporated), Mr. B. Roznoy (Morgan Matroc) and Mr. B. Ranney (Barton Mines Corporation) for providing experimental materials and device.

The author wishes to thank the Department of Mechanical Engineering, NJIT for funding this research and assistantship from Sept., 1992 to May, 1996 during Ph.D. program.

And finally, a grateful thanks to the author's family, especially, his wife, Hong Wang, for the firm support and encouragement.

TABLE OF CONTENTS

Chapter **Page**

1 INTRODUCTION 1

1.1 Surface Precision Machining 1

1.2 Surface Polishing 4

1.3 Non-Traditional Polishing Techniques 6

1.4 Abrasive Waterjet Machining 8

2 LITERATURE SURVEY 13

2.1 Abrasive Fine Finishing 13

2.1.1 Bonded Abrasive Finishing 13

2.1.2 Lose Abrasive Finishing 14

2.13 The Mechanisms of Material Removal 16

2.2 Abrasive-Waterjet Machining 19

2.2.1 Straight-line Cutting 20

2.2.2 Hole Drilling 22

2.2.3 Turning 23

2.2.4 Milling 24

2.3 Characteristics of Surface Generated by AWJ Machining 25

2.3.1 Surface Texture and Integrity 25

2.3.2 Surface Produced by AWJ Machining 28

2.3.3 Surface Finishing in AWJ Machining 29

2.4 Erosion Mechanism in the Course of the AWJ Machining 31

2.4.1 The Theory of Erosive Cutting 32

2.4.2 Study of Impinging Angle 34

2.4.3 Study of Abrasive Particle 35

2.4.4 Study of Material Effect 37

2.5 Study of Particle Motion in a Fluid Stream 37

2.6 Comments on the Previous Studies 40

3 OBJECTIVES OF THE STUDY 41

TABLE OF CONTENTS
(Continued)

Chapter **Page**

4 EXPERIMENTAL SETUP AND TEST PROCEDURE 44

4.1 Abrasive Waterjet Machining System 45

4.1.1 Hydraulic unit 45

4.1.2 Robotic Work Cell 46

4.1.3 Abrasive Feeder 46

4.1.4 Nozzle Assembly 47

4.2 Experimental Study of AWJ Polishing 49

4.2 1 Concept for Abrasive Waterjet-based Polishing 49

4.2.2 Experiment of AWJ Polishing 50

4.2.3 Experimental Material .....

4.2.4 Experimental Sample Preparation .....

4.3 Surface Texture Measurement 60

4.4 Particle Size Measurement and Micrographic Study 65

4.4.1 Laser Scanning Particle Sizer 65

4.4.1.1 Assembly of the System 65

4.4.1.2 Operating Principles 66

4.4.2 Particle Size Measurement 68

4.5 Velocity Measurement 70

4.5.1 Measuring System 70

4.5.2 Operating Principle 71

4.5.3 Velocity Measurement 73

4.6 Force Measurement 74

4.7 SEM and Microhardness Study on Surface Polished 75

4.7.1 SEM Analysis 75

4.7.2 Microhardness Test 76

TABLE OF CONTENTS
(Continued)

Chapter **Page**

5 EXPERIMENTAL RESULTS AND DISCUSSIONS 79

5.1 AWJ Based Polishing 79

5.1.1 Effect of Abrasive Particle Size 80

5.1.2 Effect of AWJ Impinging Angle 82

5.1.3 Effect of Abrasive Mass Flow Rate 83

5.1.4 Effect of AWJ Traverse Speed 85

5.1.5 Effect of Waterjet Pressure 87

5.1.6 Effect of Standoff Distance 88

5.1.7 Effect of Target Materials 89

5.1.8 Effect of Number of Passes .....

5.1.9 Effect of Focusing Tube Diameter 90

5.1.10 Effect of Initial Surface Condition 90

5.2 Momentum in the Course of AWJ-Workpiece Interaction 91

5.3 Particle Disintegration 93

5.4 Micrographic Study of the Polishing Surface and Abrasive Particle 96

5.4.1 Morphology Examination of Polishing Surfaces by SEM 96

5.4.2 Topography of Abrasive Particle 98

5.4.3 Microhardness Examination 99

6 NUMERICAL SIMULATION OF ABRASIVE WATERJET POLISHING 140

6.1 Mathematical Model of the Turbulent Flow 140

6.2 Modeling of the Turbulent 144

6.3 Near-wall Modeling with k-ε Model 147

6.4 Formulation of the Discrete Problem 151

6.5 Simulation of Free Jet Flow Impinging on a Flat Target Using k-ε Model 153

6.5.1 Modeling Two-phase Flow 154

6.5.2 Theoretical Model of Dispersed Phase 155

TABLE OF CONTENTS
(Continued)

Chapter **Page**

6.5.3 Turbulence Model of Particle Trajectories 156

6.6 Solution Procedures 158

6.7 Convergence Criteria 159

6.8 Problem Description 160

6.81 Computational Domain 161

6.8.2 Mesh Development and Boundary Conditions 163

6.8.3 Initial Condition 164

6.8.4 Particle Characteristics 165

6.9 Presentation and Discussion of Results 165

7 CONCLUSIONS AND RECOMMENDATIONS 182

7.1 Conclusion 182

7.1.1 General 182

7.1.2 Polishing Technology 183

7.1.3 Numerical Simulation 184

7.2 Recommendation 184

BIBLIOGRAPHY 186

LIST OF TABLES

Figure **Page**

1.1 Relation between Surface Roughness and Nature of Machining Operation.....2

2.1 AWJ Process and Machining Parameters.....21

4.1 Chemical Compositions of Experimental Materials.....57

4.2 Mechanical; Properties of Experimental Materials.....57

4.3 Surface Condition of Sample before Polishing.....60

LIST OF FIGURES

Table **Page**

1.1 Abrasive Waterjet Nozzle Concept 7

2.1 Schematic of Linear Cutting 22

2.2 Schematic of AWJ Drilling 23

2.3 Schematic of AWJ Turning 24

2.4 Schematic of AWJ Milling 25

2.5 Schematic of Roughness and Waviness on a Surface with Unidirectional lay and One Flaw 26

2.6 Erosion model of Material Penetration by a Solid Particle 33

4.1 Schematic of AWJ Machining System 46

4.2 Schematic of Sapphire Nozzle with Water Flow 48

4.3 SEM Image of Abrasive Used in the AWJ Polishing Study 53

4.4 Relationship between Abrasive Mesh Number and Particle Size 55

4.5 Experimental Setup 56

4.6 Diagram of AWJ Polishing Process 56

4.7 Various Surfaces of Sample Prepared for the AWJ Polishing Study 58

4.8 Dimension of Testing Sample 60

4.9 Schematic of Designations of Surface Roughness Parameters 62

4.10 Setup of Surface Roughness Measurement 63

4.11 The Matrix Videometrix Econoscope 64

4.12 Properties of the Scattered Light 66

4.13 Optical Configuration 67

LIST OF FIGURES
(Continued)

Figure **Page**

4.14 Locations Where Samples of Abrasive Were Collected 69

4.15 Schematic of the Air Catcher 69

4.16 Schematic of Schematic of Measurement System 70

4.17 Schematic of LTA Operation 72

4.18 Schematic of Piezoelectric Force Transducer 77

4.19 Schematic of the Sample for Force Measurement 77

4.20 Experimental Setup of the Force Measurement 78

4.21 Method of Sectioning Stainless Steel Samples 78

5.1 Samples Polished by Abrasive Waterjet 100

5.2 Effect of Abrasive Particle Size on Roughness of Surface Polished by AWJ for Various Materials 102

5.3 Surface Scratch Groove Generated by Abrasive Waterjet. Note: Deeper and Wider Grooves in (a) Compared that in (B) (x1000) 103

5.4 SEM Images of Surface Topography of Stainless Steel Sample Generated by Various Size of Garnet in Course of AWJ Polishing (x500). Note: the Scratch Grooves Become Thinner and Shallows as Particle Size Decreases 104

5.5 Effect of Abrasive Particle Size on the Surface Profile (R_m and R_z) in the Course of AWJ Processes 106

5.6 Effect of Abrasive Particle Size on the Surface Peak Density (N_r) in the Course of AWJ Processes 106

5.7 Size Distribution of Abrasive Particle Used in AWJ Polishing Processes 107

5.8 Effect of Jet Impact Angle on the Surface Roughness (R_a) in the Course of AWJ Processes 108

LIST OF FIGURES
(Continued)

Figure **Page**

5.9 Effect of Jet Impact Angles on the Surface Peak Density (N_r) in the Course of AWJ Processes 108

5.10 Effect of Abrasive Mass Flow Rate on the Surface Roughness in the Course of AWJ Polishing Processes 109

5.11 Effect of Abrasive Mass Flow Rate on the Surface Profile Parameters in the Course of AWJ Polishing Processes 109

5.12 Effect of Abrasive Mass Flow Rate on the Surface Peak Density N_r in the Course of AWJ Polishing Processes 110

5.13 Effect of Jet Traverse Speed on Surface Roughness in the Course of AWJ Polishing Processes 110

5.14 Effect of Waterjet Pressure on the Surface Roughness (R_a) in the Course of AWJ Polishing Processes 111

5.15 Effect of Standoff Distance on Surface Roughness in the Course of AWJ Polishing Processes 111

5.16 Effect of Material Hardness on Surface Roughness for Various Particle Size in the Course of AWJ Polishing Processes 112

5.17 Effect of Material Hardness on Surface Roughness for Various Impinging Angles in the Course of AWJ Polishing Processes 112

5.18 Effect of Number of Polishing Passes on Surface Roughness in the Course of AWJ Polishing Processes 113

5.19 Effect of Diameter of Mixing Tube on Surface Roughness in the Course of AWJ Polishing Processes 113

5.20 Effect of Initial Surface on Surface Roughness in the Course of AWJ Polishing Processes 114

5.21 Effect of Impinging Angle on Normal (F_n) and Tangential (F_t) Force Developed on Target Surface in the Course of AWJ Polishing Processes 114

LIST OF FIGURES
(Continued)

Figure **Page**

5.22 Effect of Abrasive Particle Size on Normal (F_n) and Tangential (F_t) Force Developed on Target Surface in the Course of AWJ Polishing Processes 115

5.23 Effect of Abrasive Flow Rate on Normal (F_n) and Tangential (F_t) Force Developed on Target Surface in the Course of AWJ Polishing Processes 115

5.24 Effect of Waterjet Pressure on Normal (F_n) and Tangential (F_t) Force Developed on Target Surface in the Course of AWJ Polishing Processes 116

5.25 Effect of Standoff Distance on Normal (F_n) and Tangential (F_t) Force Developed on Target Surface in the Course of AWJ Polishing Processes 116

5.26 Abrasive Particle Disintegration in the Course of AWJ Polishing Processes 117

5.27 SEM Image of Abrasive Particle Collected After Impinging Target in the Course of AWJ Polishing Processes..... 118

5.28 Effect of Impinging Angles on Particle Disintegration in the Course of AWJ Polishing Processes 120

5.29 SEM Image of 220 Mesh Garnet Fragment At Various Impinging Angles in the Course of AWJ Polishing 121

5.30 Effect of Material Hardness on Abrasive Particle Disintegration in the Course of Polishing Processes 123

5.31 SEM Image of an AWJ Polished Surface for Various Materials (x1000)..... 124

5.32 SEM Image of Polished Surface of Stainless Steel Sample by AWJ at Different Impact Angle (x1000) 127

5.33 SEM Image of Particle Embedded in Stainless Steel Sample at Various Impinging Angles (x1500)..... 129

5.34 SEM Image Clearly Shows That a Peak Was Cut off by Garnet at Near-Zero Angle with the Surface for a Stainless Steel Sample (x2000) 131

5.35 SEM Image of the Mark of Peak Cut and Bottom of Valley in the Surface of a Stainless Steel Sample (x2000)..... 131

LIST OF FIGURES
(Continued)

Figure **Page**

5.36 SEM Image of the Surface Generated by AWJ with Two Times Processing at the Same Impact Angle (3-5 degree) and with the Normal Axial Directions Each Other (x1500) 132

5.37 SEM Image of Garnets Collected in the Course of AWJ Polishing Processes 133

5.38 SEM Image of Cracks on a Garnet Collected in Course of AWJ Polishing Processes 135

5.39 SEM Image of a Garnet That Was Broken Into Several Pieces and Embedded in the Stainless Steel in the Course of AWJ Polishing Process 135

5.40 SEM Image of Garnets Collected in the Course of AWJ Polishing Processes Notice: the Scratch Mark (A) and Waviness Pattern (B) on the Surface 136

5.41 SEM Image of the Surface Topography of Garnets Collected I the Course of AWJ Polishing Processes. Notice: the Round Edge (A), Smooth Facet (B) and Wearing Marks (C) and (D) with Target 137

5.42 Microhardness Measured Through Thickness of Stainless Steel Samples Polished with Different Size of Abrasive Particles 139

5.43 Microhardness Measured Through-Thickness of Samples Polished by AWJ for Various Materials 139

6.1 Domain, Boundary Conditions and Numerical Grid for the Simulation 162

6.2 Calculated and Measured Nozzle Exit Velocity as a Function of Hydraulic Pressure 169

6.3 Streamline Flow Pattern for Various Impinging Angles in the Course of AWJ Polishing Processes (S/D_m=70) 170

6.4 Pressure Contour for Various Impinging in the Course of AWJ Polishing Processes 171

6.5 Streamline Flow Pattern for Various Standoff Distance in the Course of AWJ Polishing Processes (α=10 degree) 172

LIST OF FIGURES
(Continued)

Figure **Page**

6.6 Pressure Contour for Various Standoff Distance in the Course of AWJ Polishing Processes 173

6.7 Streamline Flow Pattern of Waterjet at Various Impinging Angles (S/D_m=70) 174

6.8 Pressure Contour of Waterjet at Various Impinging Angles (S/D_m=70) 174

6.9 Decay of Axial Centerline Velocity for a Jet Impinging on a Flat Plate 175

6.10 Axial Velocity Distribution along Radial Distance 175

6.11 Numerical Prediction of Tangential (F_t) and Normal (F_n) Force Developed on the Target Surface by AWJ At Various Impact Angles 176

6.12 Particle Trajectories for Jet Impinging Angle of 3 Degree in the Course of AWJ Polishing Processes with D_p=100 micron, P=76 MPa, M_a=68 g/min and S=178 mm 177

6.13 Particle Trajectories for Jet Impinging Angle of 10 Degree in the Course of AWJ Polishing Processes with D_p=100 micron, P=76 MPa, M_a=68 g/min and S=178 mm 178

6.14 Particle Trajectories for Jet Impinging Angle of 20 Degree in the Course of AWJ Polishing Processes with D_p=100 micron, P=76 MPa, M_a=68 g/min and S=178 mm 180

6.15 Calculated Skin Friction along a Target Surface in the Course of AWJ Polishing 181

CHAPTER 1

INTRODUCTION

1.1 Surface Precision Machining

Demands are being placed on the automobile, aerospace, electronic, medical and optical component industries to produce stronger, lighter, precision parts with advanced materials. Thus surface precision machining represent a critical and expensive segment of the overall manufacturing process.

Precision Machining is a cutting or non-cutting operation, resulting in an improvement of dimensional, form and surface accuracy, and irregularity. An important aspect of controlling this process is a knowledge of the surface texture and integrity to be expected from each operation. Only roughness R_a 1.6 to 0.008 μm may be regarded as falling within the scope of precision machining. Table 1.1 shows the relation between the type of machining operation and the roughness R_a.

There are a number of problems and cost related issues which negatively affect surface precision machining processes. In most cases the conventional processes for precision material removal such as grinding, lapping, honing, and polishing are tedious and time consuming, and cannot always provide high productivity. A recent survey by Blau (1991), for example, has shown that machining costs constitute from 50% to 80% of the cost of the final ceramic product. In the case complex surfaces, these methods are simply unacceptable and even hand operations can be required.

On the other hand, the development of new structural, electronic, photonic, and biological materials in the recent past has been very significant. Most of these materials

Table 1.1 Relation Between Surface Roughness and Nature of Machining Operation

Roughness R_a (μm)	32 ~100	8 ~25	2 ~6.3	0.5 ~1.6	0.125 ~0.4	0.03 ~0.1	0.008 ~0.025
Drilling	-	ordin.	-	-	-	-	-
Shaper planing	-	coarse	ordin.	-	-	-	-
Slide planing	Very coarse	coarse	ordin.	-	-	-	-
Milling	Very coarse	coarse	ordin.	fine	-	-	-
Turning	Very coarse	coarse	ordin.	fine	very fine	-	-
Reaming	-	coarse	ordin.	fine	very fine	-	-
Boring, finish boring	-	coarse	ordin.	fine	very fine	-	-
Broaching	-	-	coarse	ordin.	fine	-	-
Surface Grinding	-	-	coarse	ordin.	fine	-	--
Cylinder. Grinding	-	-	coarse	ordin.	fine	very fine	-
Horning	-	-	-	-	ordin	fine	very fine
Superfinishing	-	-	-	-	ordin	fine	-
Lapping	-	-	-	-	ordin	fine	very fine
Ornamental grinding	-	coarse	-	fine	very fine	-	-
Roller Burnishing	-	-	-	-	-	-	-
Calibrating	-	-	-	-	ordin.	-	-
Polishing	-	-	-	-	-	fine	very fine
				Precision Machining			

possess qualities that make them hard and difficult to machine especially under conventional precision machining methods. Some of these materials are extremely hard

such as ceramics, and glass, as well as sintered carbide. Others are soft and tough but difficult to machine, such as titanium alloys and stainless steel. Conventional machining processes are being pushed to their limits of performance and productivity with the rapid growth of hard and difficult-to-machine materials.

Interest in grinding and polishing of ceramics, ceramic based composites, diamond film deposited and glasses have grown with their widespread use as engineering materials. Unfortunately, due to the severe nature of the machining process and material susceptibility to surface damage, conventional precision machining can induce defects such as microcracks and heavy surface and subsurface deformation into the workpiece, make the material lose its special quality due to high local temperature and residual stress, or even lead to weak and stressed parts.

Obviously all the above issues in turn are forcing improvements and advancements in the machining processes that are used to make the new materials and to produce high quality and precision parts.

Abrasive waterjet devices offer several advantages over traditional and nontraditional methods of material removal, especially when working with difficult to machine materials such as advanced ceramics and composites. This technology, however, has not been sufficiently developed to allow for the precision machining of high performance materials. The purpose of this study was to explore the possibility of AWJ precision machining.

1.2 Surface Polishing

The polishing or finishing operation is the final obstacle in the development and manufacturing of quality and precision components. The definition of polishing is surface enhancement by means of material removal. Conventional polishing refers to an abrading operation that alters the surface of a substrate by physical means. It is generally done by using discs and belts, coated with very fine soft acting polishing media, or in barrels with metal balls or grains of soft acting materials like glass, ceramics, etc. The purpose of polishing with abrasives is to smooth the work surface for improving the part's appearance texture and integrity as a final operation process, and to minimize or limit the surface roughness to a predetermined magnitude for the elimination of high stress concentrations caused by microscopic surface geometry.

Typical surface conditions which, when considered objectionable, may either be removed or mitigated by polishing are (Fargo, 1980):

- Turning lines or similar cutting tool marks caused by machining operations
- Surface roughness, deep grit lines or even irregular scratches, resulting from grinding with a coarse-grain wheel
- Scale from forging in general, and parting lines resulting from closed-die forging
- Splatter, flash, and burrs from welding
- Gate, riser, and runner marks, parting lines, etc., on sand and die castings following a cleaning by rough grinding
- Rolling line, seams, extrusion lines, spin lines, draw marks, etc., caused by various hot and cold forming processes.

Polishing, in general, removes only a small amount of material from the work workpiece is small (Doyle and Aghan, 1975). Consequently, the process does not affect the workpiece size and shape produced in the preceding operations, to any significant degree. While basic forming is not achieved, a certain degree of blending can be expected from polishing, since sharp and protruding portions of the work surface are more exposed to the mild, but still effective, action of the abrasive used in polishing. These abrasives are either of the coated types or loose abrasive grains, usually carried in a liquid vehicle for application on a polishing wheel.

The mechanism of polishing is not agreed upon, but it has been placed in the category of abrasive wear because some investigators have documented that polishing produces microchip removal when a surface is acted on by hard particles that are larger than about 3 μm (0.00012 in) (Budinski, 1988). When surfaces are subjected to polishing by smaller particles, scratches and microchips are no longer observed. The mechanism of material removal under this latter condition is part of polishing. If chip removal does not occur, how is material removed? It is difficult in practice to make distinction between abrasion and polishing because the difference of the roughness is only one of degree. Rabinowicz (1968) proposes a mechanism of molecular removal. Atoms or molecules are individually removed from the surfaces by the rubbing counterface. There is no direct evidence to support this theory, but from the practical standpoint it is obvious that polishing can occur by repeated rubbing of almost anything. Steel handrails on well-used stairs often are polished from the rubbing of people's hands. In this instance, there is no abrasive on most people's hands, yet material is still removed. The likely mechanism in

such cases may be something akin to Rabinowicz's proposal. In any case, polishing is a significant wear process with an uncertain mechanism: but in cases where hard substances are part of the wear system, the material rules of low-stress abrasion usually apply.

Conventional finishing processes rely on multiple-point contact between the tool (such as a grinding wheel, honing tool or lap) and workpiece. However, large machining forces and energies, workpiece mechanical stress and machining tool wear are induced. Also, surface finishing tools are limited in material and geometric flexibility, requiring frequent tool and fixture changes to accommodate different part shapes and sizes. As one of conventional precision machining techniques, polishing could not both deliver desired performance and be cost-effective with spread application of new and advance materials. Therefore this has necessitated the development of an alternate manufacturing technology.

1.3 Non-Traditional Polishing Techniques

Many new and non-traditional machining techniques and processes have been emerging correspondingly to fill the gaps where conventional precision machining processes are inefficient. For example, over 15 different techniques of nontraditional machining methods use mechanical, thermal, chemical and radiation energy forms (Pandey and Shan, 1980). In comparison with conventional abrasive machining, these new techniques employ different physical phenomena or energy utilization and do not rely on contact between the tool and the workpiece to remove material in the form of chips. In many cases, these processes use a tool that is softer than the workpiece. These technologies have certain advantages over the conventional in performance, cost of equipment, environmental consideration or

versatility of use. However, no single process has demonstrated the ability to meet simultaneously the requirements of high finish, high effective and presence of minimal surface defects.

For example, the thermal material removal processes, some of which are limited to electricity-conducting material removed, use a variety of heat sources to melt, vaporize or sublime the workpiece surface. These process substantially change surface integrity by inducing the heat-affected zone, increasing the surface hardness and reducing the fatigue strength of material. Electrical machining, which is suitable only for electricity-conducting materials, are based upon the principles of electrolysis set forth. Slow material removal rates and high cost of equipment are among the disadvantages of these techniques. Chemical machining utilizes chemical attack or etching to remove layers of metal at very low rates, and requires highly skilled operators. The commercially available mechanical nontraditional material removal processes are all abrasive in nature and utilize a multipoint approach for removal. The mechanical forces between the "tool" and the workpiece affects the surface integrity by introducing residual stress, plastic deformation and sometime hardness alterations to the surface.

One of the more recent non-conventional machining methods, namely, abrasive-waterjet (AWJ) technique may have an opportunity to be a compatible machining technique for surface polishing. In comparison with conventional and other non-conventional machining which may have certain advantages over abrasive-waterjets for very specific applications, the AWJ technology appears to provide greater benefits in

general (Hashish 1989) and specific advantages of the abrasive-waterjet that may offset any economic disadvantages. These advantages are given as follows:

- ability to machine very hard and brittle materials
- ability to selectively machine multimaterial composites
- minimal deformation stresses
- minimal thermal effects
- reasonable material removal rates
- omnidirectional machining
- no heavy clamping needed for workplaces
- no direct "hard" contact with workpiece
- ideal for automation and remote control

Obviously, the AWJ has a potential and feasibility of becoming one of the principal machining technologies and finding application for surface polishing.

1.4 Abrasive Waterjet Machining

Abrasive water jets have been available throughout this decade and mainly used for cutting applications. Abrasive-waterjets are formed in a small abrasive-jet nozzle, as shown in Figure 1.1. Water is pressurized up to 400 MPa and expelled through a sapphire orifice to form a coherent, high-velocity waterjet. The water and a stream of solid abrasive are introduced into a hard-material mixing and accelerating tube. Here, part of the waterjet's momentum is transferred to the abrasive particles, whose velocities rapidly increase.

Typical velocities are 300-600 m/s with mass flow rate of about 3-10 g/s. A focused, high-velocity AWJ exits the accelerator nozzle and performs the material removal action.

Within the last decade there has been tremendous growth in both AWJ technology and its applications within the manufacturing environment. Over this period of time, the AWJ machining process has proven to be amenable for cutting both homogeneous and advanced heterogeneous materials.

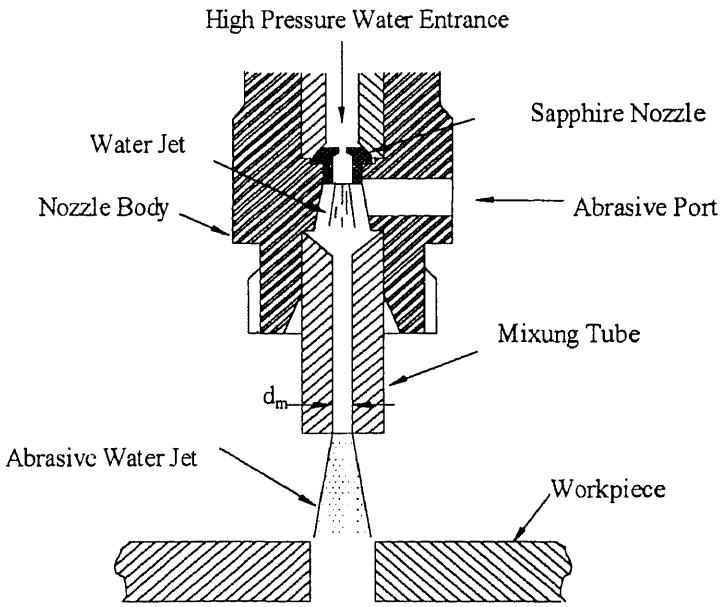

Figure 1.1 Abrasive-Waterjet Nozzle Concept

AWJ has found widespread application in primary machining and manufacturing processes. AWJ for turning, milling, drilling (Hashish, 1987a, 1987b and 1988a) and threading composite materials and glass (Sheridan, et al, 1994 and Hashish 1992) are investigated. These works predict a promising future of adaptation of AWJ systems as a precision machining tool. One important area of AWJ application which, unfortunately,

has not been investigated is the application to surface finishing. Due to low accuracy and poor topography of the generated surface (R_a=3~7 micron) AWJ process is still considered as a supplemental method of manufacturing and is employed only when conventional net-shaping proves unacceptable. Thus, development of AWJ polishing and finishing technology is necessary and critical for improving the manufacturing technology and expanding the application realm while much attention is now focused on the quality of the machined surface with rapid growth of new materials emerge.

Extensive work by Mori (1987) on Elastic Emission Machining and Namba (1978 and 1980) on float polishing indicates that highly precise surfaces can be generated by passing slurries of fine (0.001 mm) abrasive particles over glass surfaces at a grazing incidence. In the case of Elastic Emission Machining, the fluid motion is caused by a rotating sphere and in floating polishing by the motion of parts themselves over a flat lap made of tin which contains machined grooves that enhance the fluid turbulence. Obviously, it is possible to develop an AWJ polishing technology by this same relative motion which can be created by a liquid jet impinging on the surface at a low angle.

The first step of this study, therefore, will focus on the experimental trials which explore an abrasive waterjet based polishing technology; and then the surface roughness will be investigated under effect of abrasive particle size, angles of AWJ impingement, abrasive flow rate, and other process variables. Experiments will involve micrographic study of surface and abrasive particles topography. This allows identification of the surface characteristics, and aid in the visualization of effect of AWJ polishing process on the surface texture and integrity.

To develop AWJ polishing technology, it is required understanding of particle motion behavior in the case of a two-phase turbulent jet impinging on the surface at a low angle and particle erosion mechanism in the course of AWJ machining. Experimental study of the slurry jet is a difficult task due to the highly turbulent and destructive nature of the jet. It is impossible to directly measure the AWJ velocity and force developed in the workpiece. In this study a numerical simulation is conducted in order to acquire information pertinent to the slurry impact at a solid and subsequent particles motion. The simulation is based on the finite element discretization of continuity, momentum, particle motion and empirical k-ε turbulence equation for conditions developed in the course of AWJ polishing.

In this study the surface roughness of 0.3 micron was obtained for samples of ceramic and metal alloys at a reasonable rate using 500-mesh garnet. No surface defects are induced. The samples obtained by using the developed technology have been demonstrated to the industrial companies. Extremely positive response has been obtained.

This thesis contains seven chapters, The previous studies on abrasive and AWJ machining and particle motion in flow stream are discussed chronologically in Chapter 2. In Chapter 3 objective and motivation of the study are briefly stated. The experimental approaches used in the investigation of AWJ polishing and pertinent phenomena are described in Chapter 4. More specifically the developed experimental procedure involved investigation of surface and particles topography, measurement of abrasive particles velocity and forces developed in the impinging zone. Chapter 5 contains the experimental results and discussion of these results. The details of numerical simulation technique, finite

element formulation, computational domains and prescribed boundary conditions of the model are discussed in Chapter 6. This chapter also contains the computational results which are compared with the experimental data. Conclusions made as the result of this study and corresponding recommendations are presented in Chapter 7.

CHAPTER 2

LITERATURE SURVEY

2.1 Abrasive Fine Finishing

For functional reasons, technical parts may require surfaces with a very high degree of basic geometric accuracy, such as flatness or roundness, and/or with a surface texture specified as having an exceedingly low roughness and perhaps also a particular lay pattern. Such surface requirements are usually obtained by means of a finishing operation which, in the majority of cases, is an abrasive process. Abrasive finishing methods offer many and often singular advantages for the fine finishing of hard work materials, and for producing the required basic geometric form with a minimum stock removal, in combination with developing surface textures to very exacting roughness and lay specifications.

Such methods may involve the use of loose abrasives on rigid supporting members (i.e., lapping,), or bonded abrasives forced against the work surface and moved along a specific path (i.e., honing) (Farago, 1980). Very fine surfaces, such as those required for exceedingly smooth sliding or rolling contacts, are developed by the abrasive process such as Superfinishing.

2.1.1 Bonded Abrasive Finishing

For this kind of finishing, the tools used are made of abrasive, which are either bonded into a solid body, such as a honing stone, or glued on a backing such as the coated abrasives. The abrasives are forced against the work surface, while a combined relative

motion, usually composed of rotation and reciprocation, takes place between the tool and the work, such as honing, superfinishing and abrasive polishing.

The exact mechanisms of boded abrasive finishing have not been established with certainty. According to one view (Wernick and Pinner, 1972) the function of both grinding and polishing is to remove metal stock in progressively finer stages until a high luster is achieved. The opposing view (Beilby 1921) contends that in the final stages of polishing metal is displaced from the peaks into the valleys producing the much debated 'Beilby' layer of amorphous or very finely crystalline metal, but by a mechanism of plastic deformation rather than the viscous flow which Beilby envisaged. Electron microscope studies have demonstrated that the top layers of a polished surface are crushed or disordered into a very finely crystalline state.

2.1.2 Lose Abrasive Finishing

Loose abrasive are widely used for finishing various workpieces, Farago (1980). distinguished them as following three different general methods:

1. The loose abrasives, which cover the work area to be finished, are supported by a solid backing. That backing is kept in motion very close to, but not deliberately in contact with the work surface. The abrasive particles, thus, supported and moved will remove controlled but very small amounts of material from that area of the work surface which mates with the shape of the solid backing. This method is designed as lapping, in which the abrasive has the role of an intermediate medium providing the cutting ability for the tool, whose shape imparts the resulting form to the workpiece.

2. Randomly located abrasives kept in free motion by the inertial effect imparted through the movement of the container, holding both the abrasive and the work, will rub against the surface of the work; thereby exerting an abrasive action of the abrasives and the work, each having particular specific weights causing different velocities. This finishing method which operates with freely moving loose abrasive can be implemented by rotating containers such as barrel tumbling or vibrating container (i.e., vibrator finishing).

3. Loose abrasives for impacting against a specific area of the work surface are propelled by a force applied either directly to the abrasive, hurling them on the work surface, or applied by means of a fluid vehicle (Bellows, 1982, Loveless, 1994) such as Abrasive Blast Finishing, Abrasive Jet Machining, Ultrasonic Abrasive Machining and Abrasive Flow Finishing.

The loose abrasives will strike any work surface which is in the path of their forced travel, although the angle of the work surface inclination with respect to the general direction of the abrasive travel will influence the abrasives effect. Otherwise, the action of the abrasive is rather uniform over the area covered by the abrasive stream. The extent of that area, as well as the intensity of action, can be controlled over a wide range, by choice of the appropriate method, abrasives, equipment and, to some degree, even by selecting different tooling. By moving the work or source of the abrasive stream, it is possible to gradually cover very large areas and different, or even all the surfaces of the work. In the case of smaller workpieces, several can be exposed concurrently to the action of the abrasives and in general, the process is well adapted to a high degree of automation.

The rate of stock removal is commonly inferior to that which is usually attained by grinding with solidly bonded or coated abrasives applied in a firmly controlled positional relationship to the work. However, in many cases a limited penetration of the abrasives into the work material may be adequate, or even required for meeting the process objectives. The essential uniform depth of the abrasive action, accomplished without accurate positioning and travel control of the work and of the abrasive, establishes an important role for processes using propelled abrasives. Further advantages, very significant for many types of applications, result from the abrasive action produced on the surface of an odd or complex shape, and in narrow, recessed, or internal areas or when accessible to the flow of propelled abrasives, the travel path of which, in specific processes, is not even limited to a straight-line direction.

2.1.3 The Mechanisms of Material Removal

The physics of conventional loose abrasive grinding is fairly well understood. Phillips's study (1977) demonstrated that it is a fracture process where the abrasive particles, usually in a block shape, tumble in nearly a single layer under a lap, and applies a downward force. The lap rotates in a lateral shear motion via a grinding spindle. This tool force is transferred into multiple microloads which chip the brittle optical substrate, assumed to be glass in this case, and cause material removal. Phillips *et al.* proposed a model for loose abrasive machining where the impact of an abrasive particle being indented into a glass surface results in crack propagation. After unloading, chipping is

observed, which is similar to that seen in a Vickers hardness test, only with much more frequency in the loose abrasive grinding.

In 1927 Preston published an expression for wear rate in the lapping process. This expression is described by Brown (Brown, 1987) as

$$\Delta M = C\rho L\Delta S \tag{2.1}$$

Where ΔM is mass change (g); C is coefficient of proportionality (cm^2/dyne) (the Preston coefficient); ρ is density (g/cm^3); L is total load (dynes) that is weight of part and load applied normal to surface; and ΔS relative travel (cm) increment between lap and part over which wear occurs.

The equation simply states that wear is directly proportional to velocity and pressure. It has been found that velocity and pressure affect only the frequency of fracture (rate of removal) and not the magnitude of abrasion (chip size). However this model only applies to brittle materials.

Samuels (1982) summariyed interaction in the abrasive machining as following three modes:

- The abrasive particle is loose and rolls between the workpiece and another parallel surface. A corner of the particle digs into the workpiece, the particle tumbles onto an edge, and then another corner contacts the workpiece, and so on. A track of angular indentations is produced in the surface. No material removal occurs as a primary mechanism such as removal of the ridges at the sides of the indentations. Nevertheless, the efficiency of material removal approaches zero. This is known as three-body abrasion.

- The abrasive particle is fixed in one orientation with a relatively acute edge which included the angle between the advancing face and the specimen surface. A groove is produced in the surface. A standing-wave bulge forms in front of the groove. No material is removed by a primary mechanism, although secondary mechanisms are again possible. The efficiency of material removal approaches zero.
- The abrasive particle is fixed between the advancing face and the specimen surface. A groove is produced in the surface and a ribbonlike chip of material is separated from the surface. In the simplest case, all of the material that was in the groove is removed from the surface. The efficiency of material removal approaches 100 percent.

During the abrasive machining of ductile materials, considerable plastic deformation occurs on the work surface under the cumulative action of abrasive particles. The accumulation of plastic strain on the surface and subsurface causes cracks to nucleate and propagate leading to material removal. These phenomena are well described by the microcutting and abrasion mechanisms proposed by Rabinowicz (1968) and Samuels (1982). In the case of brittle solids, most observations point to the fact that fracture processes play a more dominant role than plastic flow mechanism, except in the so called "ductile regime" polishing.

Samuels (1982) observed that abrasive finishing techniques for producing smooth surfaces leave a highly strained surface layer containing dislocations, scratches, pits, embedded particles of abrasive and other forms of surface damage and contamination. Rabinowicz (1968) has demonstrated that local temperatures as high as 500^0-1000^0C can occur during grinding and polishing. Koepke (1982) has found that it is somewhat difficult

by abrasive machining to cost-effectively finish advanced ceramics and glasses and also to meet the requirements of high finish and presence of minimal surface defects, such as cracks, by forming a substantial deformation layer. The deformed layer also becomes important in abrasive machining when the plastic deformation changes the microstructure of the base material. The layer is then an important potential source of the false structures, the avoidance of which is one of the primary objectives of abrasive machining.

An energy beam was used to as an alternate manufacturing technology to the finish work surface. Sheng and Liu (1994) developed a technique to apply laser beams in the grinding and finishing process which impinges tangential to a rotating workpiece. It has been demonstrated (Johnson, 1984) that ion-beam polishing can remove surface contamination, smoothes surface irregularities and relieves the surface strain created by abrasive polishing.

2.2 Abrasive-Waterjet Machining

Commercially available abrasive waterjet (AWJ) systems are used for a wide range of trimming and shape-cutting applications. However, the AWJ process has been demonstrated for drilling, milling, turning and other machining operations (Hashish, 1988a).

In an AWJ machining operation, it is necessary to achieve certain quantitative and qualitative requirements. The geometry and quality of the machined surface directly depend on all of the process parameters, though to varying degree. The AWJ process parameters can be divided into two main groups (Hashish, 1992 b). The first group

consists of the jet-forming parameters which control the jet structure and its effectiveness and is as follows:

- water pressure
- waterjet diameter
- mixing tube diameter
- abrasive martial
- abrasive size
- abrasive flow rate

The second group is related to the machining operation itself, whether it is cutting, turning, drilling, etc. Table 2.1 lists the parameters for selected machining operations.

2.2.1 Straight-line Cutting

AWJ cutting (Figure 2.1) is the commonly used AWJ application in industry today. In most cutting applications, the cut surface needs to be free of waviness. Previous work (Hashish, 1989) indicated that the surface finish of AWJ-machined materials exhibits two distinct contributions from the AWJ: roughness due to the micro effects of each impacting particle and waviness (striations) caused by jet penetration and loss of stability as the depth increases. It has been observed that the upper portion of the cut is free from waviness. This portion of the cut is obtained by a process termed cutting wear, which is characterized by the removal of material as abrasives impact at relatively shallow angles. The lower surface of the cut is formed by a process termed deformation wear, where the

material is removed by impacts at large angles. This zone is characterized by waviness that repeats regularly.

Table 2.1 AWJ Process and Machining Parameters

Linear Cutting	Drilling	Milling	Turning
Machining Parameters			
Impact Angle Standoff Distance Traverse Rate Number of Passes Material Thickness	Impact Angle Standoff Distance Dwell time Pressure Profile Material Thickness	Traverse Rate Lateral Increment Number of Passes Number of Sweeps	Rotational Speed Direction of Rotation Angle Traverse Rate Initial Diameter Depth of Cut
Machining Requirements (Dependent Variables)			
Traverse Rate Surface Finish Width of Cut	Diameter Drilling Time Hole Shape	Volume Removal Rate Depth Control	Turned Diameter Surface Finish Machining Time

A smooth cut can be obtained by extending the cutting wear zone over the entire thickness of the material. This can be achieved by increasing the effectiveness of the jet by varying one or two of its parameters. The most common approach to reducing waviness is to reduce the traverse rate. This, however, affects taper and trailback. Taper affects the accuracy of the cuts, while trailback affects cutting around curved surfaces and corners.

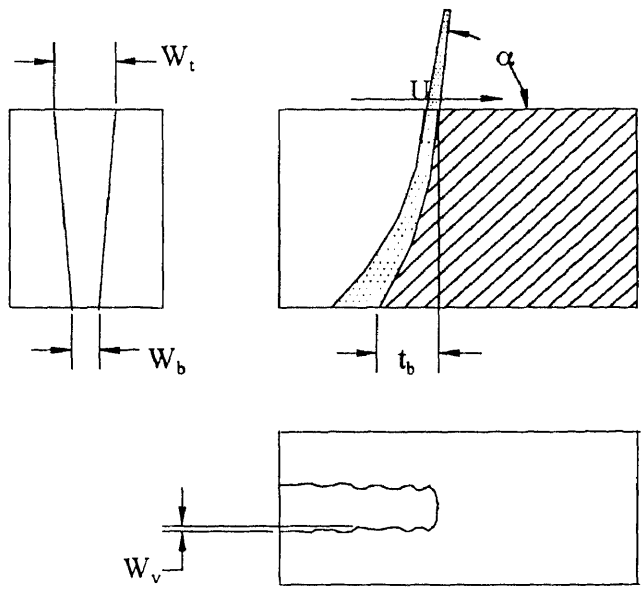

Figure 2.1 Schematic of Linear Cutting

2.2.2 Hole Drilling

Hole-drilling is the most common machining operation. Using a solid tool, the holes are always cylindrical, requiring added chamfer or taper at the ends. With AWJ, a hole can be conical, cylindrical, or even convergent-divergent. The holes do not have to be surfaces of revolution; for example, elliptical and rectangular holes can be drilled.

Figure 2.2 shows schematics of typical AWJ-drilled hole geometry. The hole rounding at the top surface is highly dependent on the standoff distance and jet coherency (Hashish, 1994), while the taper is highly dependent on the drilling rate and the jet dwell time after piercing, as well as the jet and material parameters.

The process of drilling by piercing is a highly complex phenomenon involving dynamic changes of the jet/material interaction parameters. The return flow of water, abrasives, and cutting debris interacts with the incoming jet and continually affects its

drilling characteristics. The geometry of the hole is continuously changing, influenced by both the drilling jet and the erosive action of the return flow.

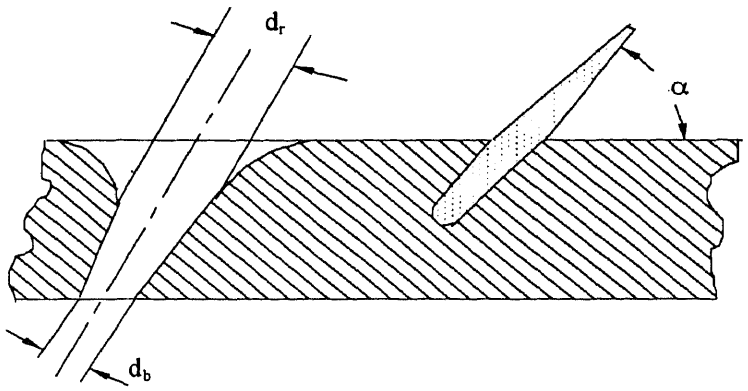

Figure 2.2 Schematic of AWJ Drilling

2.2.3 AWJ Turning

In turning with an AWJ (Figure 2.3), the workpiece is mounted in the chuck and rotated while the AWJ is traversed axially (or along a specified contour) to produce the required surface of revolution (Hashish, 1987a). The jet may also be fed incrementally (or continuously) toward the center of rotation. The complex nature of the turning process has been investigated using cinematographic visualization techniques. Under most turning conditions, the material removal process was found to take place on the cutting face rather than on the periphery (Ansari, 1990). The process is characterized by negligible forces on the workpiece and the material swept by the jet is convert to very fine debris, contrary to the chip formation in conventional machining.

Many investigators have found that the abrasive-waterjet-produced surface is generally rough and does not show any microstructure changes. A low value of roughness

can be achieved with reduce particle size and an increased number of finishing pass. This, however, is of no significance as long as surface waviness dominates the morphological features of the surface. Improvements in the traverse system and the steadiness of most influencing parameters will improve the waviness.

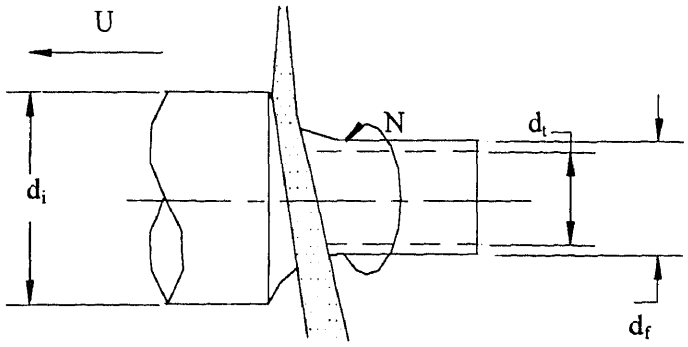

Figure 2.3 Schematic of AWJ Turning

2.2.4 AWJ Milling

AWJ milling is a process for producing pockets of a controlled depth using multipass cutting (Figure 2.4). This depth may be uniform or varied. It was found that high traverse rates are required for AWJ milling (Hashish, 1987b). This is because the uniformity of an AWJ cut improves as the traverse rate increases. An optimized milling process is one where the volume removal rate is maximized, the depth of milling per pass is minimized, and the surface texture is within tolerance values.

Ojmertz (1993) conducted an experimental investigation of AWJ milling focusing on the exposed bottom surface. The process is found to be greatly influenced by technical disturbances, that are difficult to control. He found that the AWJ milled surfaces are characterized by a variance in depth of cut, partly due to the stochastic nature of the

process, and it is sensitive to many disturbances, such as fluctuations in water pressure, abrasive mass flow, and traverse movement, but also to material properties and the different mechanisms for material removal. Further study is needed on how to overcome unwanted effects of secondary machining that is induced by the deflected jet, a problem most pronounced when cutting at low attack angles.

Despite the tremendous amount of experimental work carried out, the full potential of the AWJ application today has not been completely explored. The processes involved in the formation of a machining surface and interaction between particle and target are very complex and are far from being completely understood.

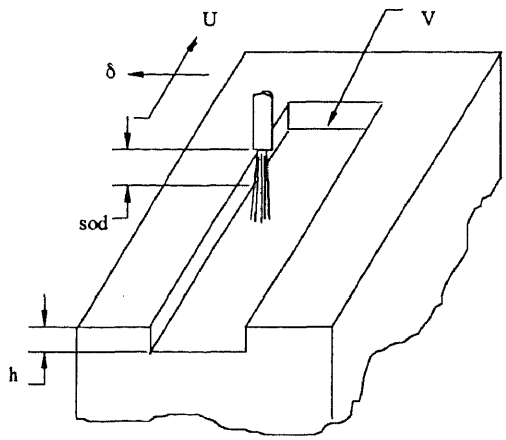

Figure 2.4 Schematic of AWJ Milling

2.3 Characteristics of Surface Generated by AWJ machining

2.3.1 Surface Texture and Integrity

A part surface has two important aspects that must be defined and controlled. The first concerns the geometric irregularities of the surface, and the second concerns the

metallurgical alterations of the surface and the surface layer. This second aspect has been termed surface integrity. Both surface finish and surface integrity must be defined, measured and maintained within specified limits in the processing of any product.

Surface finish or surface texture is concerned with only the geometric irregularities of surfaces of solid materials and the characteristics of instruments for measuring roughness (Field and kahles, 1971). Surface texture is defined in terms of roughness, waviness, lay, and flaws (Figure 2.5) as follows (Field et al, 1989):

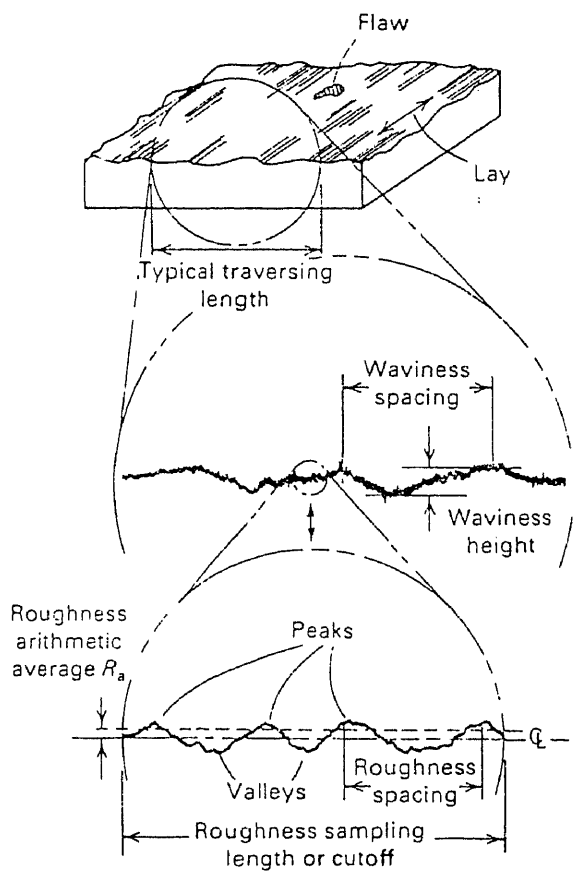

Figure 2.5 Schematic of Roughens and Waviness on a Surface with Unidirectional Lay and One Flaw

- Surface roughness consists of fine irregularities in the surface texture, usually including those resulting from the inherent action of the production process, such as feed marks produced during machining
- Waviness is a more widely spaced component of surface texture and may result from such factors as machine or work deflections, vibration, or chatter
- Lay is the direction of the predominant surface pattern
- Flaws are unintentional, unexpected, and unwanted interruptions in the surface for example, cracks, nicks, scratches and ridges.

The specification and manufacture of unimpaired or enhanced surfaces require an understanding of the interrelationship among metallurgy, machinability, and mechanical testing. To satisfy this requirement, an encompassing discipline known as surface integrity was introduced, and it has gained worldwide acceptance. Surface integrity technology describes and controls the many possible alterations produced in a surface layer during manufacture, including their effects on material properties and the performance of the surface in service. Surface integrity is achieved by the selection and control of manufacturing processes, estimating their effects on the significant engineering properties of work materials. Many of the surface integrity features that may be associated with AWJ machining include (Hashish, 1991):

- abrasive particle deposition (embedding)
- delamination
- gouging
- microstructure transformation

- microcracking
- chipping
- hardness alteration
- heat-affected zone
- residual stresses

2.3.2 Surface Produced by AWJ Machining

In conventional machining, surface texture is usually regular and homogenous, it can be characterized by measuring the roughness Ra. This is quite different in the AWJ cutting. Surface topography depends on the observation coordinate and originates from the physics of the cutting process (Blickwedel, et al, 1990, Hashish, 1991). In fact the upper part of the cutting kerf (side wall surface) is a regular and smooth surface. The surface quality in this zone is comparable to the quality generated using milling and turning techniques (Matsui et al, 1990). This is the consequence of the material removal mode in the zone. The cutting wear mechanism produces micro-craters left by the chip extraction. Roughness seems to be sweet for surface characterization. Roughness value Ra depends most of all on abrasive grain size. The depth of the upper zone depends on the specific energy delivered by the jet per unit of the workpiece area. Reductions of the cutting speed or increase of the jet velocity results in deepening the smooth zone. The bottom part of the kerf is rough and rippled. Amplitude and frequency of striations marks depend on tool parameters (focusing tube diameter), workpiece thickness and materials. Emergence of grooves from the transition zone up to the maximum cutting depth should be the issue of

an unsteady cutting process in the deformation wear zone, vibrations of the cutting head and/or the workpiece and cutting parameters fluctuations such as pressure, traverse rate or abrasive mass feed rate. In this zone, the surface is dominated by the striations and the undulations, therefore waviness can correctly characterize this portion of the cutting kerf.

Abrasive-waterjet machined surfaces may undergo external surface texture effects or internal effects on the integrity of the material. AWJ-machined surfaces are generally rough but are free from any mechanical, thermal, and metallurgical effects.

2.3.3 Surface Finishing in AWJ Machining

The goal of most metal cutting tasks is to machine a workpiece as quickly as possible, while still maintaining an adequate surface finish. Material processing, with a jet of water and abrasive particles, is relatively new technique, but the goal of minimum cutting time with an acceptable surface finish remains unchanged.

Many authors have attempted to describe, analyze and improve the finish and structure of surfaces generated by AWJ. Experimental results pertinent to the surface texture are reported by Blickwedel *et al.* (1990), Kovacevic (1991) and Singh *et al.* (1991). Chao *et al.* (1992) discussed the correlation between the vibration of the nozzle and waviness of the surface profiles. Using visualization data from Hashish (1984 b), Tan (1986) formulated a model describing the phenomenon of waviness (striation). The model shows a qualitative agreement with the experimental data.

The problem of surface quality control has been investigated by many authors. Blickwedel (1990) proposes an empirical model to predict surface quality. Guo (1993)

uses Fouier transform to analyze cutting parameters effects on the surface geometry. Tan (1986), Hunt (1988), Li (1989) and Fekaier *et al.* (1994) use the cutting force measurement to control surface texture. A very strong relationship between the forces and surface finish were found in this study and an empirical equation relating roughness to process parameters was proposed. Though this technique is widely used in conventional machining, its application on AWJ cutting needs a development of a comprehensive model for cutting forces, and experimental set up for on line force measurement.

An Experimental investigation was conducted to determine the effect of particle size on the finishing of turned and milled surface (Hashish, 1987a, 1989). It was found that the surfaces are similar and are characterized by the existence of hills and valleys about the size of one particle.

Guo *et al.* (1993) have also found that the particle size influences essentially the surface roughness. The frequency (wave length) of the grooves as well as the frequency of the striations are largely depending on the diameter of the jet. However, quantitative relations are yet to be determined.

Curhan, Reuber and Kim (1989) made AWJ test cuts in 6061-T6 aluminum to determine the relationship between cutting force, material feed rate, depth of cut, and surface roughness. Their work focused on real time controlling of surface finishing in abrasive cutting using force feedback techniques. They found that surface roughness of the cutting kerf is proportional to force applied to the workpiece by AWJ, so the controlling force will effectively control the surface finish. However Ojmertz [1993] found that both surface roughness and tolerances benefit from an inclined jet attack angle in a AWJ milling

investigation. He found that minimizing the surface roughness in AWJ milling to some extent appears to be incompatible with surface waviness amelioration. When possible, a compromise featuring the most significant promoters of each effect could produce relatively promising results. A further work should elucidate the two-factor interactions detected in this study. It was shown that abrasive mass flow, angle of jet attack, and abrasive grain size all are important factors in obtaining a smooth surface.

In turning with AWJs, Hashish (1987 a) has observed that the surface waviness improves when the jet is angled in the direction of the jet traverse, i.e., when the angle between the jet and traverse vectors is acute. similar results are obtained in linear cutting.

The goals of these analysis are (i) to characterize the topography of the AWJ surfaces in order to quantitatively describe the influence of the process parameters. This information is needed to control the machining results and to meet the imposed form and roughness tolerances, and (ii) to utilize the AWJ surface morphology as a fundamental point of the investigation of the material removal process and machining mechanism.

The structure of each technical surface documents its formation progress. The formation process of the surface in AWJ machining is not completely understood up to now. Development of AWJ machining, therefore, requires a thorough identification and control of the important parameters influencing the surface characteristics.

2.4 Erosion Mechanism in the Course of the AWJ Machining

Abrasive-waterjets are formed by accelerating solid particles within high-velocity waterjets. The resultant focused stream of high-velocity particles impacts the surface of a

workpiece and results in material removal. This phenomenon involves a complex interaction of process due to the individual and/or combined effects of the flow phase. The wear associated with solid particle impact is generally referred to as erosion; thus, AWJ machining is mainly due to the material erosion by impinging particles and is a controlled erosion process. A better understanding of the fundamental mechanisms of a material removal process under actual high pressure abrasive waterjet polishing conditions is undoubtedly necessary.

2.4.1 The Theory of Erosive Cutting

The theory of erosion by an abrasive stream was introduced by Finnie in 1958. Finnie explained a number of aspects of the erosion of ductile materials under the action of a particle stream. This theory assumes that a hard, angular particle impinging upon a smooth surface at an angle of attack α and with a velocity V, will cut into the surface, much like a sharp tool. Based on the model of erosion in Figure 2.6, three equations of motion according to Newton's law are used to describe the trajectory of an individual particle during cutting. Then the volume removal is calculated by integrating the contact area along the particle trajectory over the period of impact. The theoretical results strongly correlated with experimental data for ductile materials at shallow angles of attack, but are almost irrelevant for erosion under normal attack on the same material.

Bitter (1963a and 1963b) carried out a theoretical study of particles based on erosion. In his work, the erosion analyzed by Finnie is classified as cutting wear which is accompanied by plastic deformation of the substrate material. The erosion by particles

under conditions of normal attack on ductile materials is classified as deformation wear. This phenomenon was not accounted for in Finnie's analysis. Bitter's approach is based on the computation of the plastic energy dissipation from the impact parameters of a single erosive particle. The wear is defined as the amount of energy needed to remove a unit volume of material.

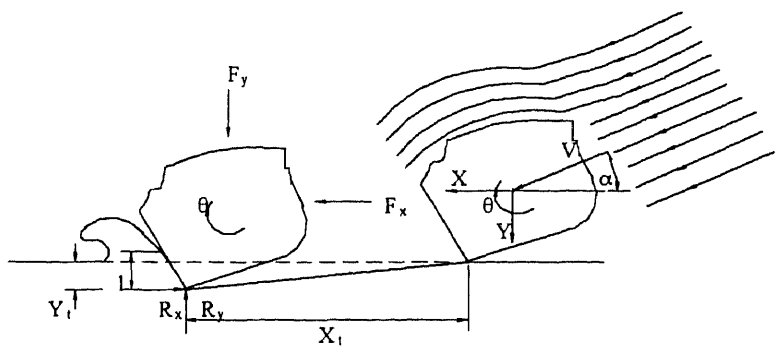

Figure 2.6 Erosion Model of Material Penetration by a Solid Particle

Winter (1974 and 1975) and Hutchings (1977 and 1979) reported that the erosion at shallow angle is characterized by plowing and cutting deformations. Plowing occurs at large negative rake angles. At more positive rake angles, cutting deformation occurs, but particle rolling will cause deep penetration rather than the scooping action for material removal. It was also found that the lip raised during the early stages of impact will be cut off by fragments of the same particle.

It was found that the erosion process is highly dependent on the angle of impact, particle size and velocity.

2.4.2 Study of Impinging Angle

The mechanism by which a high-velocity solid particle erodes material depends on its angle of impingement. The angle is defined as the angle between the jet and the plane of the target material. The angle contributes to two erosion mechanisms (Hashish, 1984a, Lansdown , 1986): The first is abrasive erosion which is the micromachining action of abrasive particles which impact the solid surface at a small angle, i.e. relative motion of the abrasive particles is nearly parallel to the solid surface. Erosion proceeds as cutting wear. This is a low-stress abrasive process where impact does not generate sufficient stress to fracture the abrasive. It is also commonly termed "scratching abrasion". The second is impingement erosion where impact of the abrasive particles occurs at a large incident angle. This erosion is due to deformation wear.

Ives and Ruff (1979) confirmed observations of particle embedment in ductile materials and showed that embedding increases with increasing angles of attack. The influence of particle embedment on the erosion process has not yet been closely examined.

Finnie (1960) derives equations to describe the trajectory of an individual particle of mass **m** striking a solid surface at an angle α, and with a velocity **V** (Figure 2.6). In this analysis it is assumed that the center of the particle translates in x and y directions while rotating at an angle θ. The particle is considered as the cutting edge of a tool for the erosion of a ductile material. The volume removal W can be found by integrating the equations of motion for the penetrating tip of the particle over the period of penetration. The final result yields:

$$W = \frac{mV^2}{p\psi K}\left(\sin(2\alpha) - \frac{6}{K}\sin^2\alpha\right) \qquad \text{if } \tan\alpha \le \frac{K}{6} \tag{2.2}$$

$$W = \frac{mV^2}{p\psi K}\left(\frac{K\cos^2\alpha}{6}\right) \qquad \text{if } \tan\alpha \geq \frac{K}{6} \qquad (2.3)$$

where p is the horizontal component of stress on the particle force, ψ is the ratio l/Y_t and K is ratio of vertical to horizontal force component on the particle. The equation shows that the amount of material removal by erosion is a function of the abrasive impingement angle.

2.4.3 Study of Abrasive Particle

Most of the previous studies of erosion were based on the earlier theories in which the properties of eroded surfaces received far more attention than those of the erosive particles.

Pioneering theories of erosion by Finnie (1958) and Bitter (1963) did not include the abrasive particle size as a parameter in their formulation. Later experimental results of other workers (for example Morrison et al., 1986) demonstrated the effects of abrasive particle size on the erosion mechanism. Tilly (1973) indirectly incorporated the effect through, what he calls, "secondary" erosion. Hashish (1987c) proposed a model based on the earlier work of Finnie that explicitly included the abrasive particle size as a parameter.

Tilly and his colleagues (1973, 1970) found that a decisive role in the erosion process (both ductile and brittle) was played by the particle fragmentation upon impact. Tilly suggested a two-stage mechanism. The first stage consists of chips cut and also gouges and vulnerable extrusions plowed up by the impinging particles. The Second stage is produced by radically flying fragments which cause further damage on the eroded surface.

An important element in Tilly's two-stage erosion theory is the variation of the erosion rate with that of the particle size observed experimentally. The abrasiveness W of quartz particles below the threshold size (5 μm) was found slight (Tilly, 1969 a); it increased (normally as the square of the size, i.e. $W=kd^2$), until, for some target materials, it reached a saturation point and continued on a plateau. The fragmentation was used to explain the particle size dependence of erosion. Below the threshold size, no fragmentation occurs, and the secondary stage is missing. Erosion increases with fragmentation as the particle size is increased. Maji and Sheldon (1979) examined the secondary erosion concept proposed by Tilly and confirmed the evidence of its role in increasing erosion.

Sheldon and Finnie (1966 a) also found that the particle size effect is an important consideration for all erosion processes during experimentation of eroding plate glass by three sizes of angular SiC grit. Small enough particles can produce the effect of ductile erosive cutting in nominally brittle materials All but the small size (9 μm) grit displayed brittle erosion characteristics; the small size grit produced typical ductile erosion. They explained that the size effect is due to the distribution of flaws throughout the material. These produce stress concentration upon contact loading, and probability of encountering these decrease with decreasing dimensions of the contact region. Thus the fracture strength effectively increases for small size indenters, and the material will tend to flow instead of fracturing.

2.4.4 Study of Material Effect

Many investigators (Preece 1979) have observed greater erosion from the impact of a single particle at shallow angles of impact (15 to 20 degree) on ductile materials and at normal angles on brittle materials. Figure 2.3 illustrates this behavior. Material that are both ductile and brittle, such as hard steel, exhibit erosion characteristics that are intermediate between these two cases, with maximum erosion at relatively large angles of impact (around 45 degree). It has also been observed (Sheldon and Finnie, 1966 a) that nominally brittle materials may exhibit ductile material erosion behavior under certain erosion conditions. Thus, ductility and brittleness are conditions resulting in different type of erosive behavior that may be displayed in either nominally ductile or brittle materials.

Material parameters relevant to the erosion process may include both static and dynamic mechanical properties together with thermal and physical properties. The indentation hardness of the work-hardened surface proposed by Sheldon (1977) seems the most applicable measurement to use in this instance.

2.5 Study of Particle Motion in a Fluid Stream

Benchaita (1983) proposed that the general problem of erosion involves two interdependent phenomena the wear of materials by collisions of abrasive particles on the metallic surface as discussed above and the fluid mechanics of the solid-fluid two-phase flow (or momentum exchange between the solid and liquid phase). The effect of the carrying-fluid flow conditions have previously been considered only to determine prior-to-impact particle erosion parameters. The carrying fluid/cutting process interaction has not

yet been considered by any investigator. Finnie (1962) discussed the effect of fluid velocity on erosion when the abrasive-carrying fluid turns a bend. When a fluid stream containing solid particles is turned in pipe bends or tees, the abrasive trajectories are different from those of the fluid motion, and for a large ratio of inertia force to drag force acting on the solid particles, almost all abrasives impact on the wall. In the case of suspension particles, turbulent fluctuations in the flow velocity propel the abrasives to the wall and thus increase the rate of erosion, especially for fine particles, for which case the frequency of collisions with the metallic surface is much greater than in the case of large particles. Bitter (1963 a) described the attack of abrasive turned in a bend as "gouging". Barkalow *et al.* (1979) indicated that the true angle of attack, particle velocity and impact density (number of particles per unit area) vary along the surface of a cylinder cross-flow as a function of the particle size. Several equations were proposed for particles entrained in a laminar flow. The forms of these equations depend on the forces considered in a particular study. Finnie (1961) employed an equation governing the motion of particle to analyze the motion of erosion particle in a fluid stream, in which the particle was considered subjected to the drag force. Soo (1967) gave a deduction of the equation for the motion of particles subjected to different forces. Sheldon (1966,b), Neilson (1968), Benchaita (1983) and Finnie (1967) discussed the various applications of this equation.

Hinze (1959) discussed the motion of particle in a turbulent flow, Tchen (1947) and Hjelmfelt(1965) derived an equation for the motion of particles and discussed the particle response to the oscillatory motion of the carrying fluid. As a result of their work, for a particle of density ρ_p and diameter d, the following equation was proposed:

$$\frac{\pi d^3}{6}\rho_p\frac{du_i^p}{dt} = 3\pi\mu\rho d(u_i - u_i^p) + \frac{\pi d^3}{6}\rho\ \frac{du_i}{dt} + \frac{1}{2}\frac{\pi d^3}{6}\rho\ (\frac{du_i}{dt} - \frac{du_i^p}{dt}) +$$

$$\frac{3}{2}d^2\sqrt{\pi\rho\mu}\int_{t_0}^{t}\frac{\frac{du_i}{dt'} - \frac{du_i^p}{dt'}}{t - t'}dt' + f_i^p \qquad (2.4)$$

where u_i and u_i^p are velocity of the fluid and particle respectively, f_i^p is the combination of force acting on the particle, μ is the viscosity of the fluid and t_0 is the starting time.

Danon(1977), Melville(1979), Maxey (1983), Situ (1987), Givler (1987) and Ahmadi (1989) calculated numerically the trajectories and velocities from the differential equation under various initial and boundary conditions.

The velocity and direction of solid particles traveling in the stream of a fluid may greatly differ from those of the surrounding fluid. Small particles may change their trajectories in the vicinity of a solid surface obstructing the flow. An analysis of the velocities attained by particles introduced into the fluid flow was given by Tilly (1969b). The trajectory of a particle approaching a surface may be numerically calculated from the differential equations of particle motion. It has been shown that in an air stream (104m/s) directed against a perpendicular and an inclined plane, the trajectories for large particles (60 μm) are hardly deflected while 5 μm particles behave nearly like air in the vicinity of the obstacle, and pass around the target.

Investigations, however, seldom combine theories of fluid mechanics of solid particles in a fluid stream, and the wear of material by abrasive, especially in the case of a turbulent jet. The theoretical prediction of motion are hindered since complete solutions of

the complex turbulent free jet flow are lacking, and since the interaction between the turbulence of the mainstream and the dispersed phase is not well understood.

2.6 Comments on the Previous Studies

1. It is a logical to expect that AWJ which is successfully applied to cutting drilling, milling and turning can also be applied for finishing operations.

2. The geometry and quality of the machined surface depend on all of the process parameters, though to varying degree.

3. The characteristics of the erosive particle and its motion has received less attention than those of eroded surface of target materials.

4. In the relatively mature field of fluid dynamics there are two issues which are poorly understood because of experimental difficulties. they are turbulence and two-phase flow. In this situation, therefor, direct numerical simulation appears to be the only practical alternative for understanding of the physical phenomena which bring about AWJ erosion.

5. The understanding of the particle trajectory in a fluid stream is of considerable practical interest since there is a direct correlation between effect of turbulent jet on particle motion and thus on erosion mechanisms in the course of AWJ machining.

CHAPTER 3

OBJECTIVE OF THE STUDY

With the rapid growth of hard and difficult-to-machine materials, conventional machining processes have reached practical limits of performance and productivity. At the same time requirements to parts precision become more and more stringent. Precision machining represents a critical and perhaps the most expensive segment of the present day manufacturing. Space technology, bioengineering, micromechanics and microelectronics, etc. are based on the use of ultraprecision components fabricated from composites, ceramics, superalloys. Conventional, rather than exotic processes must be used for cost effective fabrication of such components. The necessity to produce precision and ultraprecision parts from hard -to-machine materials and inability of existing machining processes to accomplish this at an acceptable cost constitute one of the main problems of the manufacturing industry. Because existing processes are not able to meet this challenge, creation of new technologies of precision machining is a must.

Perhaps the most urgent, and at the same time the most difficult task, is the development of a practical technique for formation of precision and ultraprecision surface texture. Existing technologies definitely are not able to meet the challenge. In fact in a number of cases , for example in the production of telescope mirrors, manual polishing is the only acceptable technology. AWJ machining constitutes one of the more promising approaches to surface processing technologies. The interaction between abrasive particles and substrate in the course of slurry impact is similar to that of ultrasound or float

polishing. At the same time, it is much easier to accomplish and control the interaction using an abrasive nozzle than any other tool. Existing surface machining processes change surface integrity by inducing a heat-affected zone, increasing the surface hardness, and reducing the fatigue strength of the material. Flooding of the substrate surface by incoming water in the course of the slurry jet impact prevents the above problems (Geskin, E.S., 1991 and 1993).

However, the accuracy of existing AWJ based processes (cutting, milling and turning) is far below that of conventional milling and turning technology. Due to low accuracy and poor topography of the generated surfaces, the AWJ process is still a supplemental method of manufacturing and is employed only when conventional net-shaping proves insufficient.

Thus, there is a gap between the potential use of AWJ for surface improvement and manufacturing practice. It is the mission of this work to develop the knowledge base needed for the implementation of AWJ processing into manufacturing practice. More specifically, our objective is to determine feasibility the improving the of surface topography by the impingement of a high speed slurry jet. Due to the complexity of the phenomena in question, only a direct evaluation of change to the substrate topography can be used to determine the effect of AWJ on the surface texture. As long as the feasibility of AWJ polishing can be determined, it is necessary to evaluate the effect of various process variables on the process result. Such evaluation is another objective of our work. Particles impacting the substrate surface constitute a machining tool in the course of polishing; thus the information about particles properties is necessary for process design. The

specification of the abrasive materials provides sufficient information about geometry and the structure of particles prior to entering into the focusing tube. However, due to disintegration in the course of impact and mixing the characteristics of the abrasive particles at the impact site are expected to be different from those entering the focusing tube. Because the available information concerning particles's behavior prior to the impact is limited, it is still another objective of this work to investigate particles disintegration in the course of slurry formation and impingement on the workpiece surface. Due to the limitation inherent in current theoretical and numerical methods, the experimental techniques study the jet characteristics and their effect on the results of polishing.

Finally, the objective of this study is to investigate the motion of particles prior and after impingement. In the final analysis this motion determines the surface processing and final substrate topography. The experimental technique is used to monitor jet properties (velocity distribution, impact force), while the motion of individual particles is investigated numerically.

Because there is no prior experience of the AWJ-based topography improvement and numerical evaluation of the slurry impacts, these parts of our study constituted a special challenge.

CHAPTER 4

EXPERIMENTAL SETUP AND TEST PROCEDURE

The objectives of the experimental study was the exploration of the feasibility of abrasive waterjet-based polishing technology, evaluation of the correlation between control variables and surface texture, and the examination of the topography of generated surface and abrasive particles. Four kinds of experiments were carried out.

The first experiment involved the determining of feasibility of AWJ polishing by directly studying the topography and integrity of surfaces subjected to the slurry impact with various parameters of the machining. An industrial scale abrasive waterjet machining system was used in this study.

The second experiment involved measurement and analysis of abrasive particles disintegration during mixing and impacting under various varables of processes and their size distribution in the process of the polishing by the Laser Scanning Sizer. The particle topography after impacting are examined by SEM.

The third experiment consisted of LTA measurements of AWJ velocity along and across the jet and monitoring of forces developed at the jet-workpiece interface in the course of polishing using the piezoelectric force transducer.

Finally, SEM examination and analysis of polished surfaces were carried out to evaluate the surface topography. Surface integrity was examined by through-thickness microhardness test and SEM observation.

The experimental facilities, test materials and samples, the measurement instruments and procedure are described in the following sections

4.1 Abrasive Waterjet Machining System

The AWJ polishing tests were carried out at a waterjet machining cell manufactured by Ingersoll Rand Co. It has a 5 axis robotic manipulator controlled with an Allen Bradley 200 robot controller. The cell consists of four major components: the hydraulic unit, the robotic workcell, the abrasive feeding system and the nozzle body (Fig 4.1).

4.1.1 Hydraulic Unit

The principal part of the hydraulic unit is the intensifier, which is a special type of a pump. A basic system pressurizes a large piston at hydraulic pressure up to 45,000 psi. The control system cycles the piston in a double-acting motion. The piston is mechanically connected to a smaller diameter piston cylinder and is intensified by the ratio of the area of large and small pistons. Using this principle, it is possible to create a water flow having a pressure between 50,000 and 60,000 psi. A series of check valves allow the water to enter the high pressure cylinder on the suction stroke and leave on the discharge stroke. A booster pump is used to assure continuous flow into the suction side of the high pressure cylinders. Filters and softeners are used to condition the water. High pressure tubing, swivels, flexible joints and fittings are used to connect the intensifier to the cutter, i.e. the nozzle.

4.1.2 Robotic Work Cell

The movement of the nozzle and the change in the angle between nozzle and workpiece surface can be controlled accurately by a 5-axis robotic workcell with Allen-Bradely 8200 controller. The programming capability of the controller enables the movement of a continuous path control of all axes. The positioning accuracy is +/- 0.005" and the repeatability is also +/- 0.005".

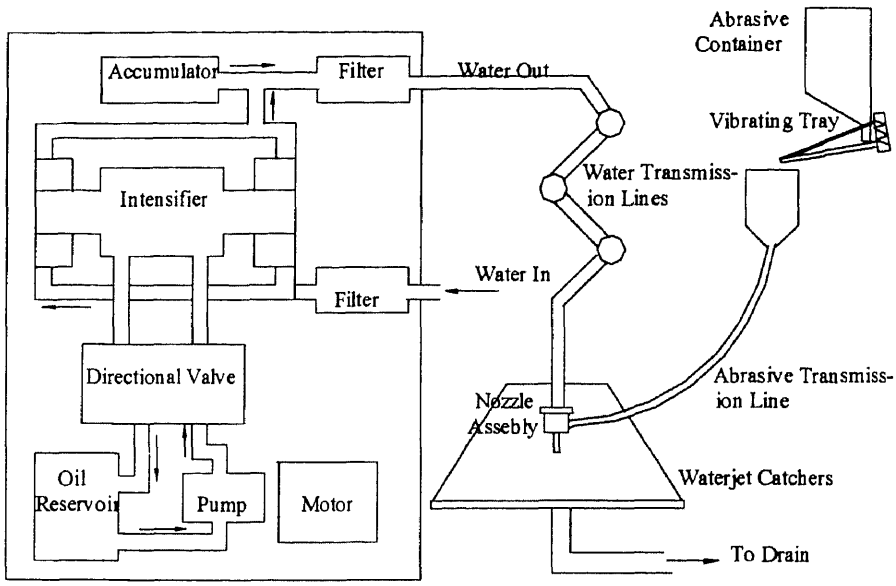

Figure 4.1 Schematic of AWJ Machining System

4.1.3 Abrasive Feeder

A vibrator feeder is used to control the federate of the abrasives. The bulk abrasive is stored in a larger hopper and an electromagnetic vibratory tray regulates the flow of abrasive from the hopper by changing the applied voltage which in turn changes the frequency of vibration. The suction created in the nozzle assembly draws abrasive from the

vibratory. In the course of the experiment, the size of the abrasive varied from 50 to 500 mesh with garnet sand being the material. The abrasive particle size significantly affects the abrasive feed process (in the abrasive control valve and in transmission hoses) and its method. The entrainment of dry powder is practically limited to a mesh size of 240. The fines in average-sized abrasives can result in abrasive feed halt either due to caking, moisture absorption, and/or coating of the feed lines with a fine layer of powder that affects hose frictional characteristics. Therefore, a special feeding system, vibrator and screw feeder, are used with an abrasive size smaller than 240 mesh in this work. It consists of a vibrating hopper and an screw deliver system whose entering port is located under the exit of the hopper. The vibrating frequency of hopper and rotating speed of screw regulate the powder flow rate.

4.1.4 Nozzle Assembly

The pressure head of water is converted into kinetic energy in the nozzle assembly (Figure 1.1). Two kinds of nozzles assembly can be housed in the main body. In a pure waterjet machining system, the nozzle is normally a small sapphire orifice with a diameter d_N between 0.1778 mm to 0.3556 mm. In an abrasive waterjet machining system the same nozzle, as in pure waterjet machining, is used in conjunction with a secondary nozzle, known as a focusing tube, with 0.8636 mm, 1.09 mm, and 2.4 mm of internal diameters d_m. The focusing (carbide) tubes are made from tungsten carbide to resist wear.

The high pressure water supplied from the water distribution line pass through a sapphire nozzle (Figure 4.2) and accelerates to a velocity of 600 to 800 m/sec. In the case

of AWJs, the abrasive enters from the side port behind the sapphire nozzle. Water from the sapphire nozzle and abrasive particles are mixed in the focusing tube made from tungsten carbide. Here abrasive particles are accelerated and the final energy transformation takes place. The performance of the sapphire nozzle and the carbide mixing tube depends on the diameter, length, angle of convergence and weight. Also, the entry angle of the abrasive, the diameter of port, the vertical and horizontal distances between the abrasive inlet and the sapphire nozzle are typical variables which affect the nozzle performance.

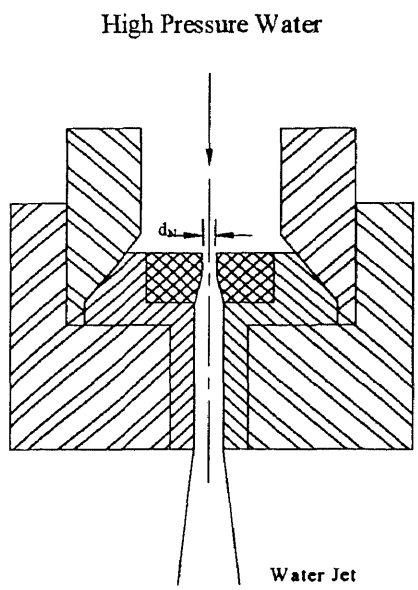

Figure 4.2 Schematic of Sapphire Nozzle with Water Flow

4.2 Experimental Study of AWJ Polishing

4.2.1 Concept for Abrasive Waterjet-based Polishing

In AWJ the cutting process, abrasive particle impact angle and size are found to be the dominant parameters affecting the surface finish of the generated kerf.

Based on erosion studies by Bitter (1963) and Finnie (1958), the smooth cutting zone is the upper portion of the kerf in which the primary surface irregularity is roughness, and which is free from jet-induced waviness "striation", as material removal occurs primarily by particle impact at shallow angleswith the wall of the kerf. A rough striation zone which appears at some depths of penetration is termed the deformation wear zone, as the impact at large angles causes material removal. This implicates that the surface finishing or polishing could be achieved by changing the impinging angle of AWJ.

Mechanical finishing or polishing processes usually rely on contact and abrasion between a multiple-point tool (such as a grinding wheel, horning tool or lap) and a workpiece. The tool is composed of many grains of material with high hardness (Knoop hardness above 2000) embedded or bonded on a base material (Kalpakjian, 1984). Upon tool/workpiece contact, each grain shears away a small chip of workpiece material, that is material at the apex or peak of workpiece surface. For AWJ cutting, the volume removal caused by impact at a small angle was given by Hashish (1987 c) as:

$$\delta\upsilon = \frac{14dm_a}{\pi\rho_a}\left(\frac{V_a}{V_c}\right)^{2.5}\alpha^{1.5} \qquad (4.1)$$

where α is the abrasive particle impact angle, dm_a is the infinitesimal abrasive mass flow rate, ρ_a is the density of abrasive material, V_a is abrasive particle velocity and V_c is

characteristic velocity. Obviously, it is possible that at a small impact angle the abrasive waterjet may remove only a small volume of material from target surface; thus, precision material removal is feasible by AWJ.

Finnie et al. (1977) showed that the depth of penetration of an impact particle into a material surface is by one order of magnitude less than the particle size. Hence it is logical to predict that the surface will range from one-tenth of the particle size up to the particle size, and this suggested that AWJ could only shear away the apex or peak on the target surface by controlling the abrasive particle size in addition of impact angle.

4.2.2 Experiment of AWJ Polishing

Based on the above analysis and material erosion theory, it follows that the results of material erosion by a stream of solid particles is controlled by such particle features as particle size and shape, impinging angle, flow rate, and velocity, etc., as well as the properties of the target material. Therefore, the initial experiments were designed to explore the feasibility of AWJ polishing and to discover major trends in surface evolution. This goal was attained by comparing the roughness of AWJ generated surfaces produced at a different impact angles α and abrasive particle size d_p.

The tests were carried out using 50 to 500 mesh Barton garnet. SEM micrography of the particles surfaces prior machining are shown in Figure 4.3. Almandine garnets (iron aluminum silicates), was selected for testing because of its demonstrated effectiveness, flowability, availability, and reasonable cost. Prior to the test the abrasive particle size distributions was determined by the optical analysis described later. Relationship between

abrasive mesh and actual particle size (Figure 4.4) shows that the abrasive with a larger mesh number has a smaller average value of particle size, that is, there are more particles per unit weight.

Figure 4.5 shows the experimental setup of AWJ polishing The general arrangement of the experiment is shown in Figure 4.6. Impact angle α of the jet is defined as the angle between jet and the plane of the target. Standoff distance S is the distance anlong the jet axis between the exit of jet and striking point on the plane. In the experiment AWJ is sprayed onto the sample surface under high pressure, from a certain standoff distance S and at a angle of incidence α, while jet is traversing in the direction of perpendicular jet axis at speed V and moving backward at the feed increment δ. To catch the defected jet a collecting tank is made which houses the portion of the workpiece to be machined.

The AWJ performance according to Hashish (1987 b) is related to a number of hydraulic, abrasive, mixing nozzle, and cutting parameters. Since the machining process is a result of interaction between the abrasive jet and the target material, work material properties, such as hardness, also determine process output. To explore the influence of the participating parameters on basic AWJ polishing performance, the following parameters were selected for this investigation as being important for process control and optimization:

- angle of impact α
- garnet size mesh d_p
- abrasive mass flow rate m_a

- water pressure P
- traverse speed V
- standoff distance S
- target material
- focus tube size d_m
- number of passes N_p

These parameters, which are the factors of our experiment, were recorded and analyzed for each roughness observed in the course of testing.

4.2.3 Experimental Materials

One of objectives of this investigation is to find a new polishing technique used to a very wide range of materials which are difficult to machine using conventional methods. Therefore, some of difficult-to-polish material, such as alumina ceramic, stainless steel and titanium alloy, were selected as experimental materials to verify the feasibility of AWJ polishing process. Two ductile materials, an aluminum alloy and carbon steel, were also tested for studying mechanism of AWJ polishing. The chemical compositions and mechanical properties of the above materials are listed in Tables 4.1 and 4.2, respectively.

(a) 150 Mesh Garnet

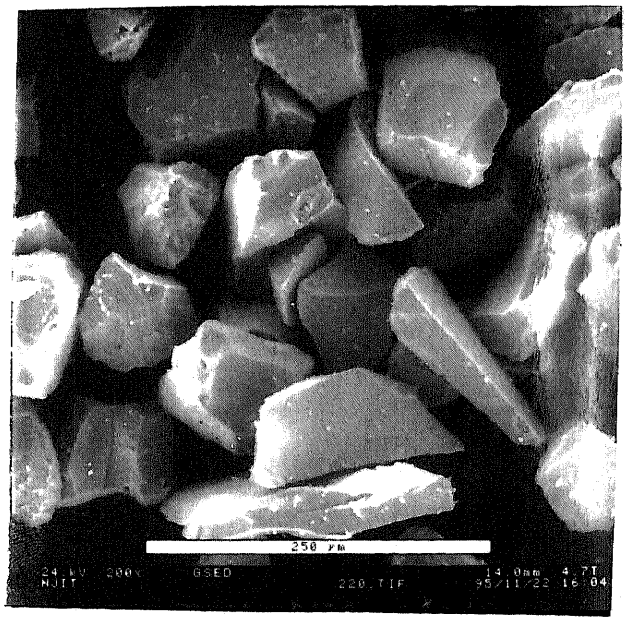

(b) 220 Mesh Garnet

Figure 4. 3 SEM Image of Abrasive Used in the AWJ Polishing Study

(c) 240 Mesh Garnet

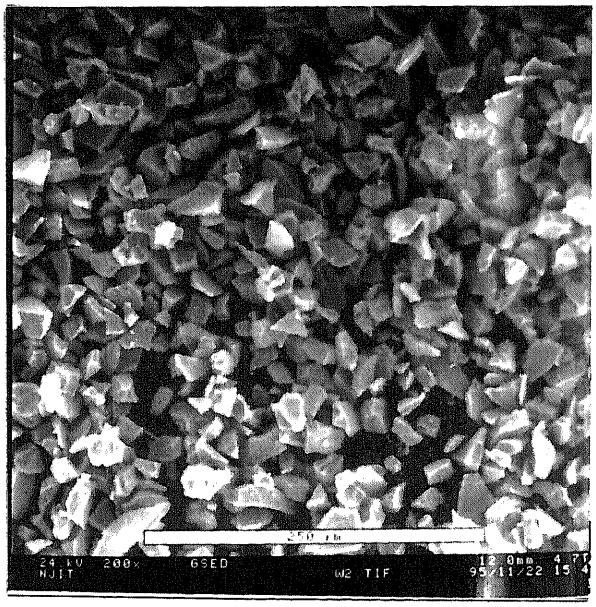

(d) 500 Mesh Garnet

Figure 4. 3 (Continued)

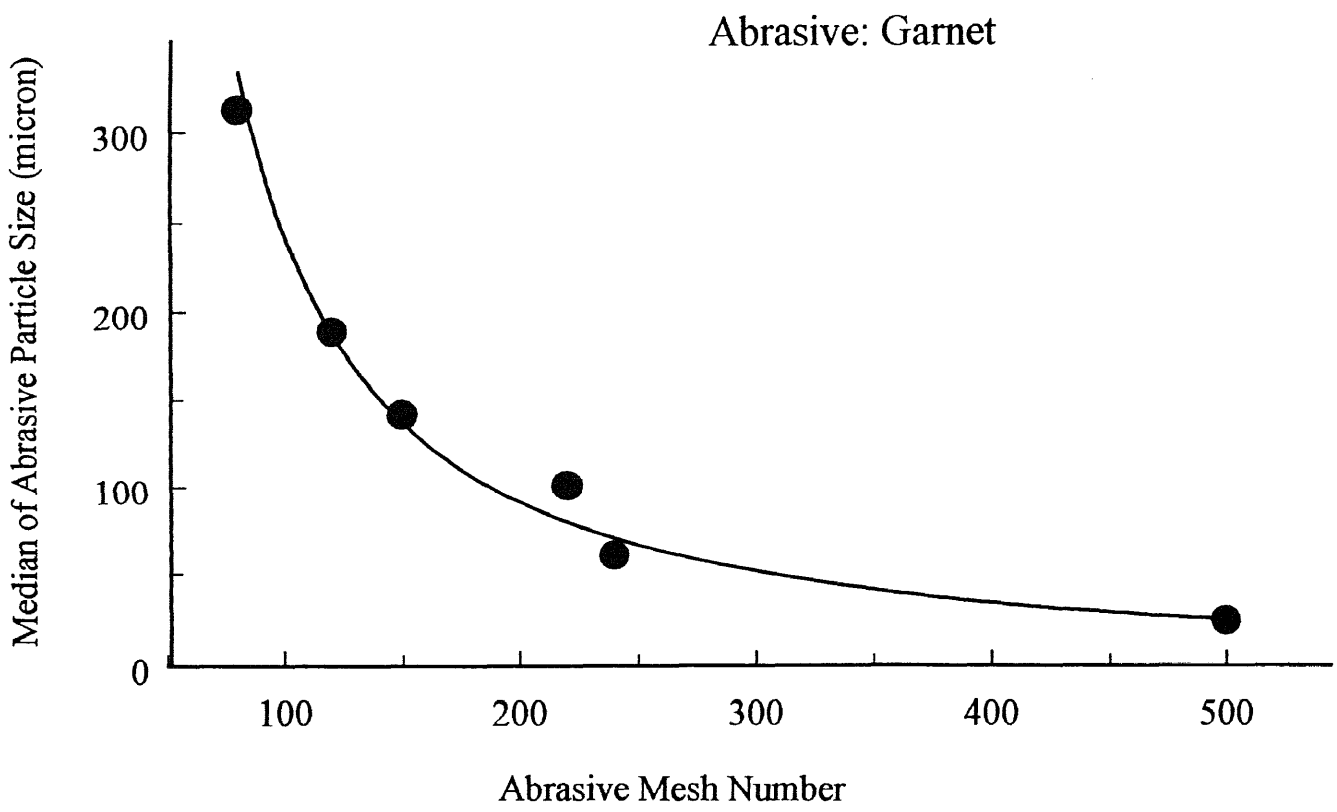

Figure 4.4 Relationship between Abrasive Mesh Number and Particle Size

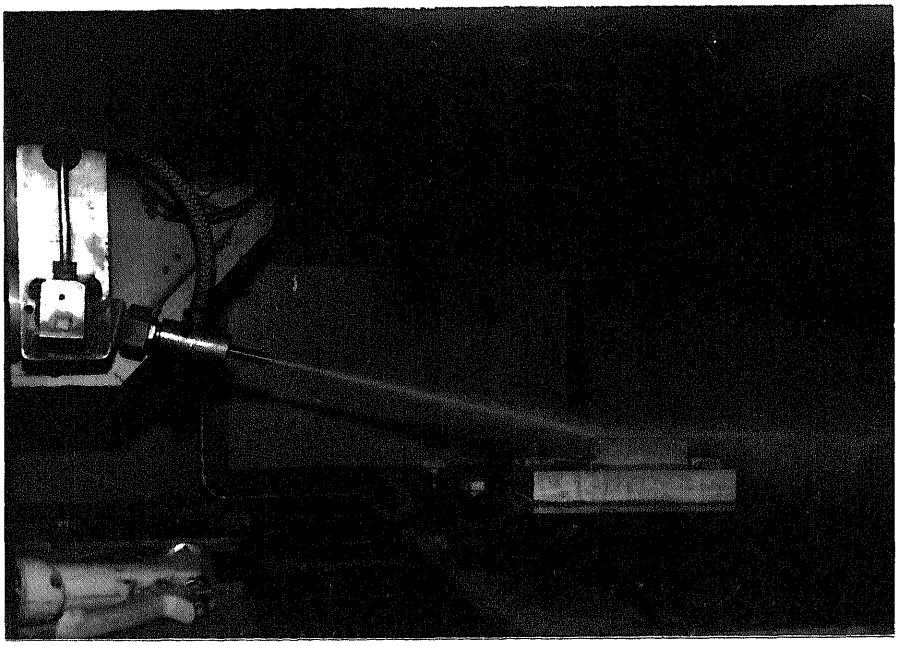

Figure 4.5 Experimental Set-up

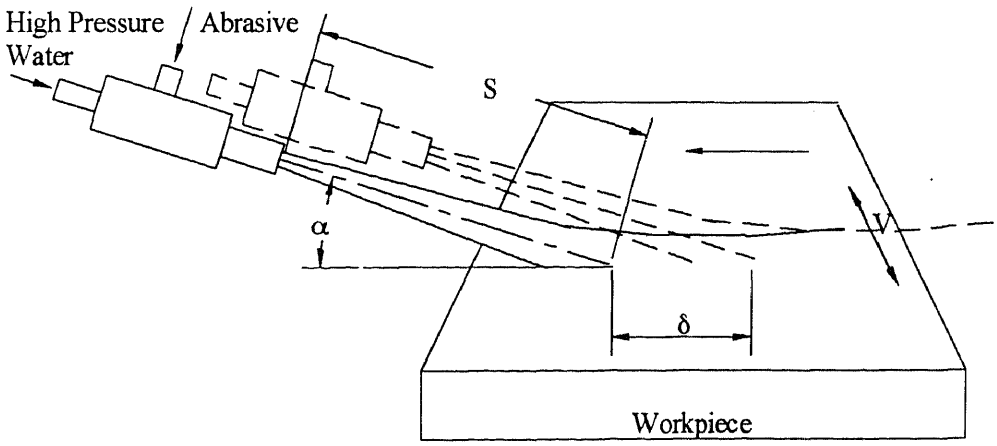

Figure 4.6 Diagram of AWJ Polishing Process

Table 4.1 Chemical Compositions of Experimental Materials

Material	Composition					
Al 6061-T6	% Mg	% Si	% Gr	% Cu	% Al	
	1.0	0.6	0.2	0.27	97.93	
AISI 1018	% C	% Mn	% P	% S	% F	
	0.15-0.2	0.6-0.9	0.4	0.05max	remainder	
Ti Gr2	% N	% C	% H_2	% Fe	% O_2	% Ti
	0.03	0.1max	0.015max	0.3max	0.25max	reminder
AISI 304	% C	% Mn	% Si	% Cr	% Ni	
	0.08	2.0	1.0	18~20	8~20	
Alumina Ceramic	% Aluminium-oxid 94	-	-	-	-	-

Table 4.2 Mechanical Properties of Experimental Materials

Material	Tensile Strength (MPa)	Yield Strength (MPa)	Elongation (% in 2 in.)	Hardness (HB)
Al 6061-T6	310	275	12	60
AISI 1018	450	380	16	86
Ti Gr2	345	275	20	92
AISI 304	515	205	18	100
Alumina ceramic				70 (RC)

4.2.4 Experiment Sample Preparation

In order to investigate the effect of the original surface on AWJ polishing process. The processes of rolling, AWJ cutting, milling, and grinding were used for various samples preparation. Figure 4.7 shows surface characteristics of some of the prepared samples of stainless steel.

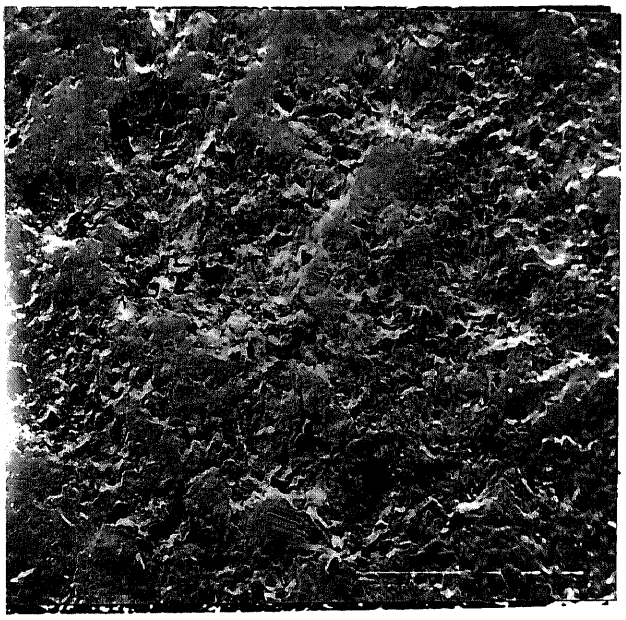

(a) Surface Rolled (R_a=9~15 micron)

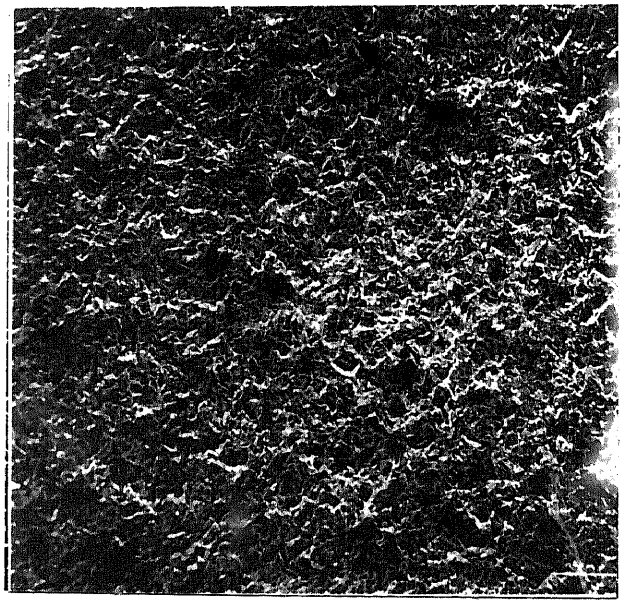

(b) Surface Cut by AWJ (R_a=6~9 micron)

Figure 4. 7 Various Surface of Stainless Steel Sample Prepared for the AWJ Polishing Study

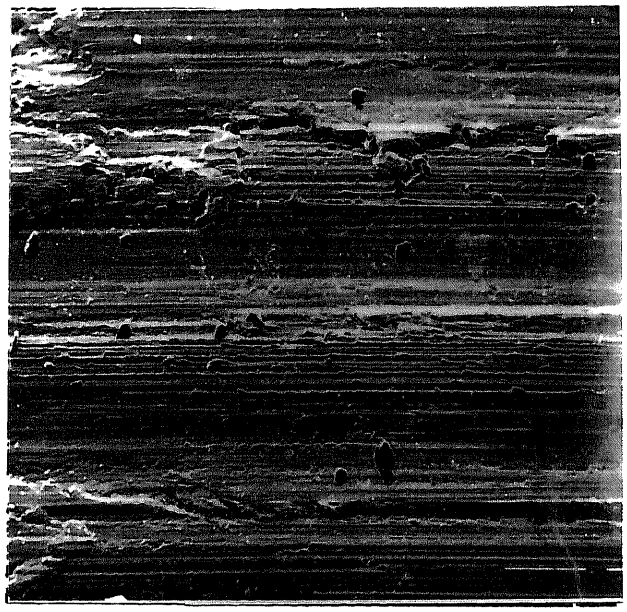

(c) Surface Milled (R_a=3~6 micron)

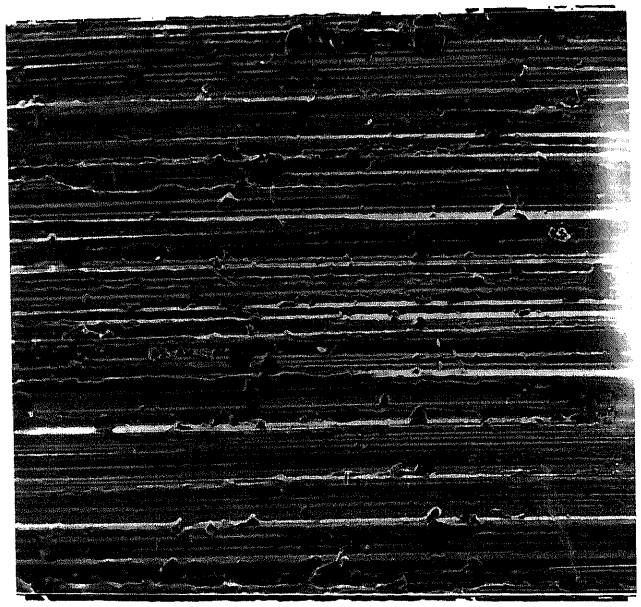

(d) Surface Grinded (R_a=1.5~0.8 micron)

Figure 4. 7 (Continued)

As it is shown in Table 4.3, three levels of the initial surface roughness (low, medium, high) were selected. The range of values of surface roughness for each of the level varied for different processes.

The test specimens were rectangular parts (Figure 4.8).The sample thickness was kept constant at 0.5 inch.

Table 4.3 Surface Condition of Sample before Polishing

Factors	Level 1	level 2	level 3
Process	Rolling/AWJ Cutting	Milling	Grinding
Surface R_a (μm)	High (7~12)	Medium (1~6)	Low (0.9~0.6)

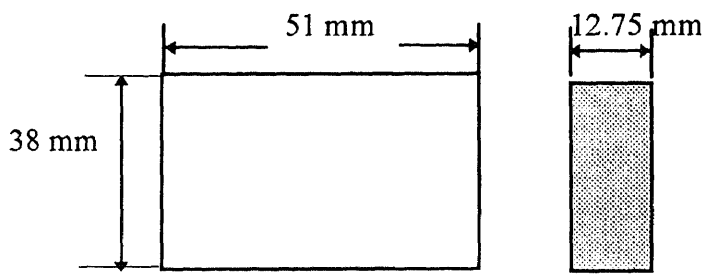

Figure 4.8 Dimension of Testing Sample

4.3 Surface Texture Measurement

Surface profile characterization or surface roughness is commonly used to evaluate surface quality. Surface roughness is the irregularity in the machined material's surface texture and is prevalent in industrial use and consequently was selected as a reference in this investigation. The parameters of surface characterization are arithmetic average roughness value R_a defined as:

$$R_a = \frac{1}{l_m}\int_{x=0}^{x=l_m}|y|dx \tag{4.2}$$

where l_m is length of the profile used for parameter evaluation, y is the ordinate of the profile from the centerline (Figure 4.9 a).

The other characteristics of surface roughness used in the investigation are R_z, the average height difference between the five highest peaks Y_{pi}, and five lowest valleys Y_{vi} contained within a chosen evaluation length l_m, defined as (Figure 4.9 b):

$$R_z = \frac{1}{5}\left(\sum_{i=1}^{5}|Y_{pi}| + \sum_{i=1}^{5}|Y_{vi}|\right) \tag{4.3}$$

R_m is the maximum individual peak-to-valley height Z_i obtained from the five sample lengths l_e (0.8~2.5 mm) within the evaluation length l_m, defined as (Figure 4.9 c):

$$R_m = \max(Z_i) \quad i=1, 2,\ldots,5 \tag{4.4}$$

One of the more interesting surface roughens parameters evaluated in this study is the profile of peak density or peak count N_r taken over a length l_m of filtered roughness profile

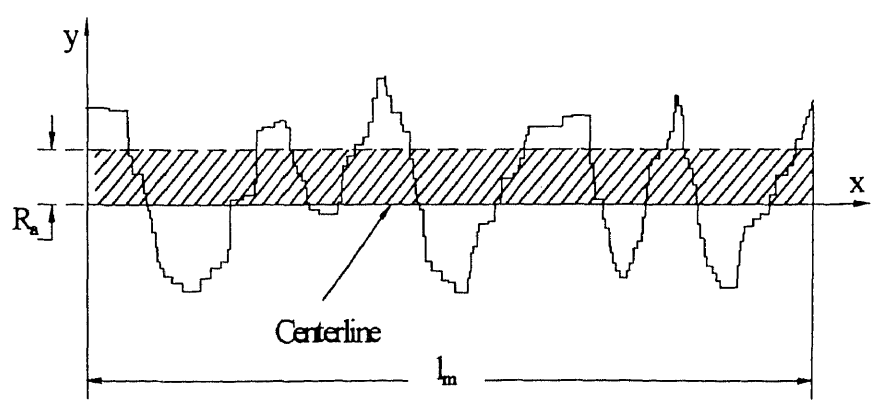

(a) Arthmetic Mean Roughness Value R_a

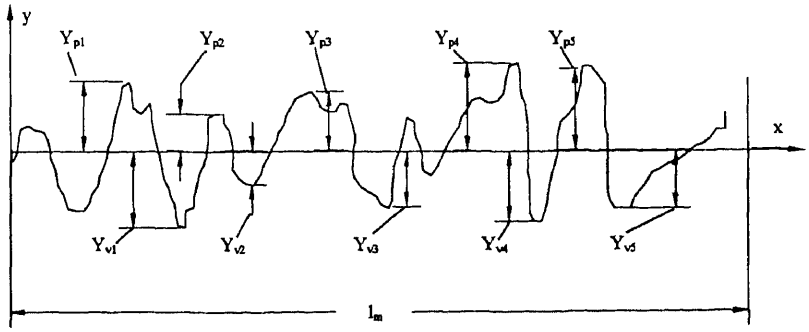

(b)Ten Point Height R_z

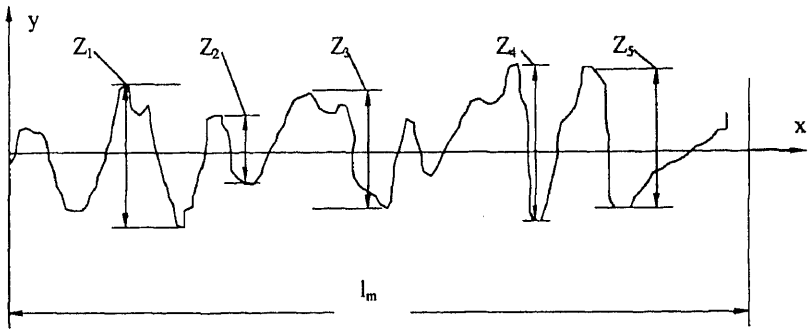

(c)Maximum Peak-toValley Roughness Height R_m

Figure 4.9 Schematic of Designations of Surface Roughness Parameters

Whereby a peak is only read after the profile has passed through both a lower and an upper variable preset threshold C_1 -C_2 . Both threshold lines are set parallel to the center line.

The surface roughness measuring device, the HOMMEL TESTER T 1000S was used to investigate the texture of surfaces. This device consists of a motor driven traverse unit, inductive pick-up, digital display unit, and digit graphic printer (Figure 4.9).

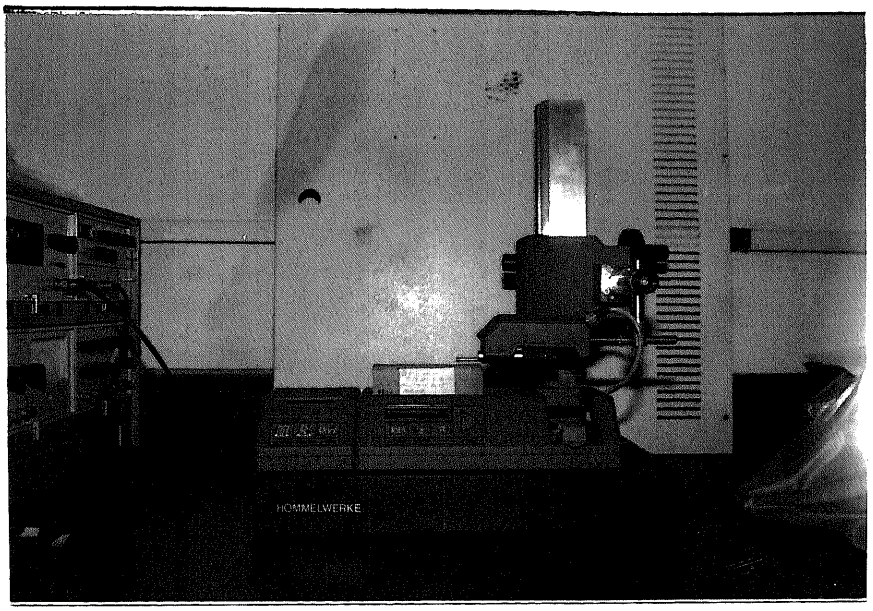

Figure 4.10 Setup of Surface Roughness Measurement

The surface-roughness readings were taken before and after AWJ polishing using stylus with radius of 5 μm. Four measurements of R_a, R_m, R_z and N_r were taken for each sample and the average values were used. for further analysis. All of the roughness measurement were taken in the middle of the piece, in the direction of the flow, from edge to edge The cut-off length was set at 0.8 ~ 2.5 mm which gave the maximum evaluation length l_m across the workpiece of 4.0~12.5 mm. The value of threshold C_1 and C_2 were set at 1 and 0.5 micron, respectively.

The Matrix Videometrix Econoscope was used to measure and analyze the topography include flatness and roughness of the original surface of the sample before

polishing process. The Econoscope uses non-contact techniques to provide rapid dimensional verification of the complete parts or specified features of a part. It comprises a general purpose computer (HP-9000 series), a 3-axis positioning control system, a digital image processor and part monitor section as shown in Figure 4.11. The software has six major functions. The topo function is the module that we used in this study. After the points to be sampled, the size of the measurement matrix, magnification lenses and the light intensity are specified, it executed the automatic measurement of the main features of the surface topography. The data representing the surface profile include the X, Y, and Z coordinates of the points sampled. They are stored in the computer memory and then download to PC via the RS-232 port for further analysis.

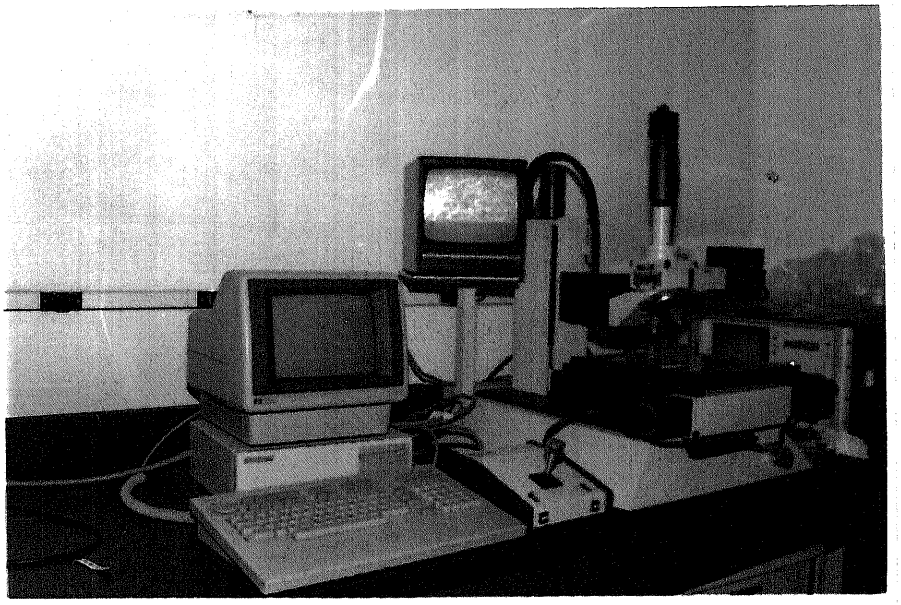

Figure 4.11 The Matrix Videometrix Econoscope

4.4 Particle Size Measurement and Micrographic Study

The use of abrasive material in high pressure water jet machining is one of the means for the intensifying of the effects exerted by the waterjet on the material to be machined. Understanding the mixing process which creates the abrasive waterjet and determining the critical properties of the abrasive material represent key factors in finding ways of increasing the efficiency of abrasive water jet polishing.

4.4.1 Laser Scanning Particle Sizer

4.4.1.1 Assembly of the System Particle size analyzers using Low Angle Light Scattering techniques have become highly respected and popular in the last few years.

Laser light scattering is an exceptionally flexible sizing technique capable in principle of measuring the size and structure of any individual phase in a multiphase system. The MasterSizer X system, produced by Malvern Instruments Ltd, is a particles sizers based on laser scattering. It comprises an optical measurement unit that forms the basic particle size sensor including a transmitter, a receiver, sample area cover and optical bench, and the computer system that manages the measurement and performs result analysis and presentation. The transmitter houses the laser, its power supplies, and the beam expanding optics that creates the analyzer beam. The receiver houses the range lens and the detector.

The system uses a low power laser beam to probe the particle size. It can give high resolution size discrimination. Up to 100 size bands can be displayed covering a range of

up to 600:1 in size capability on any single range. It successfully adapts to measure wet dispersion, dry powders and sprays

4.4.1.2 Operating Principles When light is scattered by particles the pattern of light intensity shows variations with angle. In the simplest description, small particles scatter the light at large angles while the angle of scattering for large particles is small. When a particle scatters light it produces a unique light intensity characteristics with angle of observation. It scatters light so that the measured energy on the detector has a peak at a favored scattering angle which is related to its diameter. Large particle have peak energies in small angles of scatter and vice versa as illustrated in Figure 4.12.

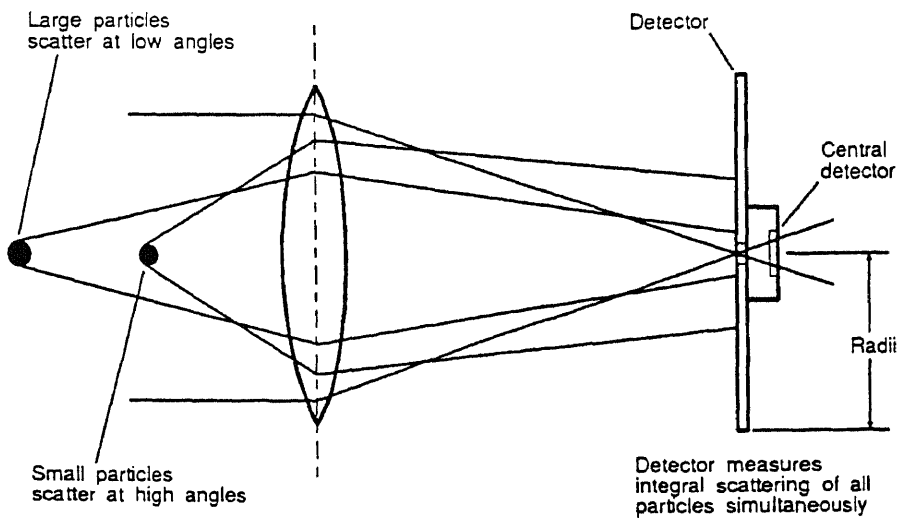

Figure 4.12 Properties of the Scattered Light

The instrument measure the light scattered from a system of particles via an optical arrangement to a series of detector which record a current proportion to the intensity of the scattered light falling upon them. The system optical configuration is shown in Figure 4.13.

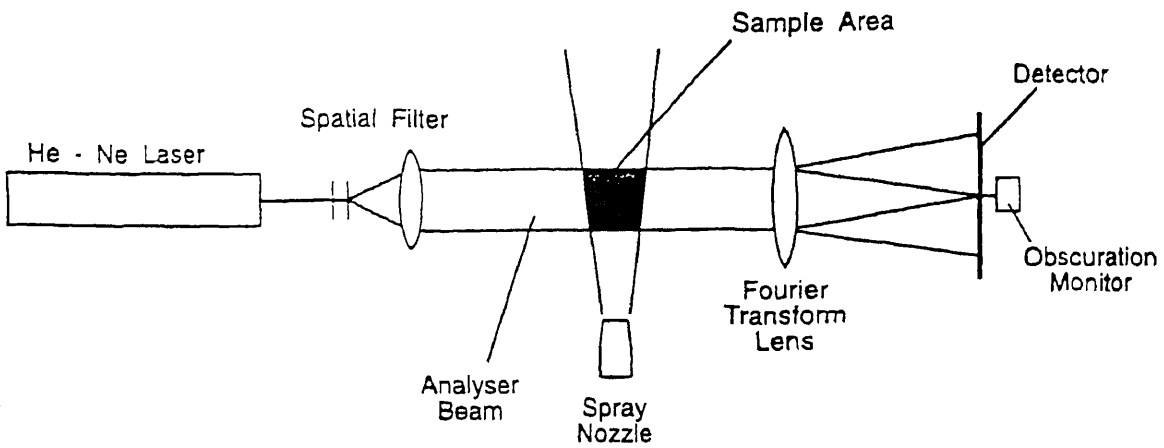

Figure 4.13 Optical Configuration

The radiation of a low power Helium-Neon laser is used to form a collimated and monochromatic beam of light. This beam of light is the analyzer beam and any particles present within it will scatter this laser light. The particles are introduced to the analyzer beam by the sample presentation modules or by direct spraying through the measurement area. The light scattered by the particles and the unscattered remainder are incident on a receiver lens also known as the range lens. This operates as a fourier transform lens forming the far field diffraction pattern of the scattered light at its focal plane. Here a

custom designed detector, in the form of a series of angular sectors, gathers the scattered light over a range of solid angles of scatter.

The unscattered light is brought to a focus on the detector and passes through a small aperture in the detector and out of the optical system. The total laser power passing out of the system in this way is monitored allowing the sample volume concentration to be determined.

The detector provides an electronic output signal proportional to the light energy measured over all separate solid angles of collection. The computer reads this signal and perform the time averaging by successively reading the detector.

4.4.2 Particle Size Measurement

To determine the crucial properties of the abrasive particles that influence the performance of the AWJ, changes in the abrasive particle size distribution and shape characteristics in AWJ forming and AWJ polishing were investigated.

The break-down of particles during abrasive jet machining occurs in two stages as follows:

1. Particle-particle, and particle-water jet, and particle-wall collisions in the mixing chamber/focusing tube assembly
2. Particle-particle, and particle-target material collisions at the target surface.

Thus, to establish the particle size distribution and shape samples of the abrasive were taken at three locations: (A) before entering the mixing chamber, (B) after exiting the focusing tube, (C) after the impact of the specimen surface. These points are schematically drawn in Figure 4.14.

The changes in particles size distribution were established during the tests. To analyze the particle disintegration during the acceleration a special catcher, able to decelerate particles without further destruction was designed. The catcher consists of a 170 mm PVC pipe as a stream guidance and an air container to collect particles. The abrasive jet was directed into the catcher and collected (Figure 4.15). The samples were then analyzed using the Laser Scanning Particle Sizer.

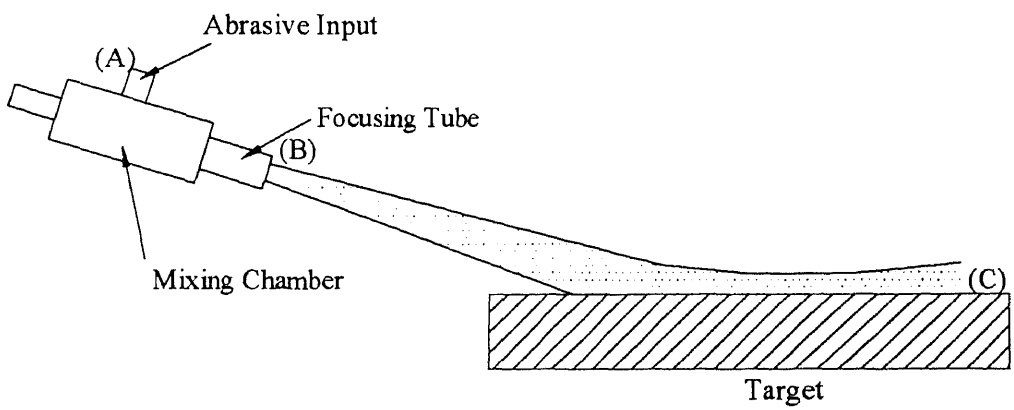

Figure 4.14 Locations Where Samples of Abrasive were Collected

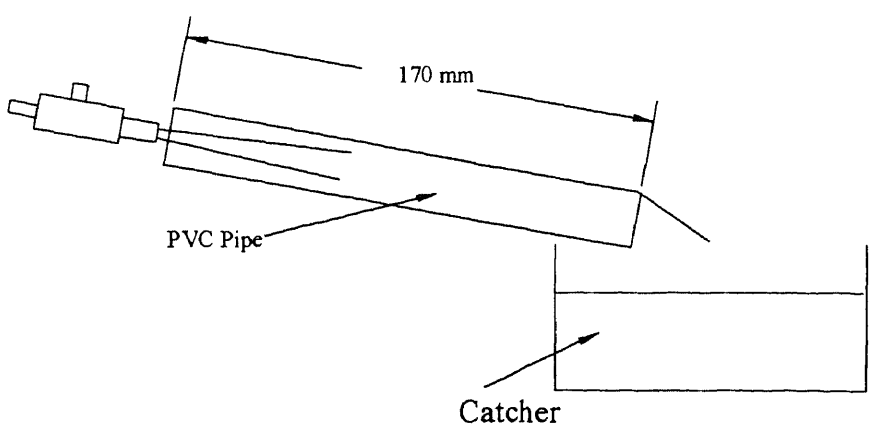

Figure 4.15 Schematic of the Air Catcher

4.5 Velocity Measurement

4.5.1 Measuring System

The measuring system used in this study was developed by Dantec Electronic Co. Here 15 mV He-Ne laser is used as the light source. As shown in Figure 16, the system consists of an optical head and a data processing system. The Data processing System of the LTA measurement has three major functional components: 1) Counter Processor, 2) Oscilloscope and 3) Computer. The Counter Processor receives the voltage signals from the photomultiplier in the optical head and conveys these signals, in analog form to the oscilloscope and in digital form to the computer. The function of the computer is to determine the time period between two successive signals which are fed from counter processor, and hence, calculate the velocity.

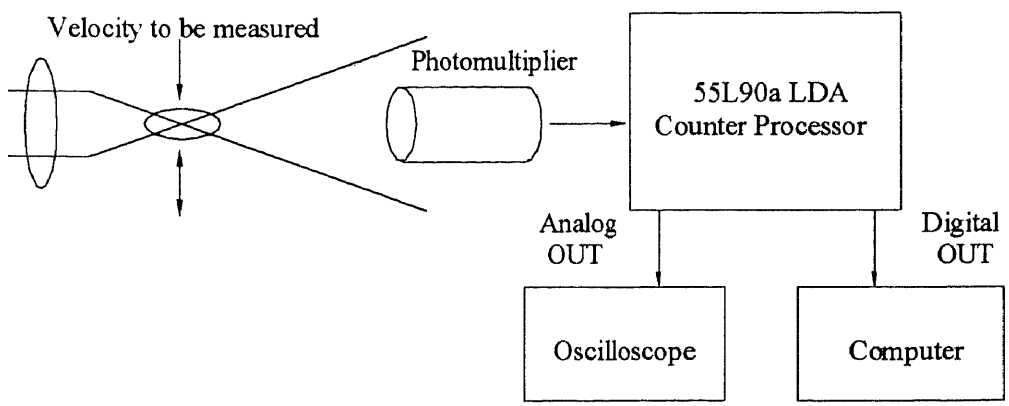

Figure 4.16 Schematic of Measurement System

The setup of the optical head is illustrated in Figure 4.17. The beam splitter BS1 receives the source light and creates two beams. The beam plane formed by these beams can be rotated by two polarizers P1 and P2 to ensure its coincidence with the direction of

the flight of particle. The two beams are focused by the lens system to form the measuring volume and the image of two focal points is received by the same lens system and transmitted via the mirrors M1 and M2 to the beam splitter BS2. The scattered light, generated by a particle passing through the measuring volume is detected and converted to the voltage signals by the photomultiplier PM. Thus, the signals are transmitted to the data processing system to determine the particle velocity by measuring the time period between the signals.

4.5.2 Operating Principle

Laser Transit Anemometer(LTA) is an optical instrument for nonintrusive measurements, which produces no interference with the flow. It has a unique lens system that splits a single incoming laser beam into two equal intensity beams and focuses the beam to a small region. Thus, a particle passing through the focal point of either of these split beams generates a scattering light of high intensity. The design of LTA is such that it ensures the signals that are generated are due to only those particles passing through the focal points. With a knowledge of the distance between the two foci and the time taken for a particle to travel through these two focal points, it is possible for us to calculate the velocity of the particle.

Time period t between two successive logical signals is then determined by the computer and the velocity is computed using the equation

$$V=d/t \tag{4.5}$$

where d is distance between the two focal points.

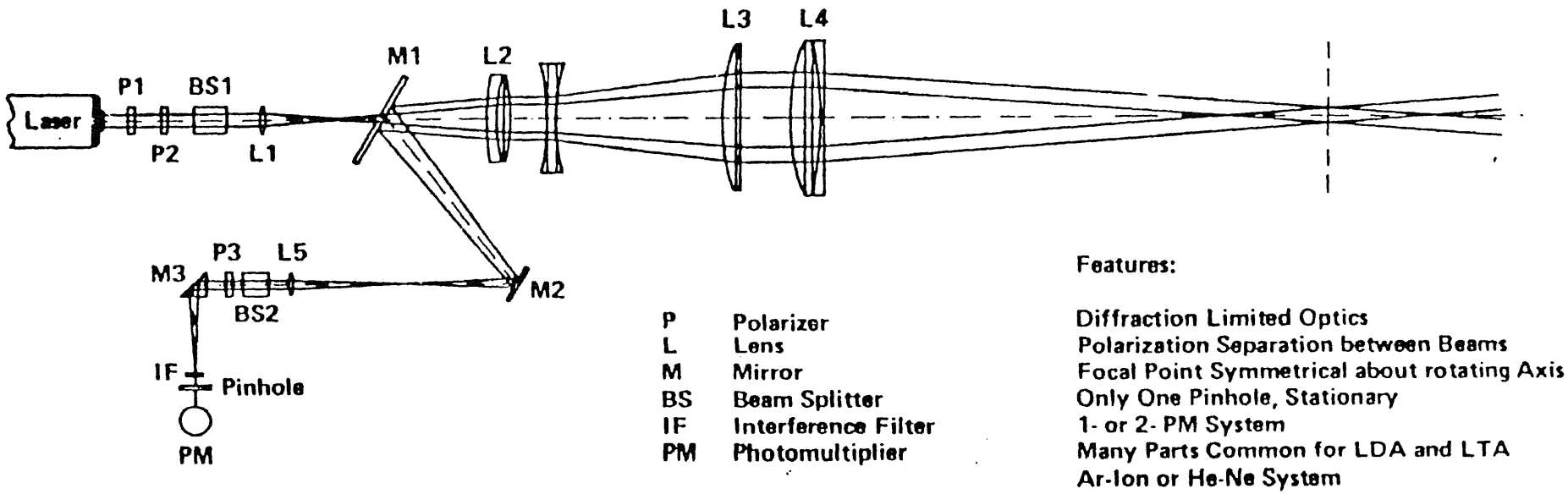

Figure 4.17 Schematic of LTA Operation

4.5.3 Jet Velocity Measurement

The velocity measurement by the use of LTA is based on the measuring the time of flight of the particle. However, as reported by Schodl (1982), the velocity of a pure waterjet can be measured by LTA based on the flight of submicron particles which are normally contained in a real fluid. The velocities of such particles are strongly correlated with the water velocity (Yanta, et al, 1971). The size difference between the added particles and particles contained in the water determines the difference in the intensity of the light, scattered by both kinds of particles. This enables us to differentiate between the signals obtained from added particles and those obtained from contained particles. In measuring the velocities of added particles, the signals generated by submicron particles become noise signals by the selection of an appropriate amplifier gain. Thus, the time intervals measured between such noise signals are ignored by the data counter system.

The velocity of the sapphire waterjet formed by the highly pressurized water passing through the sapphire nozzle was measured. Then, the velocity of carbide waterjet formed by sapphire waterjet passing through the carbide tube was also monitored. Finally, the velocities of particles entrained in the corresponding AWJ were thereafter measured. Abrasive velocity distribution along and across the jet was measured for a combination of sapphire-carbide nozzle (d_N= 0.3556 mm and d_m=2.36 mm) with an abrasive particle size of 220 mesh and an abrasive mass flow rate of 68 g/min. at various standoff distance.

4.6 Force Measurement

The objective of this study is to provide information about the jet action while impinging on the workpiece surface and to determine the process variables effecting this action. It will also enable us to develop a experimental procedure for the evaluation of some basic characteristics of the AWJ polishing technology.

The sketch of the transducers setup is shown in Figure 4.18. Two identical three-components force measurement platforms were used in the study. Each multi-components transducer is assembled by stacked quartz disks loaded mechanically in a series with electrode interlayers. The force to be measured acts on the workpiece so each quartz disk will generate a certain amount of charge. A stainless steel plate, 356 x 102 x 19 mm, is shown in Figure 4.19, The plate has for 20 holes each of diameter 0.953 mm. This plate is attached to the insulation wood and transducers by means of screws. The bottom surface of the workpiece is fine machined to prevent possible vibration of the workpiece and for insulationtion of the wood.

In our study, two Kistler three-components force measurement platforms 9257A were used. The signal was amplified by a charge amplifier which was used as a classic electrometer to enable charge alteration on quartz transducers to be measured. Each component of the charge amplifier has its own sensitivity switch and measuring range scale switch according to each measuring axis. In this study, Kistler three component charge amplifier Model 5007 was used. A Nicolct 2 channel oscilloscope was used to record the signal from the charge amplifier The oscilloscope was connected with a 486 PC

through RS232 port for measuring procedure control automatically. The schematic of experimental setup is shown in Figure 4.20.

In the experiment, measurements of the force exerted on the workpiece in normal and tangential direction were carried out during both abrasive and non-abrasive waterjet polishing of stainless steel samples, under different impinging angles, water pressure and standoff distance.

4.7 SEM and Microhardness Study on Surface Polished

4.7.1 SEM Analysis

Scanning electron microscopy (SEM) is a necessary tool for studying the surface topography of machined components because it can show the detailed characteristics of the surface produced by machining, including cracks, tears and tool marks.

The electron microscope provides a narrow beam of electrons that can be focused on a sample for the purpose of image formation or elemental analysis. The beam may be moved or scanned across the sample surface, or fixed at one point. The formation of an image depends on the detection of a signal that varies with the topography or composition of the sample. Scanning electron microscopy detects the emissions from the upper surface of the particle or target sample. The electron beam is scanned in the x and y direction across the sample and the detected signal is processed and displayed on a CRT screen, resulting in an image that appears to be three-dimensional. The ability to focus an electron beam to a very small dimension (0.1 μm in diameter), as well as scanning the beam over the sample surface to pinpoint the beam at some portion of the sample surface, allows for

microanalysis of a single particle by examining the emissions from the particle that are induced by the electron beam.

For this investigation, SEM examination were carried out for characterizing the surface structure at the Material Research Center in NJIT, using a JEOL JSM 840A microscope. The optimal magnifications were selected for each individual process. The same magnification was used for comparison of surface characteristics. An accelerating voltage of 10 KV used for the photographs. The samples were situated in the position identical to that used during polishing as discribed in Art 4.72. The examination is focused on surface topography and integrity of stainless steel samples polished at various impact angle and particle size.

4.7.2 Superficial Hardness and Microhardness Test

To evaluate the variation of surface and subsurface integrity due to the machining, through-thickness microhardness of cross-sections of the polishing samples were measured using a LECO M-400 microhardness tester with Vickers diamond pyramid indentor loaded at 500g, and surface hardness test was carried on the polishing surface using Wilson/Rockwell hardness tester 500 with 120^0 sphero-conical diamond indentor. The polishing samples were sectioned in the longitudinal and transverse directions as shown in Figure 4.21 to examine the micronhardness and to provide specimens of appropriate size (2 cm x 2 cm) for scanning electron microscopy of the polishing surface.

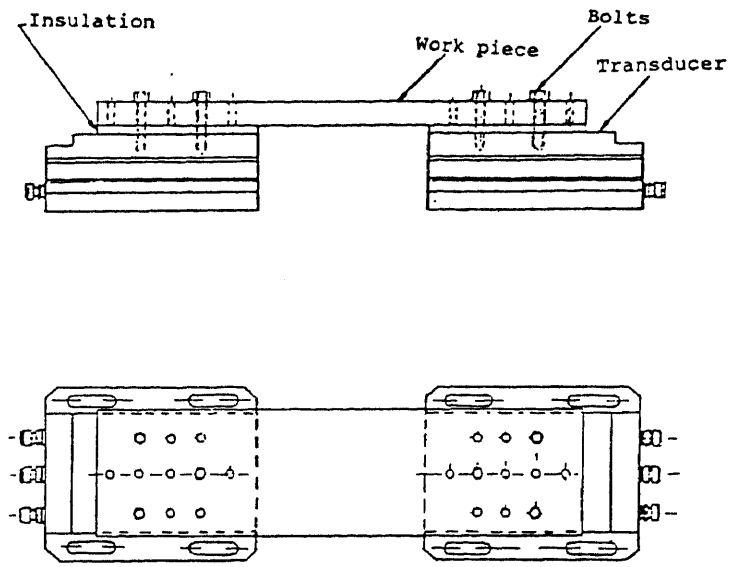

Figure 4.18 Schematic of Piezoelectric Force Transducer

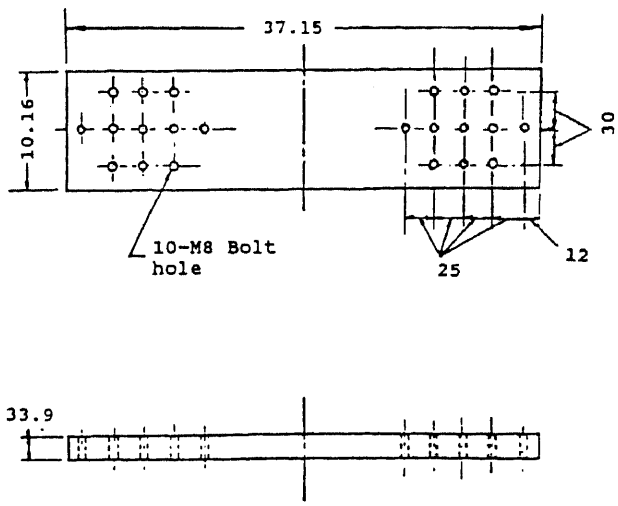

Figure 4.19 Schematic of the Sample for Force Measurement

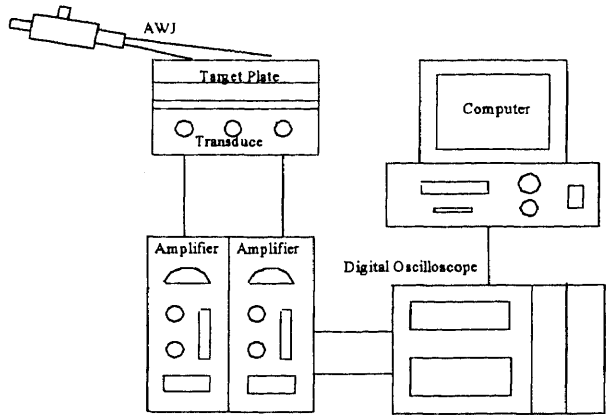

Figure 4.20 Experimental Setup of the Force Measurement

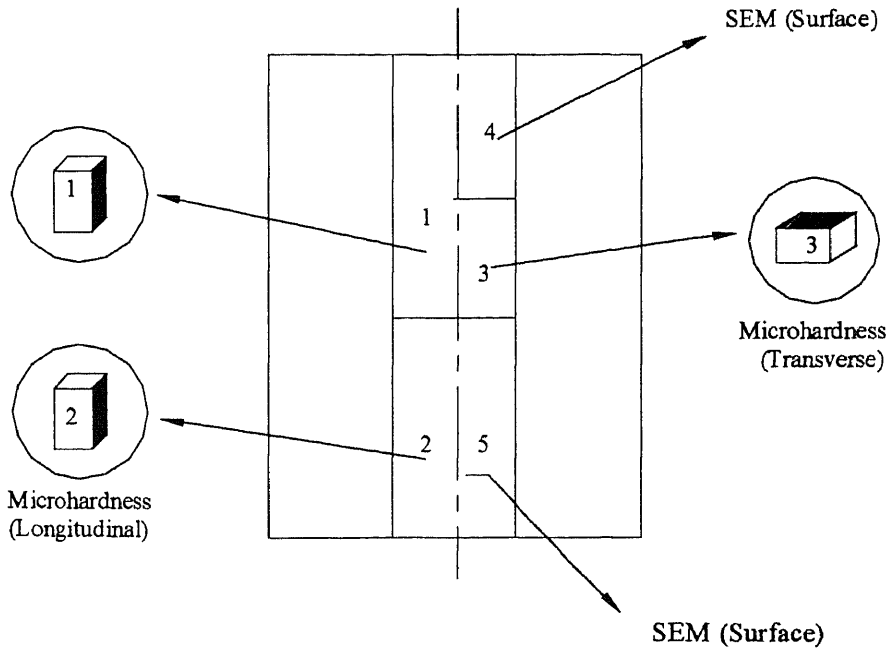

Figure 4.21 Method of Sectioning Stainless Steel Samples

CHAPTER 5

EXPERIMENTAL RESULTS AND DISCUSSIONS

Fundamentally, material machining operations can be divided into primary operations (turning and milling) and finishing operations (grinding, lapping and polishing). Obviously, the surface finish is one of the primary factors determining component quality. In this study the feasibility of polishing difficult-to-machine materials such as ceramics and stainless steel using a relatively new non-traditional process called AWJ machining has been demonstrated. Surface roughness of $R_a = 0.3$ micron can be achieved from a previous roughness of 2~12 micron R_a by AWJ at a near-zero angle of impact, while no surface defects are induced. Figure 5.1 shows samples polished by AWJ. Note the mirror-like behavior of the generated surface (Figure 5.1 d).

5.1 AWJ Based Polishing

The main purpose of this experiment was to explore the possibility of using AWJ for polishing and to examine effect of process parameters, such as abrasive particle size, AWJ impact angle, abrasive mass flow rate, water pressure and etc. on the process results. Improvement of the surface roughness was used as a criterion determining process feasibility as well as the effect of various factors on AWJ performance. Initially, the feasibility to use WJ to improve surface topography was investigated. Several setups were used to examine the effect of the impinging water stream on the substrate surface. No substantial improvement was found. These experiments should continue, however, this

study was limited to the examination of the effect of slurry flow on the substrate geometry.

5.1.1 Effect of Abrasive Particle Size

Figure 5.2 shows that as the size of abrasive particle size is reduced from 50 mesh (295 micron) to 500 mesh (23 micron), the surface roughness (R_a) of Alumina ceramic substrates decreases from 2 μm to 0.3 μm in the course of AWJ polishing proceses. The same trend is also held for other materials investigated.

As seen from Figure 5.2, the results of polishing are heavily effected by the particles size and the material hardness. The reduction of particles size brings about a consistent and significant decrease of the surface roughens. Individual abrasive particle strikes the target and removes small chips from the surface of the target material. Such particles behavior is quite predictable. Smaller impacting abrasive grits, that is smaller cutting edges, generate thinner microchips. Thus, a smoother surface is obtained. The incentive to use a finer abrasive lies in the feasibility to generate a better surface. According to the Finnie investigation (1977), the depth of penetration of an impacting particle into a material is by the magnitude of one order less than the particle size. Thus, the diameter of a crater generated by an impinging particle does not exceed the 1/10 of the particles diameter. We can expect that the same correlation is correct for scratch grooves generated at the material surface by particles impinging at a low impact angle. Although, the ratio between the particle diameter and the groove width and depth, was not investigated, it is reasonable to assume that the groove width is a function the particle

diameter. In general, it is quite obvious that larger particles create heavier surface deformation, and thus, less perfect surface topography. This result is supported by SEM observation (Figure 5.3). Most important, analysis of the surface topography shows the consistent trend of reduction in the surface roughness with the decrease of particles size (Figure 5.4).

It is important to notice that while decrease of the integral topography characteristics (R_m and R_z) fades as the particles size is reduced (Figure 5.5), the reduction of the number of surface peaks (Figure 5.6) grows as the size of particles drops. These phenomena are due to the effect of the peak height on the correlation between impact conditions and surface erosion. The larger peaks are, the more susceptible to impacts and, thus degenerates faster as the number of impacts grows. Another, reason is the kinematics of particles motion along the material surface. The probability of collision between the particle and surface unevenness and thus the change of the particle trajectory is much higher in the case of larger particles. Small particles more probably will attack and destroy larger peaks than small surface unevenness.

It should be noted that a nominal particle size is just a median value. Actual particle dimension (Figure 5.7) varies around the values. Thus, the difference in surface roughness with a comparatively small difference in particles size is not substantial.

5.1.2 Effect of AWJ Impinging Angles

The effect of the impingement angle α on the surface roughness with an abrasive particle size of 220 mesh and an abrasive mass flow rate of 68 g/min. is depicted in Figure 5.8. It is shown that the impinging angle has a profound effect on the quality of a surface generated by AWJ. Note the significant growth in surface roughness at the increase of impact angle determines the sense and feasibility of AWJ polishing. However, the increase of this angle above about 20 degrees does not practically effects R_a of the generated surfaces. Existence of such "a saturation point" was observed for all tested materials.

The groove geometry is strongly affected by the impact angle. At a small angle, the depth of the groove is smaller, but it is longer than those at a large impact angle. Because of this, the reduction of the angle is a necessary condition for effective polishing. As it follows from Figure 5.8, the low roughness of about 0.5 micron for 220 mesh grit can be attained at a small (0-3 degrees) impact angle and the roughness is mostly affected by the strike angle at the angle level of 0-20 degrees. At a higher angle of attack the depth of particles penetration, and thus, surface roughness is less dependent on the impact direction (Figure 5.8). The length of the contact area during the particle impact increases as the impact angle decreases. It becomes maximal when the particle trajectory is parallel to the substrate surface. Thus, the amount of peaks stroked by a particle increases as the length of its trajectory along the surface increases. Therefore, the peaks density is reduced when the value of α decreases (Figure 5.9). The strong correlation between R_a and the impact angle at the range of the angle value of 0 to 20 degrees suggests that α is one of critical parameters in the AWJ polishing technology, while there may be a change in the

mechanism of the interaction between particles and the material at about 20 degrees (the saturation point) .

Thus the increase in the angle of attack changes the character of the interaction between the jet and the polished material and strongly effect the topography of the generated surface. The objective of polishing is the removal of peaks, while the bulk is unchanged. This condition is best met when the angle between particle trajectory and the substrate surface is minimal. Our results (Figure 5.8-5.9) demonstrate that effective polishing is feasible only at a small (0-3 degree) angle of attack.

5.13 Effect of Abrasive Mass Flow Rate

The effect of the change in the abrasive flow rate from 0 to 180 g/min during the course of polishing at a near-zero angle on generated surface roughness is shown in Figure 5.10 for stainless steel. It was found that the optimum abrasive mass flow rate is 68 g/min. With the increase of abrasive mass flow rate, the roughness decreases rapidly, though not linearly, and then reaches a plateau at the flow rate of about 68 gm/min. Figures 5.11 and 5.12 show the abrasive flow rate has a similar effect on R_z, R_m and N_r. The optimal flow rate, of course, depends on the kinds of particles and the material.

The primary energy carrier in the course of AWJ machining is the waterjet. In the mixing chamber and the mixing tube, this energy is partially transferred to the abrasive particles. The velocity of the AWJ can be estimated by a simple momentum balance:

$$U_a = \eta\left(\frac{U_w m_w}{m_w + m_a}\right) \tag{5.1}$$

$$\frac{U_a}{U_w} = \frac{\eta}{1+R} \tag{5.2}$$

and

$$R = \frac{m_a}{m_w} \tag{5.3}$$

where U_w is the waterjet velocity, U_a is the velocity of the slurry stream, m_a is the abrasive mass flow rate, m_w is the water mass flow rate, and η is the momentum transfer efficiency. Equations above illustrate the correlation between the abrasive flow rate and material removal. An increase in the number of abrasive particles increases the number of impacts and, thus accelerates material machining. At the same time, increase of the particles number reduces the slurry velocity and has adverse effect on the machining rate. Therefore, there is an extremal value of the mass flow rate which assures maximum rate of machining. Effect of abrasive flow rate on the polishing results is also determined by the peculiarities of the peaks destruction and grooves formation. Each impacting particle destroys existing peaks, but generates new grooves. The polishing occurs when the peaks destruction has greater effect on the surface topography than grooves formation. The rate of peaks destruction increases as the number of impacts (particles flow rate) increases (Figure 5.10 and 5.12). However, increases in the particles flow rate also promote groove formation; and at a certain value of flow rate, the effects of both phenomena become practically equal. With this in mind, we now examine the influence of the abrasive flow rate on surface roughness for various process conditions.

The maximum abrasive flow rate that can be handled by an AWJ nozzle is limited by two factors: the entrainment capability of the waterjet and the inner diameter of the

mixing tube. At the water pressure of 76 MPa and the mixing tube diameter of 2.36 mm the maximum abrasive flow rate was about 180 g/min. (Figure 10).

Note that the entrainment capability refers to the ability of the waterjet to draw abrasive into the waterjet body. For a given length and diameter of the focusing tube and the geometry of the mixing chamber, the entrainment capability is a function of the waterjet velocity (pressure) and flow rate (orifice diameter). At a higher waterjet pressure the abrasive flow rate increases, and the waterjet entrains more abrasive until the mixing tube ultimately gets choked. With a larger mixing tube it is possible to entrain a higher abrasive flow. However, beyond a certain optimal value the benefit of carrying larger abrasive flow rate declines, as it is evident from Figure 5.10. Determining the optimum abrasive to water mass flow rate ratio to maximize productivity of polishing is an important topic for further research.

5.1.4 Effect of AWJ Traverse Speed

Figure 5.13 shows the effect of the traverse speed on AWJ polishing at the impact angle of 3 degrees, the average particles size of 100 μm, flow rate 68 g/mm and the water pressure of 76 MPa. From this figure, it follows that there is a critical value of the traverse speed, which is equal to 2 m/min. for the condition of the experiment in question. At the traverse speed below the critical value surface roughness does not depend on the traverse speed. At larger traverse speed the surface roughness is proportional to the speed.

The traverse speed is inversely proportional to the residence time and thus it is inversely proportional to the number of particles impinging a unit of the substrate surface.

Each impinging particle destroys existing peaks. At lower speeds, more particles strike peaks with shallow angle, thus wear out more peaks and repolishing and smoothing already generated surface. The traverse speed determines the time of surface exposure to the impinging jet and, thus, a number of particles impinging material surface. The effect of traverse rate is similar to that of particles flow rate (Figure 5.10). At a small traverse rate, similarly to large flow rate, the final roughness is minimal. The roughness increases if the rate of the jet motion increases (Figure 5.13). At a small traverse speed, as it is at a high flow rate, the value of the speed does not effect the roughness. At our conditions the optimal traverse speed is 2 m/min. where further decrease of speed reduces productivity, further increase negatively effects surface topography. However, the minimal size of peaks which can be destroyed depends on the size of impinging particles. When all peaks which can be removed by the given particles are destroyed, further increase in the number of particles does not effect the surface topography. Thus, the minimum attainable surface roughness depends on particles size. If a number of impinging particles are less than the critical number, a part of peaks which can be destroyed by the impacting abrasive will survive and the surface roughness will be larger than the minimum attainable level. Thus, for a given process condition, there is minimal attainable surface roughness which depends on the particle size. The maximum (critical) traverse speed at which this roughness is attended constitute the critical value of the speed. Below the critical value, the change in the traverse speed does not effect the surface topography. (Figure 5.13). Above the critical value, the surface roughness increases almost proportionally to traverse speed.

The traverse rate may also effect the cutting mechanism (Hashish, 1981). That is, cutting wear may occur more often at low traverse rates and deformation wear at high traverse rates.

5.1.5 Effect of Waterjet Pressure

Figure 5.14 shows the relationship between the water pressure and the roughness of the stainless steel surface generated by AWJ polishing of 220 mesh garnet at the near-zero angle of impact. In the process, abrasive mass flow rate and traverse speed are held constant at quasioptimal value for all pressures investigated. The results indicate that a better surface polishing is obtained when a lower water pressure is used.

Because the water pressure influences the waterjet machining in numerous ways, it is considered to be one of the principal variable of AWJ polishing. The effect of water pressure on jet spreading, abrasive particle fragmentation, nozzle suction capability, wear of nozzle components, mixing efficiency, etc., has been documented by Hashish (1989). However, most important is the effect of water pressure on the waterjet velocity determined by the equation:

$$U_w = \sqrt{\frac{2P}{\rho}} \tag{5.4}$$

Here the compressibility effects are not included. Though the experimentally measured waterjet velocity agrees reasonably well with that determined by the above equation, the AWJ velocity (U_a) also depends on abrasive loading ratio ($R = m_a/m_w$), mixing efficiency, and length and diameter of the mixing tube. However, under "normal" operating

conditions a perturbation of U_w results in a corresponding change of U_a at least in the neighborhood of the operating point.

5.1.6 Effect of Standoff Distance

The relation between standoff distance and surface roughness is displayed in Figure 5.15. From this figure, it follows that there is an extremal value of standoff distance relating a best improvement of surface for all tested materials, and the correlation between R_a and the standoff distance is practically linear beyond the region of the extremity.

As the distance between mixing tubee exit and workpiece increases, the jet becomes wider and more diffuse due to jet diversion. The density of energy transmitted to the target material thereby decreases, resulting in less sufficient force for peaks destruction. At the same time the reduction of standoff distance increase the force developed in the impact site. Particle impact results in the destruction of existing peaks and creation of new grooves. The impact force must be sufficient for peaks destruction but not sufficient for grooves formation. If the impact force exceeds the critical value, when a particle is able to penetrate in the body of substrate, particles impact will increase rather than decrease surface roughness. Thus there is the extremal value of the standoff distance when the minimal roughness is attained. If the standoff distance exceeds this value, the roughness increases due to the reduction of density of the strikes. If the standoff distance is below the extremal value, the roughness increases due to intensive deformation of the substrate body.

5.1.7 Effect of Target Materials

Figure 5.16 and Figure 5.17 shows the effect of material hardness on the polishing result for different sizes of grit and impact angle. Obviously R_a decreases with an increase of material hardness in all cases. Figures 5.2, 5.8 and 5.13 show the data trend obtained for different types of materials and alloys (Table 4.1). As follows from these figures, polishing of a soft material results in a larger roughness than that of harder material under the same conditions. For example, R_a of the polished surface of aluminum alloy is much rougher than that of stainless steel (Figure 5.13). At a low traverse speed, the material hardness positively effects the final texture, because the groove depth for these materials is smaller. However, at a higher traverse speed the roughness of soft materials is smaller because the reduction in the impact numbers effects hard materials more strongly. Since a given material may be very sensitive to one form of wear and relatively insensitive to the other, the value of a transition traverse rate is material-dependent. This implies that the roughness versus traverse-rate curve is of a complex nature.

The before mentioned figures demonstrate that under various parameters of polishing the roughness of a harder material will always be less than that of a relatively soft material. The Alumina ceramic in these figures appears to be the most resistant to erosion, while aluminum alloy is the least resistive. These results obviously follow from the ability of impinging particles to form larger grooves at the surface of a softer material. The conclusion above takes place at various particle sizes (Figure 5.2) as well as at various angles of attack (Figure 5.8).

Substrate hardness is conventionally considered as a primary factor determining material erosion. A linear correlation exists between the reciprocal material hardness and the erosion rate (Finnie et al., 1967). Sheldon and Kanhere (1972) indicated that the hardness of the material determines erosion resistance at shallow angles of impact.

5.1.8 Effect of Number of Passes

It is expected that the increase in a number of passes improves the surface texture as shown in Figure 5.18, while all other variables are held at optimal value. It is equally obvious that this increase adversely effects productivity. It is important, therefore, to identify a practical value for this parameter. As it follows from Figure 5.18 in most cases only one pass is needed. If however, roughness reduction is the primary concern, the number of passes should be four.

5.1.9 Effect of Focusing Tube Diameter

Figure 5.19 shows the correlation between the surface roughness (R_a) and the focusing tube diameter. Increase of the mixing tube diameter reduces the stream power density. This results in improved polishing performance. Thus, a smaller value of R_a occurs at a larger diameter.

5.1.10 Effect of Initial Surface Condition

Three levels of the roughness in samples prior to polishing were identified.(Table 4.4). and the effect of this roughness on the results of polishing was evaluated. The initial surface

roughness determines the amount of material to be removed in the course of polishing, and the size of peaks to be destroyed. It is obviously that the larger are peaks prior to treatment; the higher is the final roughness. Figure 5.20 shows that the roughness in the polished surface of stainless steel varies linearly with the initial value of the surface R_a.

The effect of various process variables on the topography of the surfaces generated during AWJ polishing was evaluated. It is shown that the jet impact angle and particles dimension are two critical parameters controlling the process. The former determines the feasibility of AWJ polishing and the later controls the extent of improvement in the surface topography.

5.2 Momentum in the Course of AWJ-Workpiece Interaction

Information about the magnitude and change of the momentum developed during the course of the jet-workpiece interaction enables us to understand the mechanism of AWJ polishing and to optimize the control variables.

The abrasive waterjet action force can be decomposed into two parallel components:

$$F=F_t + F_N \tag{5.5}$$

where F_t is the tangential force including F_f friction force and F_c cutting force, F_N is the normal force. The friction force depends mostly on the flow characteristics and the surface roughness. The cutting force F_c presents shear stress acting on the material surface and varies with the impinging angle and flow velocity.

In this study the correlation between the normal and tangential forces and AWJ impact angle, abrasive particle size, water pressure, abrasive flow rate and standoff distance was examined. With four of these variables fixed, the relationship between force and a changing one was examined.

Figure 5.21 shows that the tangential force decreases and normal force increases with an increasing in the impact angle. Comparing this result with the correlation between R_a and α (Figure 5.8) suggests that increase of the tangential force and the reduction in the normal force improve the surface topography. Thus development of a waterjet-based polishing technology should include analysis of the values of both force components. Figure 5.21 shows that at an impact angle below 15 degrees the slope of change in both components are steep, while at the impact angle exceeding 20 degree the effect of α on both components is insignificant. This explains the peculiarities of the correlation between the impact angle and the surface roughness.

The relationship between the impact force and abrasive particle size was investigated because of the dominant effect of particle size on final surface roughness. Figure 5.22, however, shows that there is no correlation between particle size and tangential and normal force components developed on the surface being polished.

The effect of an abrasive flow rate on the tangential force was studied at a low impact angle. The result is shown in Figure 5.23. Tangential force increases with the increasing abrasive mass flow rate and arrives to a platform at the flow rate of approximately 70 g/min. Note that this trend is similar to that in Figure 5.12 where a platform is also formed for R_a after about 70g/min. This suggests that surface

improvement by the increase of an abrasive mass flow rate results from the shear action of tangential force, developed by the impacting particles at the substrate surface.

Figure 5.24 shows the changes in two components of force with the water pressure for variation at the impact angle of 3 degrees. It is obvious that both components of the force developed on the surface increase when the pressure increases. The rate of increase of the normal force is higher than that of the tangential force although the former locates below the latter for the all pressure examined. Comparing polishing results obtained under the same test conditions (Figure 5.14) with that of Figure 5.24 shows that a rapid increase in the normal force increases the surface roughness.

Figure 5.25 shows the relationship between the tangential force and standoff distance for various process variables. The test condition corresponds to those that assure minimal surface roughness. It has been found that the increase in standoff distance results in the significant reduction of the tangential force while the normal force is not effected substantially.

5.3 Particles Disintegration

It was shown previously that the size of impinging particles is the major factor that determines the topography of a generated surface. Our study, as well as all other pertinent research, relates surface texture with size of particles prior to machining. At the same time, acceleration and impact result in the disintegration of particles; and actual particles dimension which in the final analysis determines the surface topography is very much different from the original one. Because of this, it is necessary to evaluate particles

disintegration in the course of polishing in order to evaluate the actual geometry of abrasives which determine the process result. During the acceleration process, abrasive particles are exposed to extremely high stresses during acceleration in the mixing chamber and the mixing tube. The load imposed by the acceleration, waterjet impact during entrainment and the impacts on the side walls of the mixing tube, generally cause fracture and disintegration of the abrasive. Therefore, the abrasive particles impacting the workpiece have a different mean size and size distribution than the abrasives entering the focusing tube. Actually material removal by abrasive particles in of the course polishing is determined by the size of particles exiting the focusing tube rather than that of entering particles entering the tube. Further particles disintegration occurs upon impacting the specimen. The particle-target fracture effects the secondary erosion which occurs when rebound particles are re-entrained by the impinging jet.

Figure 5.26 shows that in the course of AWJ polishing particles disintegration occurs in the mixing tube and on the workpiece surface for all examined processes. It was found that the larger abrasive particles underwent much more intensive breakage in the mixing tube and at the workpiece surface, and there was almost no particle disintegrating for fine abrasive. SEM examination (Figure 5.27) shows that heavier mixing occurs for big size particles (Figure 5.27 a) and uniform particles in size were collected for smaller abrasives (Figure 5.27 d). The reason of this phenomena may be a higher probability of cracks and defects in larger abrasive particle comparatively to finer ones. These figures also show that main particles fragmentation occurs during the acceleration in the mixing tube.

The abrasive particles were collected and analyzed after impacting the workpiece surface at a variety of impact angles for abrasive of 220 mesh. The particles dimension distribution (Figure 5.28) determined by the use of Laser Scanning Sizer shows that the average particle size after impacting reduces linearly with increases of the impact angle. SEM observation also demonstrates particles fragmentation (Figure 5.29).

Figure 5.30 shows the effect of material hardness on abrasive particle disintegration for five materials treated by 220 mesh garnet at the 3 degree impact angle. It is observed that the average particle size reduces with an increase in the material hardness. This may indicate that less plastic deformation occurs on the surface of a hard material in the course of particles impact than at the surface of a softer material.

A recent study of abrasive particle fragmentation (Simpson, 1990) indicates that the percentage of silica sand, reduced in size during passage through the AWJ nozzle, increases as the pressure grows, and the total percentage of the abrasive which breaks down is greater for the larger size particles. As mentioned above, the reason for the latter phenomenon is a higher probability of cracks and defects in larger abrasive particles compared with that of finer ones. The study also identified that abrasive particles impact at the mixing tube wall results in a catastrophic disintegration while the effect of the waterjet impact is much less substantial. Hashish (1989) observed that increase of the waterjet pressure above 207 MPa does not result in further significant particle fragmentation.

Ansari (1995) gave a possible explanation for dependence of volume removal rate on particle size. The drag force responsible for accelerating the abrasive particles varies with the square of the particle diameter, whereas the buoyancy force that tends to lift the

particle is related to the cube of the particle diameter. Thus, the buoyancy force changes at a faster pace than the corresponding drag force. Furthermore, smaller particles are more susceptible to change their trajectory and follow the waterjet than the larger size particles. This also explains the higher stability of the smaller particles in the course of polishing.

5.4 Micrographic Study of the Polished Surface and Abrasive Particle

5.4.1 Morphology Examination of Polished Surfaces by SEM

To evaluate the effects of various factors on the topography of a polished surface and to understand the material removal mechanism in the course of polishing, SEM surface examinations was carried out on Aluminum, carbon steel, titanium alloy, stainless steel, glass and ceramic samples. This allowed identification of the surface characteristics and visualization of the effect of AWJ process on the impact damage pattern.

It is known that a particle can interact with the target in three different ways: (1) it can chip the material if the particle penetrates deep enough in the material; (2) it can perform plastic cutting, producing spiral chips if a sharp cutting edge and a high speed are involved; (3) it can force the material into plastic flow if a high localized pressure is applied.

Figure 5.31 shows the topography of surfaces of different materials impacted by AWJ at near-zero angle. The impact pressure is much lower than that of AWJ cutting. Scratching marks are visible on all machined surface and the evidence of plastic flow is clearly noticeable, even for brittle materials such as glass and ceramic (Figs. 5.31 e and f).

The effect of the impact angle on the surface topography is shown in Figures 5.32. In the case of 90^0 impingement (Figure 5.32 e), the eroded surface is subjected to a large number of normally impinging particles. Therefore, one can observe the eroded surface dominated by numerous pits or craters. The deformation involves mode 3 (plastic flow), mode 1 (digging) or 2 (chipping) or a combination of above. In the course of impact particles penetrates into the substrate, deform and chip the material. It is observed that the most of surfaces generated at large impingement angles are imbedded with fragmented abrasive particles.

The ratio between the different modes of deformation, and subsequently the embedding depth, varies with the impact angle as shown in Figure 5.33 (a) (90 degree), 5.33 (b) (70 degrees) and 5.33 (c) (30 degree). With the reduction of the impact angle below 30 degree the crater decreases and groove or scratch mark increases, while the particle trajectories along the surface become longer. A noticeable difference between the low and normal impingement resides in the traces of the plastic flow which are shorter and fewer under the normal impact. It is difficult to find the crater or any cracks on the surface polished at the angles below 20 degree (Figure 5.32 a and b). Figure 5.34 provides the evidence that only the peaks were cut off by impacting particle at near-zero angle, while the bottom of the valley remains unchanged. (Figure 5.35).

Figure 5.4 shows surface topography generated at near-zero angle impact with different abrasive particle size. Obviously the surface topography improves with the reduction of particles size while the dimension of groove decrease.

Figures 5.36 shows the topography of the surfaces generated by sequential impacts of two jets at the same impact angle (3-5 degree) and the normal axial directions. The change of the flow direction dramatically improves substrate surface. The depth of groove generated in the course of the first stage was substantially reduced during polishing by the jet having the axis normal to the first jet. New grooves generated during the second stage of polishing are much more shallow than those created during the first stage.

5.4.2 Topography of Abrasive Particle

In order to understand the interaction between AWJ and target materials, SEM examination of abrasive particles topography was carried out for garnet mesh 220.

Figure 5.37 shows that the sharp edge of the particle was broken. Figure 5.38 shows cracks generated within the particle and Figure 5.39 shows that a particle was broken into several piece embedded into the stainless steel sample.

SEM observation provides evidence of abrasive particle wearing due to the interaction with material surface. Figure 5.40 shows the wear trace left on the particle surface. Figure 5.41 shows the smooth surface of particle, generated due to the friction between the particle and the surface in the course of motion along the substrate surface. The particles wear mirrors the wear, that is polishing, of the surface, and the study of this wear provides the substantial information about process mechanism. For example, the groove on the particles surface is generated by the peaks penetrated in the particle body and the reduction of the groove width (Figure 5.40) indicates the wear destruction of the peak. The smooth particles surfaces generated in the course of impingement are generated

by an equally smooth substrate surface and, thus, indicate the elimination of unevenness at the substrate surface.

5.4.3 Microhardness Examination

In order to identify the influence of the AWJ polishing process on material surface integrity, microhardness of cross sections of polished materials was measured in longitudinal and transverse directions. Through-thickness microhardness measurements are given in Figure 5.42 for stainless steel samples polished with different garnet size. Comparison of polished and virgin surfaces show that for the investigated samples there is no obvious hardness difference caused by the polishing process. Figure 5.43 shows the results of hardness measurement of four different materials. No hardness change across the section as well as the difference with the sample hardness prior to polishing was observed.

Combined analysis of the generated surfaces using SEM and microhardness tests evidently demonstrated that the polishing procedure induced no visible defects at the sample subsurface while substantial improvement of the surface topography has been achieved. This conclusion corresponds with the available information about non-damage of substrate during waterjet machining (Hashish, 1991).

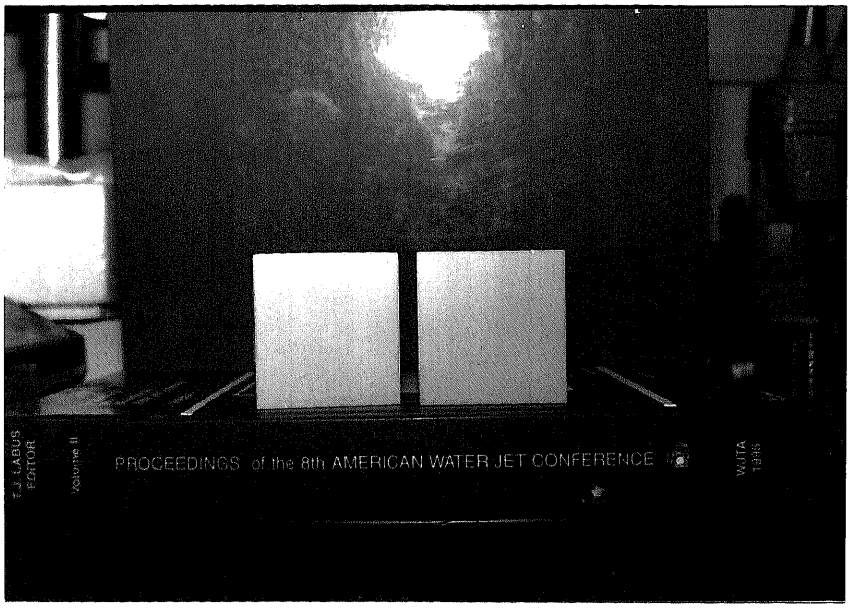

(a) Polished Samples of Ceramic

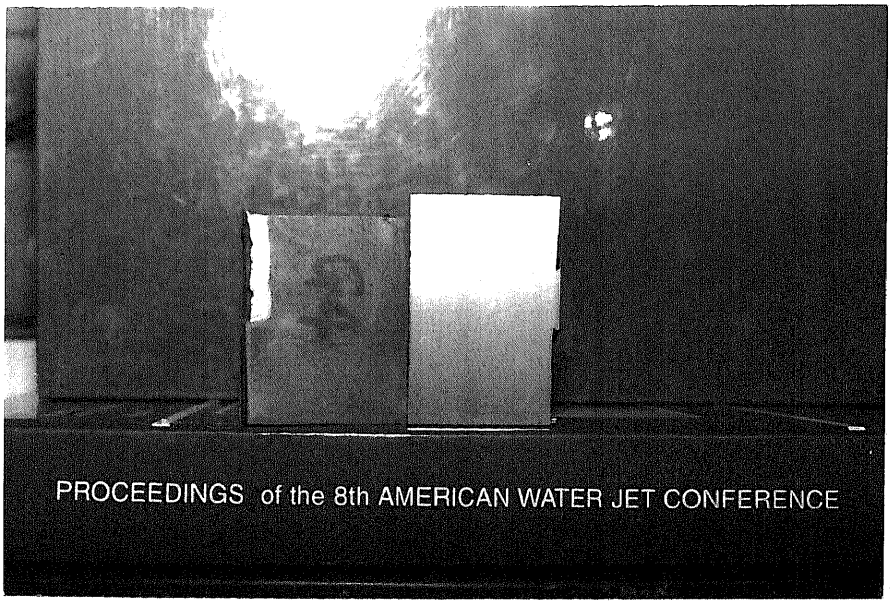

(b)Comparison of Stainless Steel Samples before (left) and after Polished (right)

Figure 5.1 Samples Polished by Abrasive Waterjet

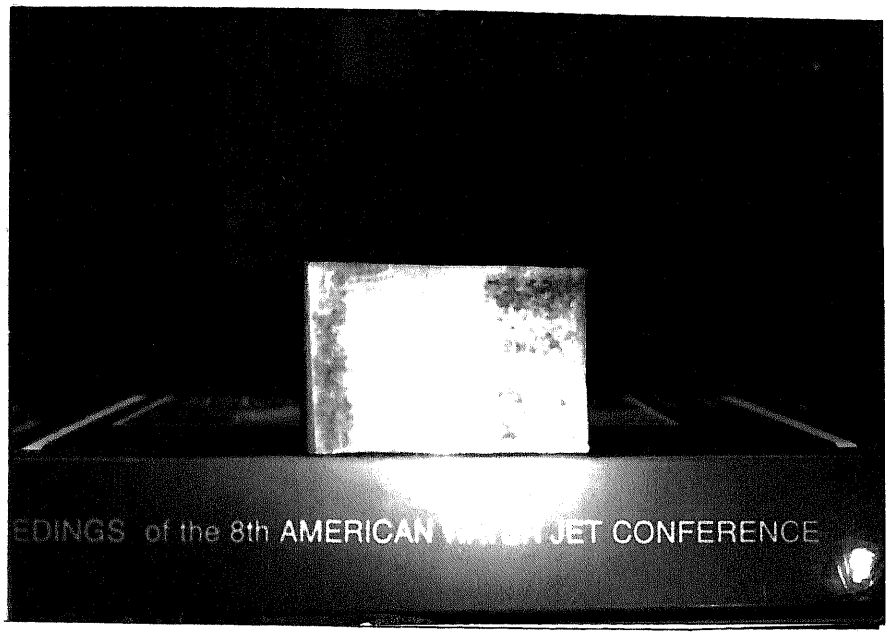

(c) Polished Sample of Titanium Alloy. Note:Polished Zone in the Middle of the Sample

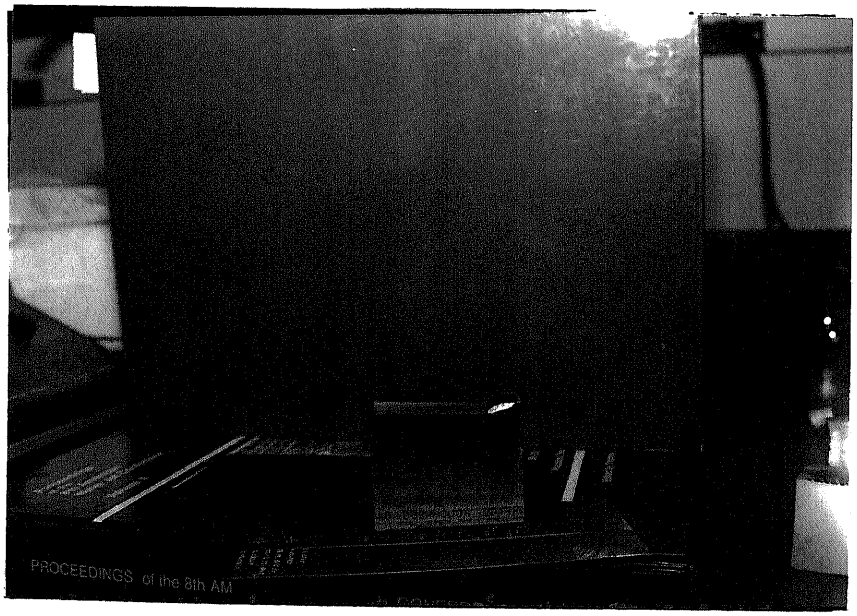

(d) Reflection of Surface Comparator on the Polished Surface

Figure 5.1 (Continued)

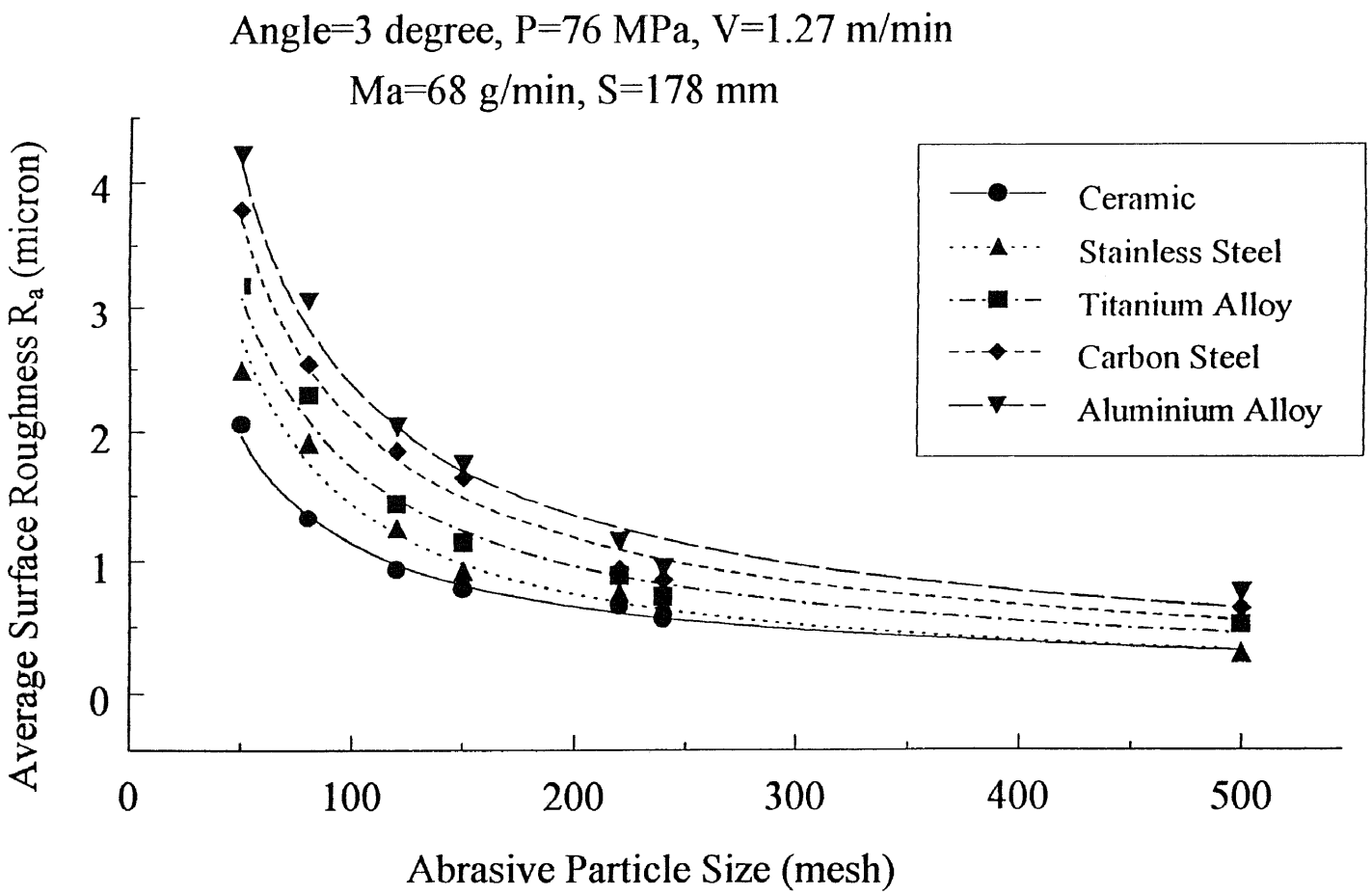

Figure 5.2 Effect of Abrasive Particle Size on Roughness of Surface Polished by AWJ for Various Materials

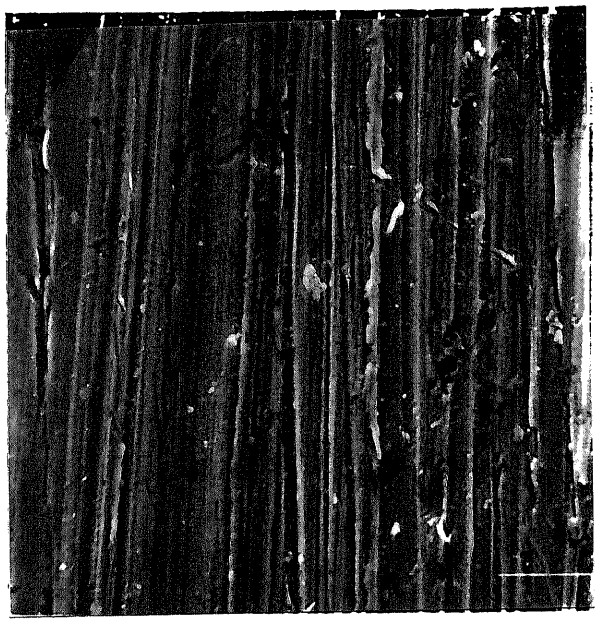

(a) Processed by 240 Mesh (d_p =60.28 micron) Garnet

(b) Processed by 500 Mesh (d_p = 23.79) Garnet

Figure 5.3 Surface Scratch Groove Generated by Abrasive Waterjet. Note: Deeper and Wider Grooves in (a) Compared with that in (b) (x1000)

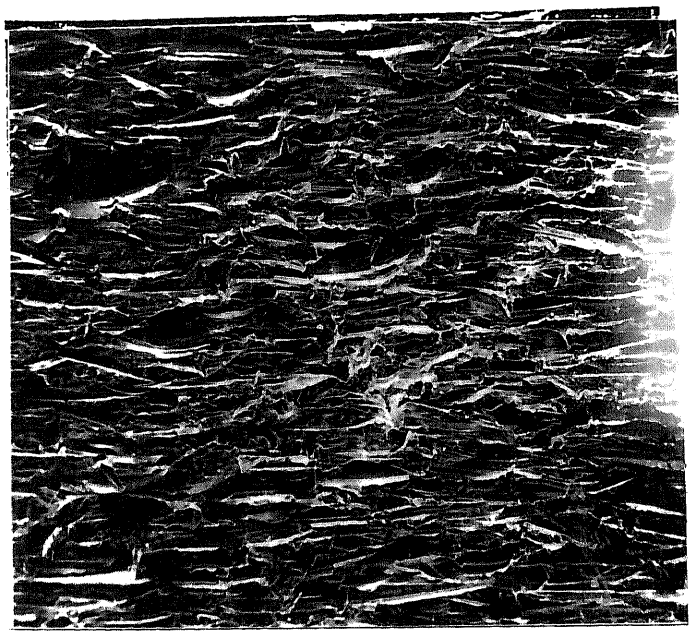

(a) 80 Mesh (311 micron)

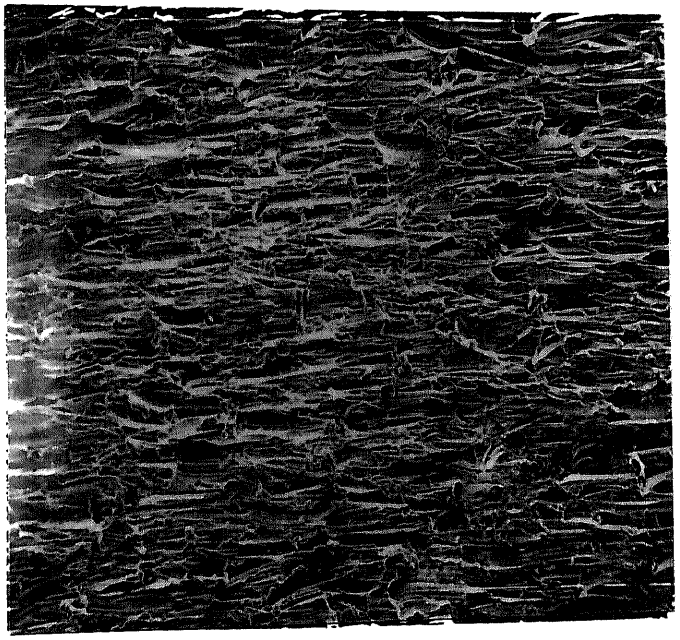

(b) 120 Mesh (188 micron)

Figure 5.4 SEM Images of Surface Topography of Stainless Steel Sample Generated by Various Size of Garnet in Course of AWJ Polishing (x500). Note: The Scratch Grooves Become Thiner and Shallower as Particle Size Decreases.

(c) 150 Mesh (141 micron)

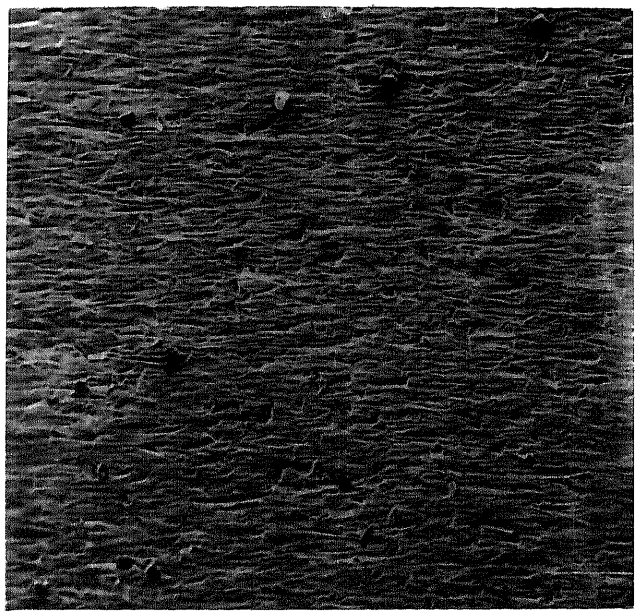

(d) 220 Mesh (100 micron)

Figure 5.4 (Continued)

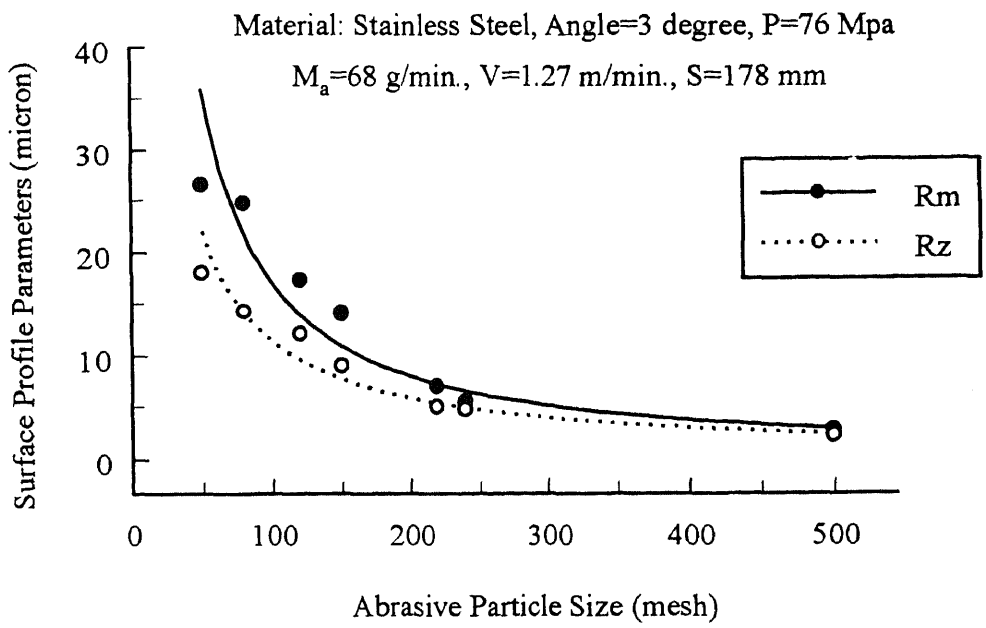

Figure 5.5 Effect of Abrasive Particle Size on the Surface Profile (R_m and R_z) in Course of AWJ Processes

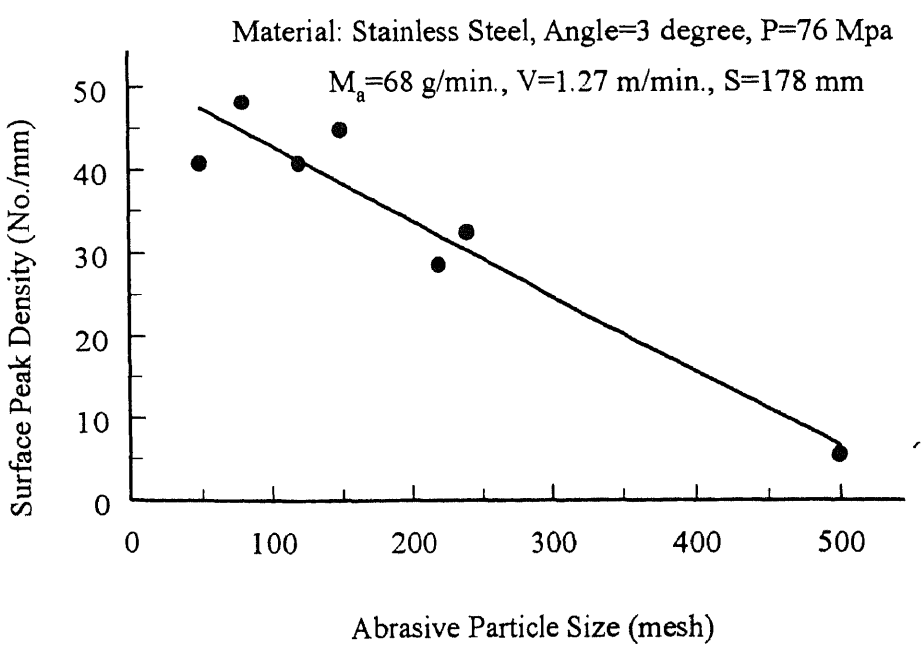

Figure 5.6 Effect of Abrasive Particle Size on the Surface Peak Density (N_r) in Course of AWJ Processes

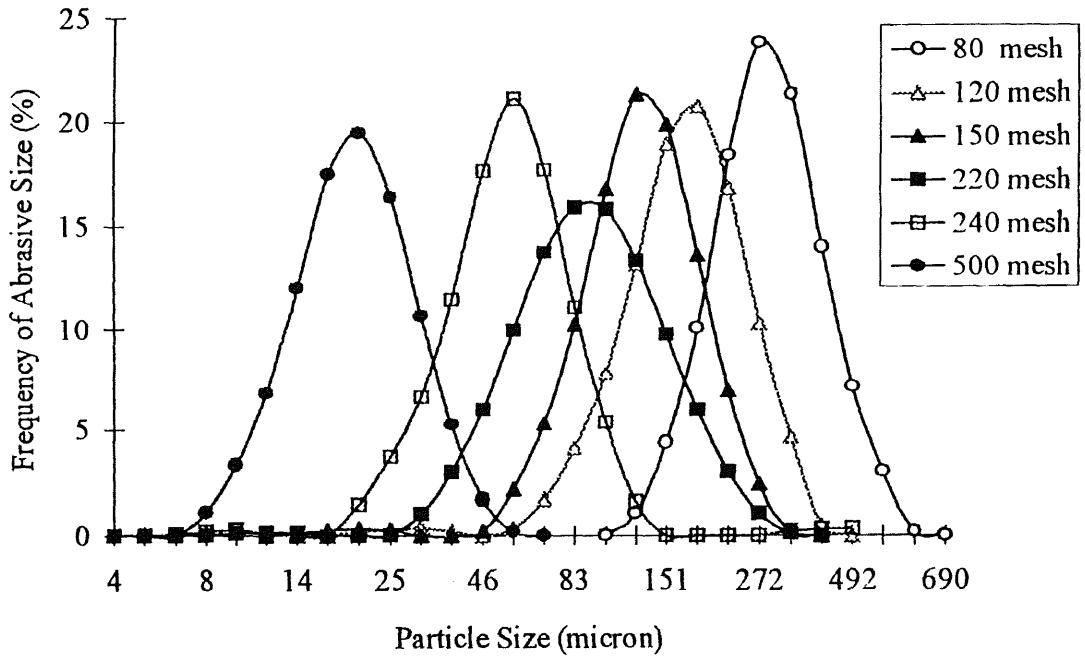

Figure 5.7 Size Distribution of Abrasive Particle Used in AWJ Polishing Processes

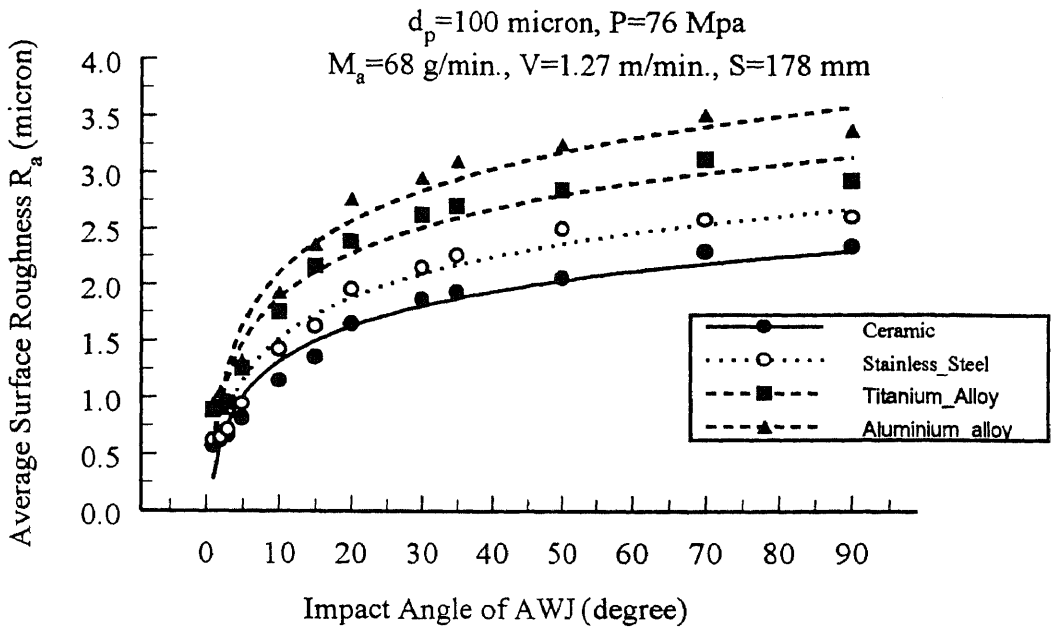

Figure 5.8 Effect of Jet Impact Angles on the Surface Roughness (R_a) in Course of AWJ Processes

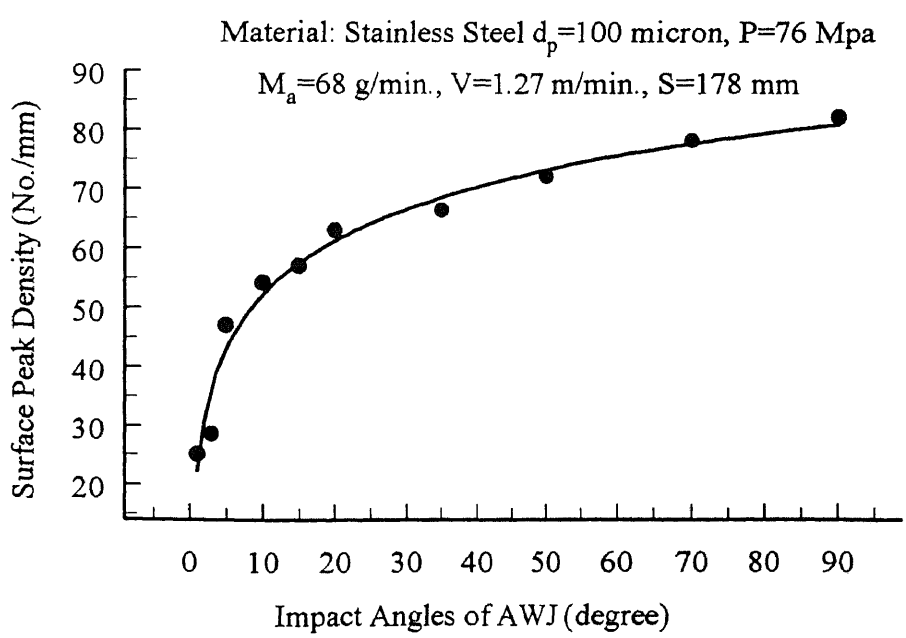

Figure 5.9 Effect of Jet Impact Angles on the Surface Peak Density (N_r) in Course of AWJ Processes

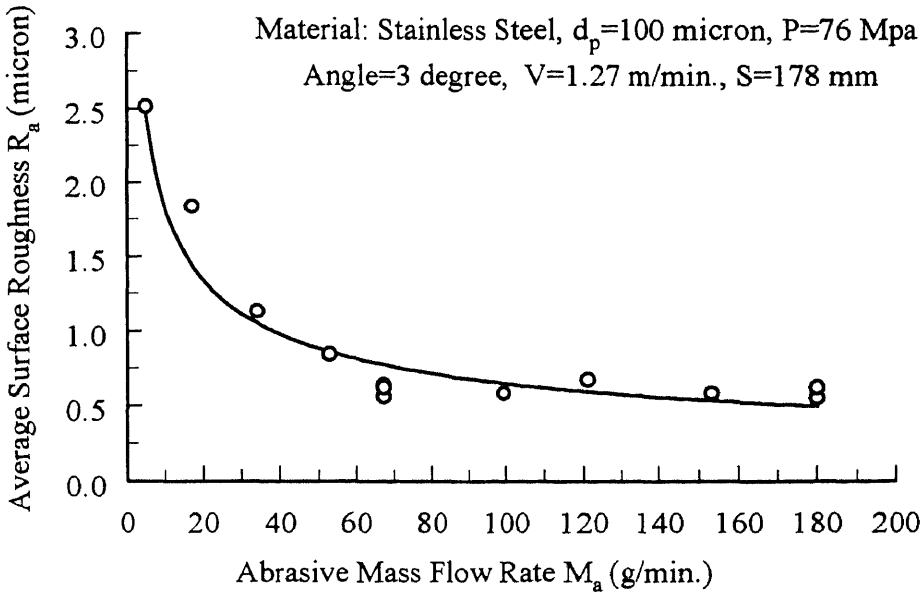

Figure 5.10 Effect of Abrasive Mass Flow Rate on the Surface Roughness in Course of AWJ Polishing Processes

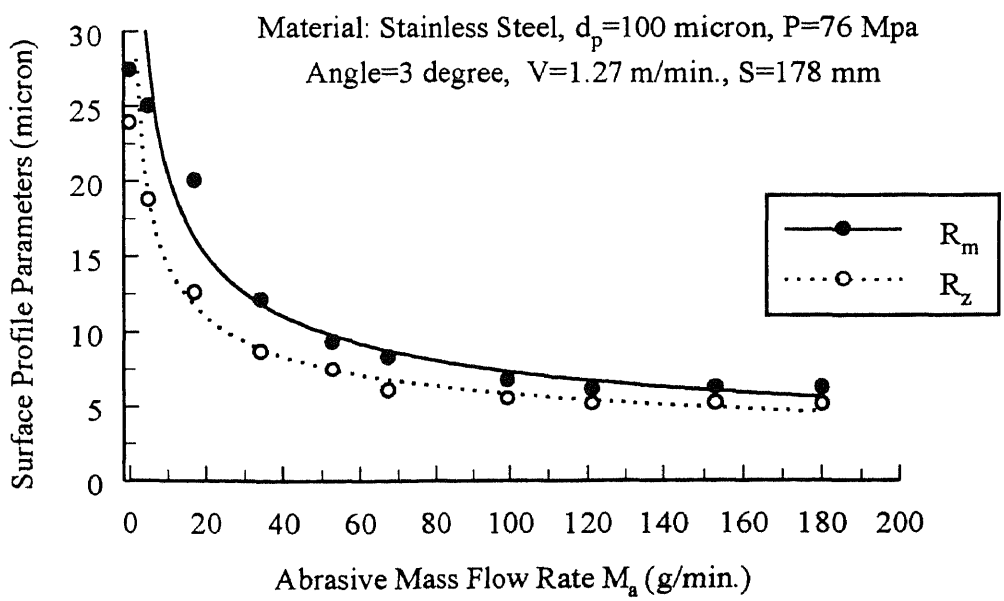

Figure 5.11 Effect of Abrasive Mass Flow Rate on the Surface Profile Parameters in Course of AWJ Polishing Processes

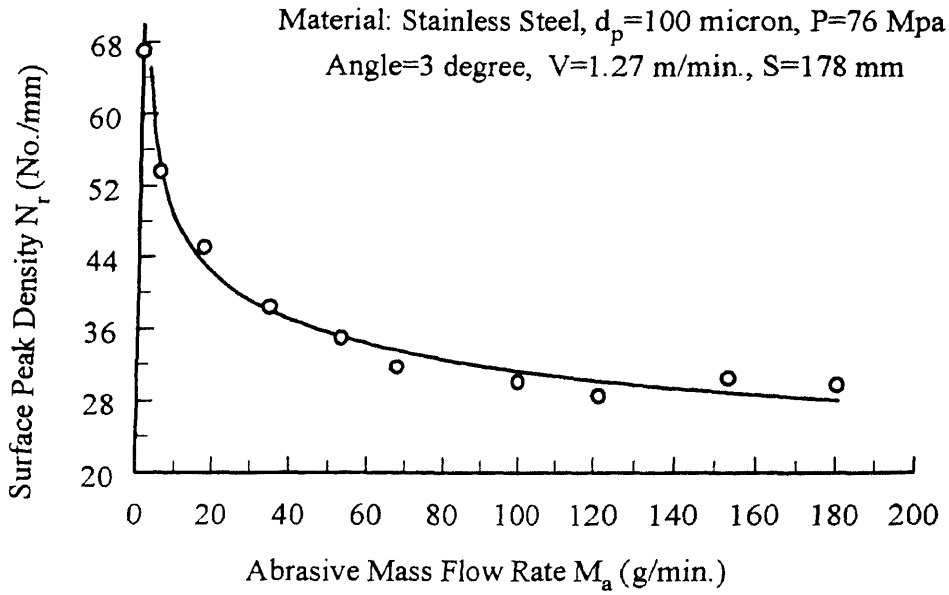

Figure 5.12 Effect of Abrasive Mass Flow Rate on the Surface Peak Density N_r in Course of AWJ Polishing Processes

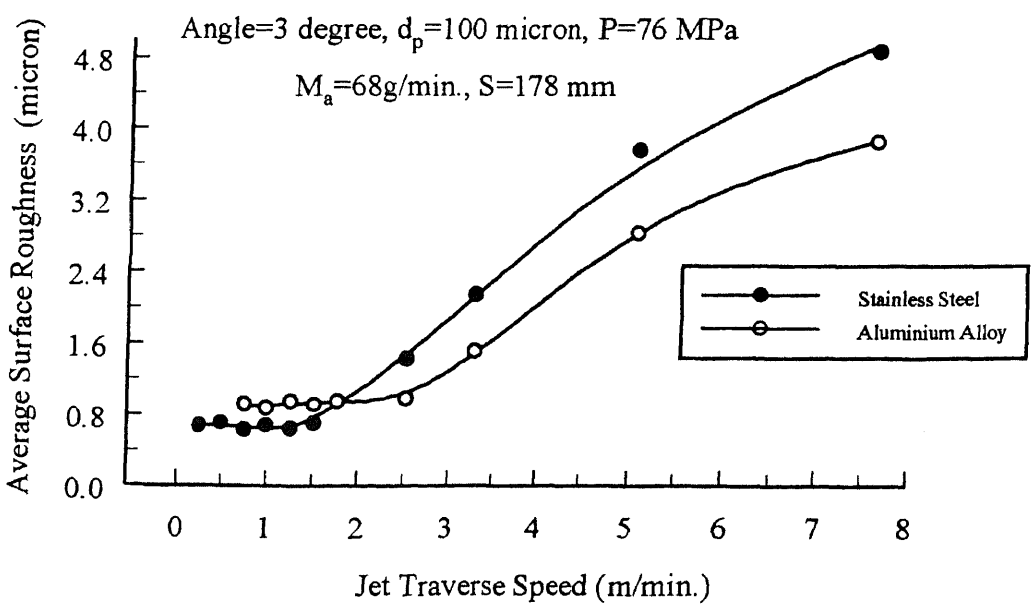

Figure 5.13 Effect of Jet Traverse Speed on Surface Roughness in Course of AWJ Polishing Processes

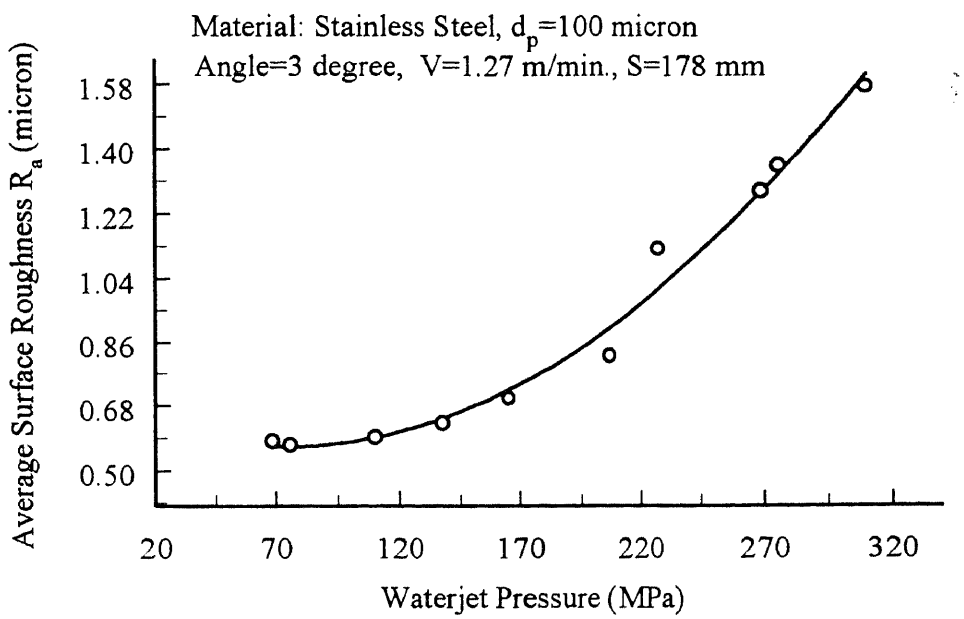

Figure 5.14 Effect of Waterjet Pressure on the Surface Roughness (R_a) in Course of AWJ Polishing Processes

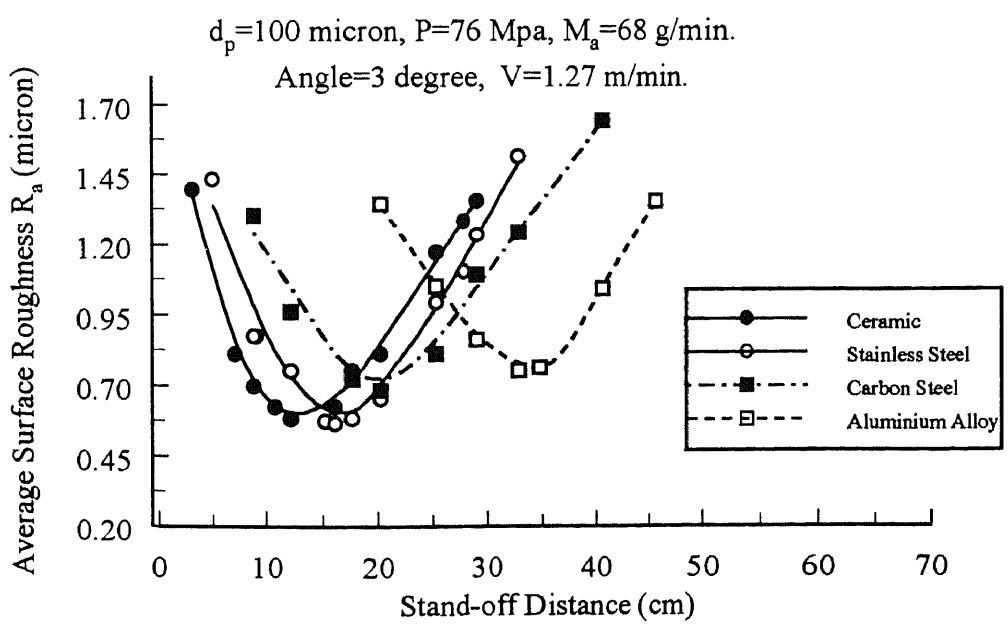

Figure 5.15 Effect of Stand-off Distance on Surface Roughness in Course of AWJ Polishing Processes

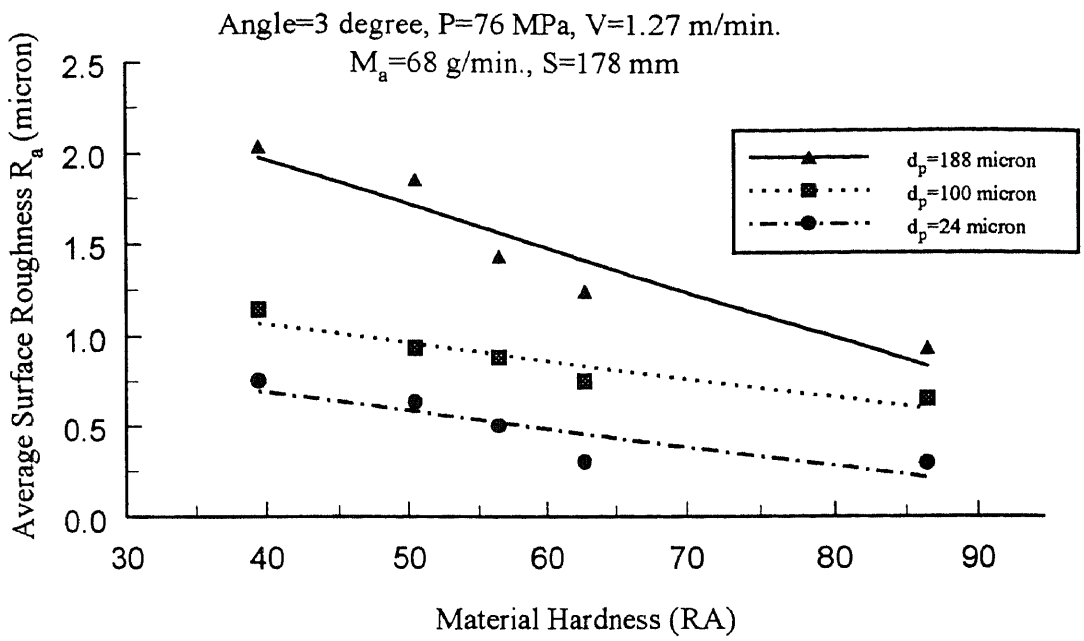

Figure 5.16 Effect of Material Hardness on Surface Roughness for Various Particle Size in Course of AWJ Polishing Processes

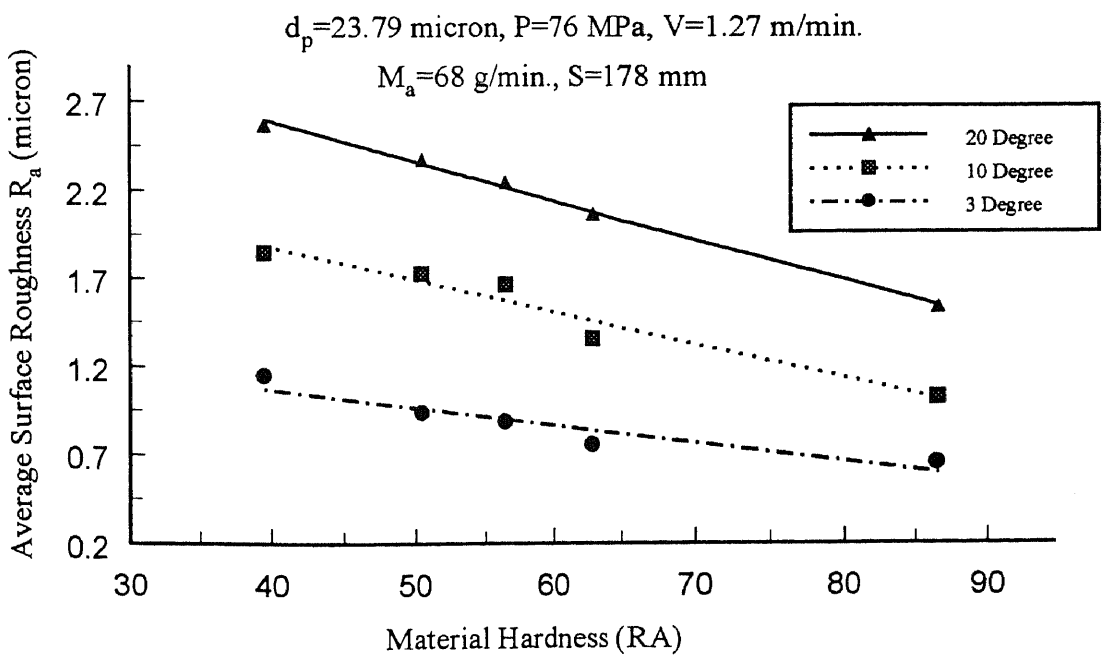

Figure 5.17 Effect of Material Hardness on Surface Roughness for Various Impinging Angles in Course of AWJ Polishing Processes

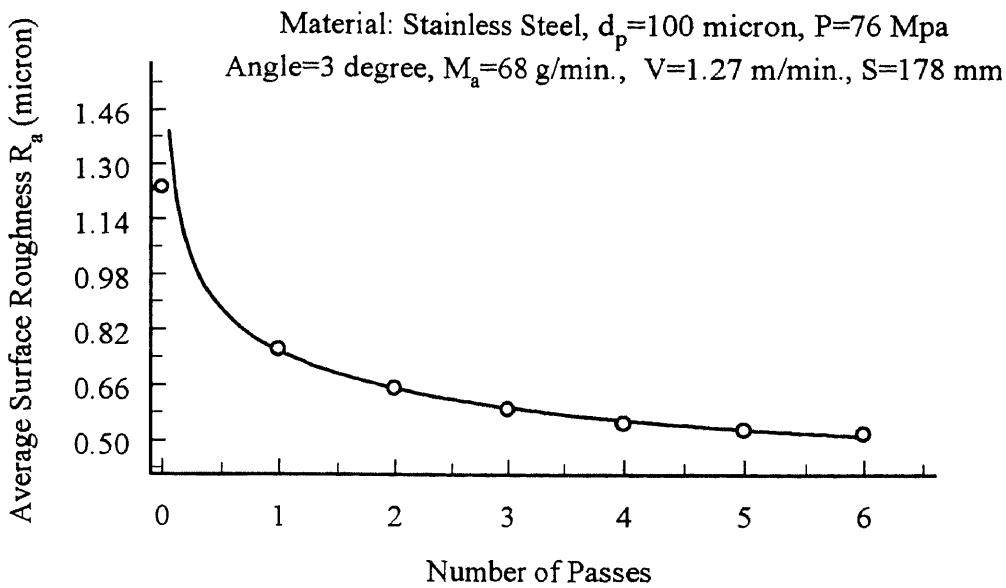

Figure 5.18 Effect of Number of Polishing Passes on Surface Roughness in Course of AWJ Polishing Processes

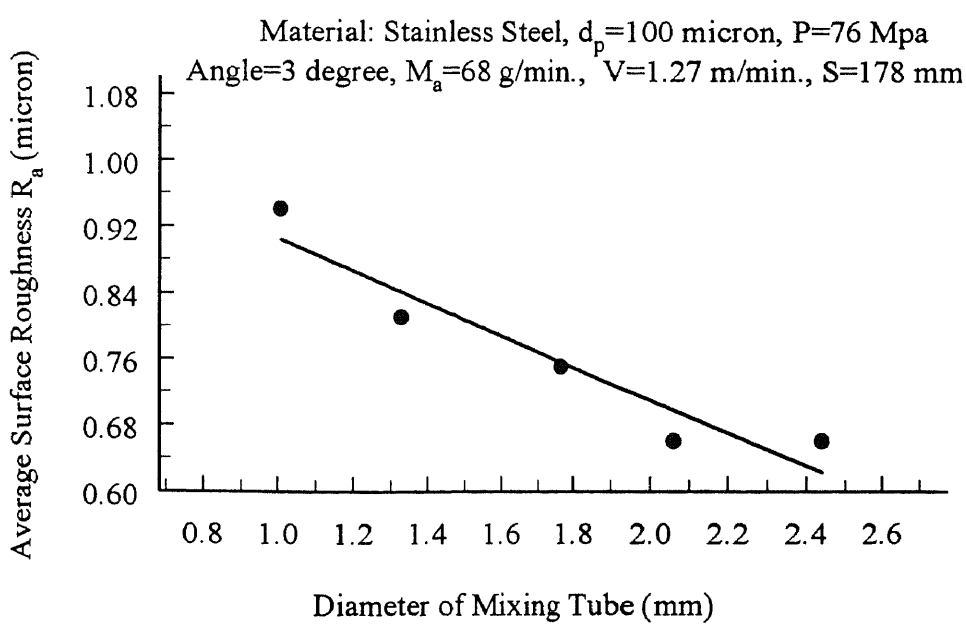

Figure 5.19 Effect of Diameter of Mixing Tube on Surface Roughness in Course of AWJ Polishing Processes

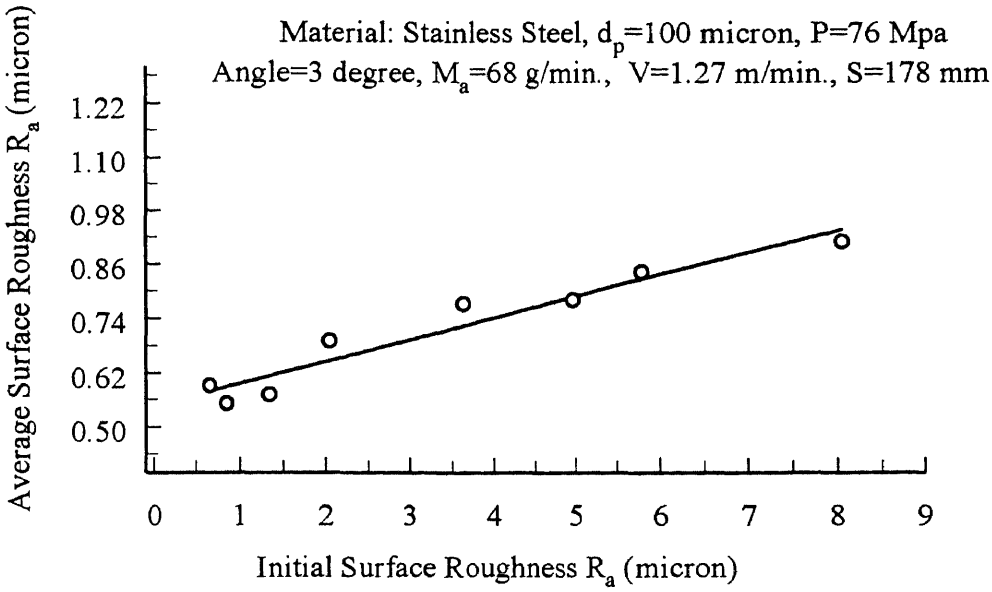

Figure 5.20 Effect of Initial Surface on Surface Roughness in the Course of AWJ Polishing Processes

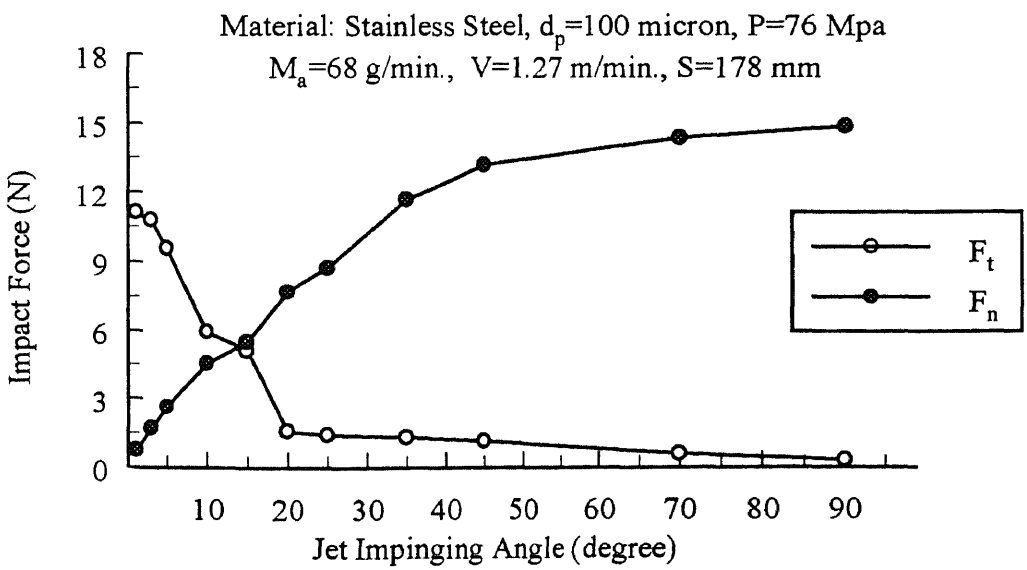

Figure 5.21 Effect of Impining Angle on Normal (F_n) and Tangential (F_t) Force Developed on Target Surface in Course of AWJ Polishing Processes

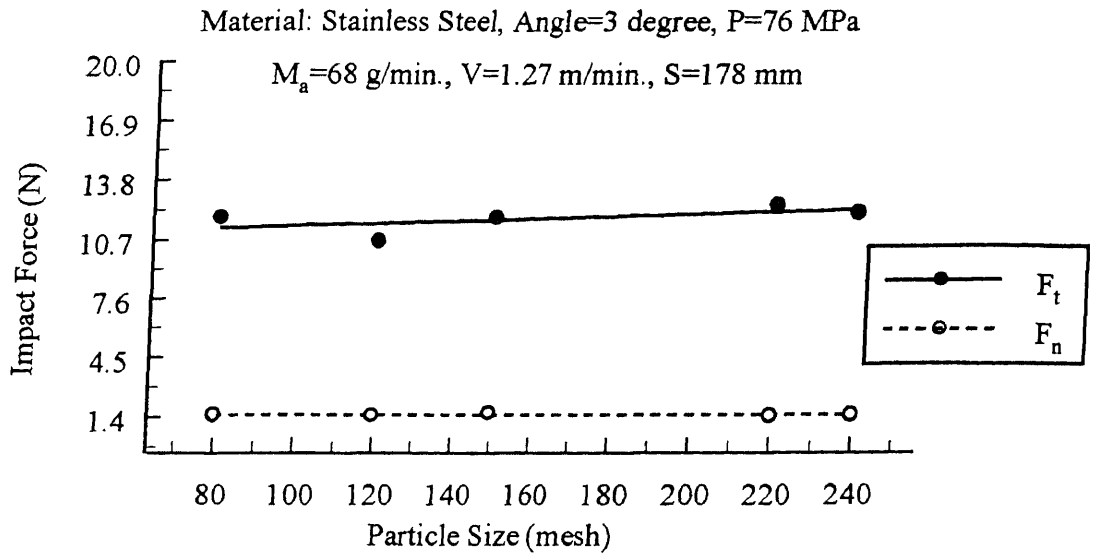

Figure 5.22 Effect of Abrasive Particle Size on Tangential (F_t) and Normal Force (F_n) Developed on Target Surface in Course of AWJ Polishing Processes

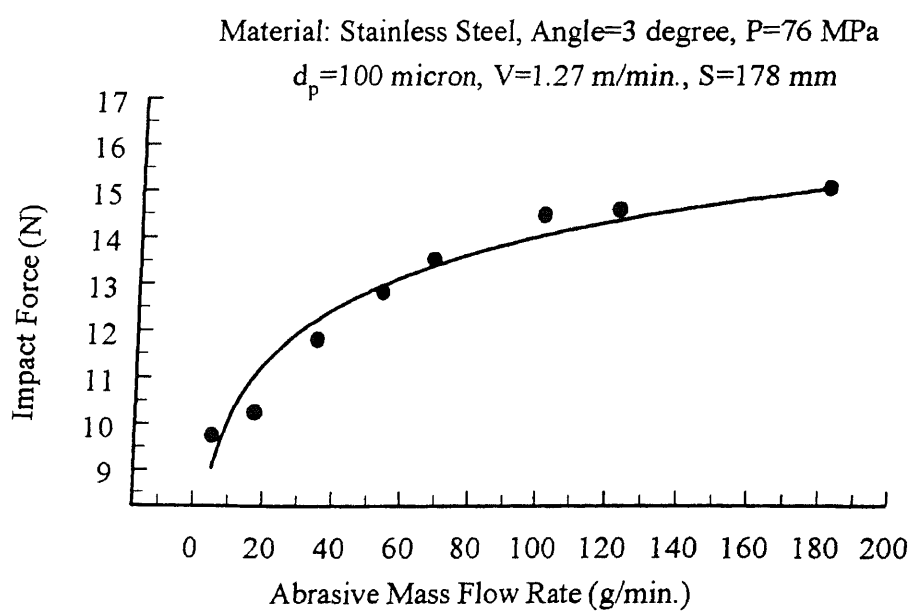

Figure 5.23 Effect of Abrasive Flow Rate on Tangential (F_t) and Normal (F_n) Force Developed on Target Surface in Course of AWJ Polishing Processes

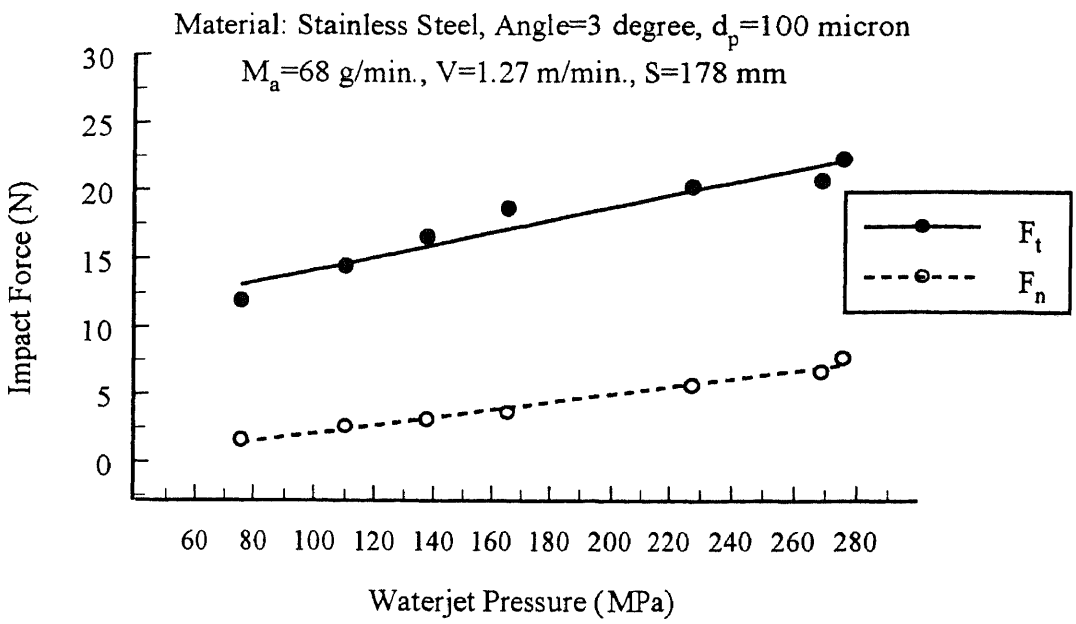

Figure 5.24 Effect of Waterjet Pressure on Tangential (F_t) and Normal (F_n) Force Developed on Target Surface in Course of AWJ Polishing Processes

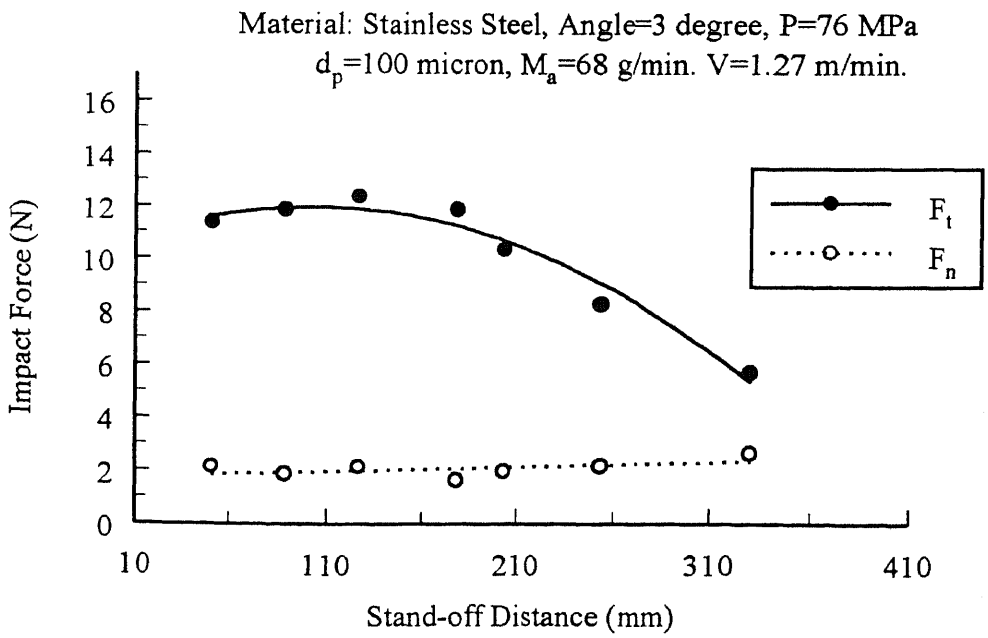

Figure 5.25 Effect of Stand-off Distance on Tangential (F_t) and Normal (F_n) Force Developed on Target Surface in Course of AWJ Polishing Processes

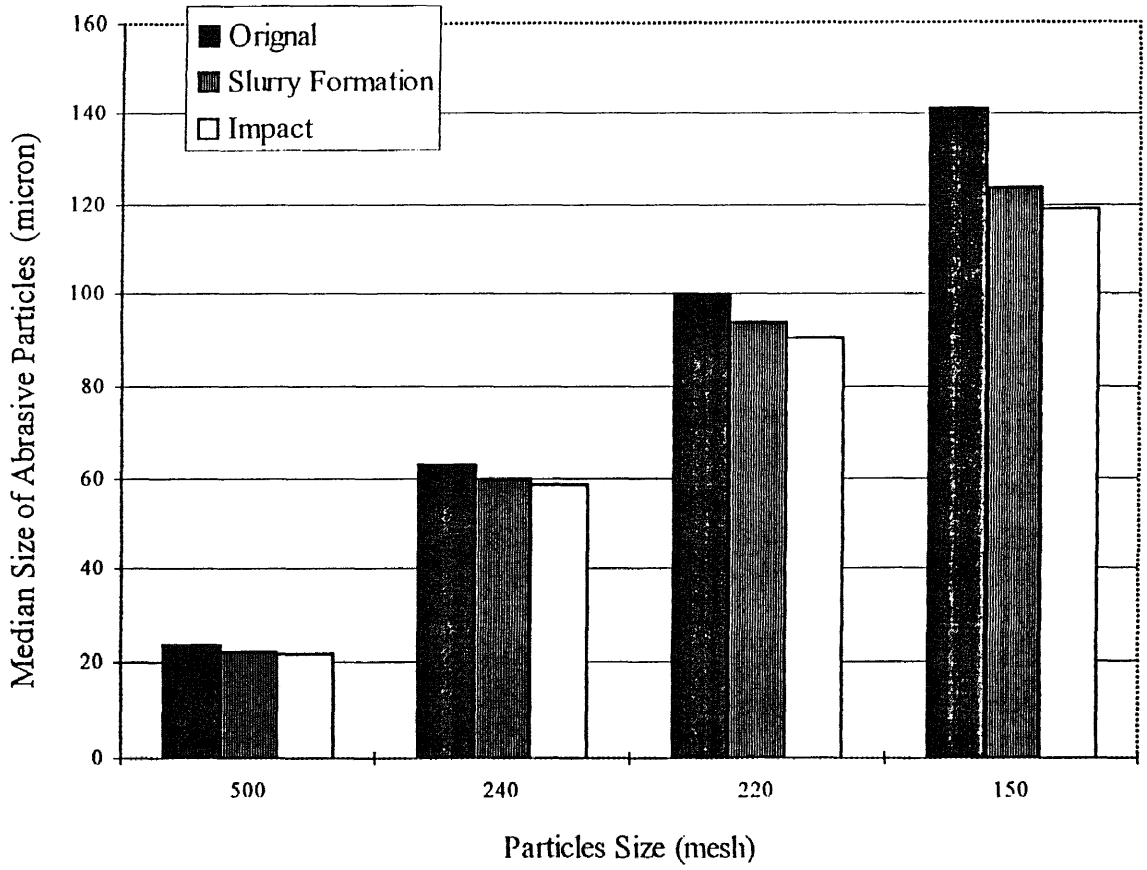

Figure 5.26 Abrasive Particles Disintegration in the Course of AWJ Polishing Processes

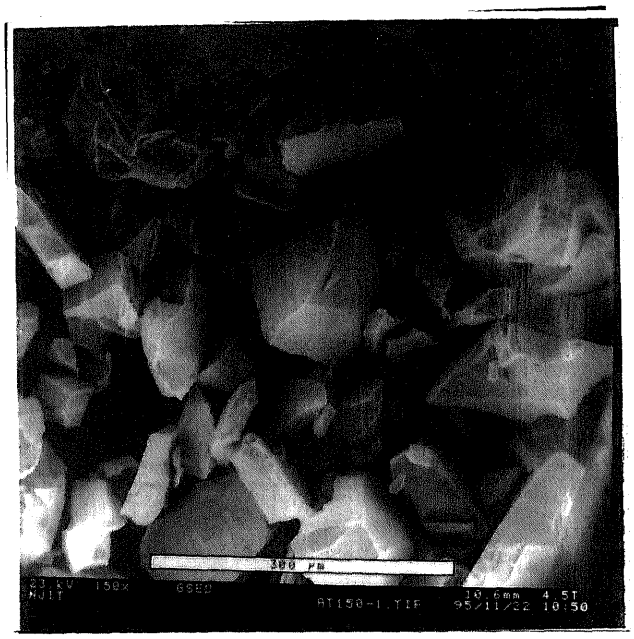

(a) 150 Mesh Garnet
Note: The Large Difference in Size can be Clearly Observed

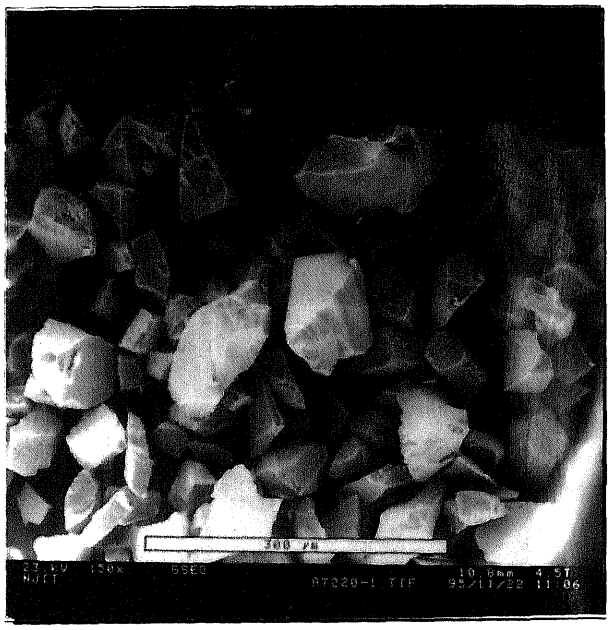

(b) 220 Mesh Garnet

Figure 5.27 SEM Image of Abrasive Particle Collected after Impinging Target in AWJ Polishing Processes

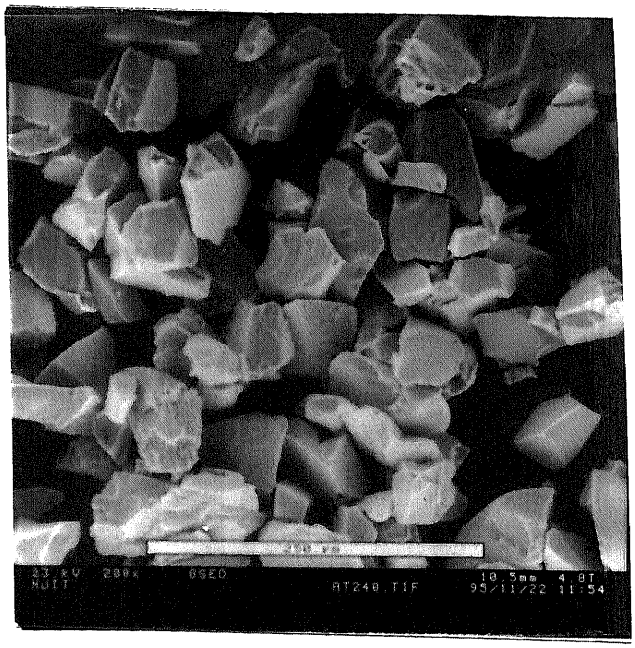

(c) 240 Mesh Garnet

(d) 500 Mesh Garnet
Notice: the Uniform Particle Size and Sharp edge

Figure 5.27 (Continued)

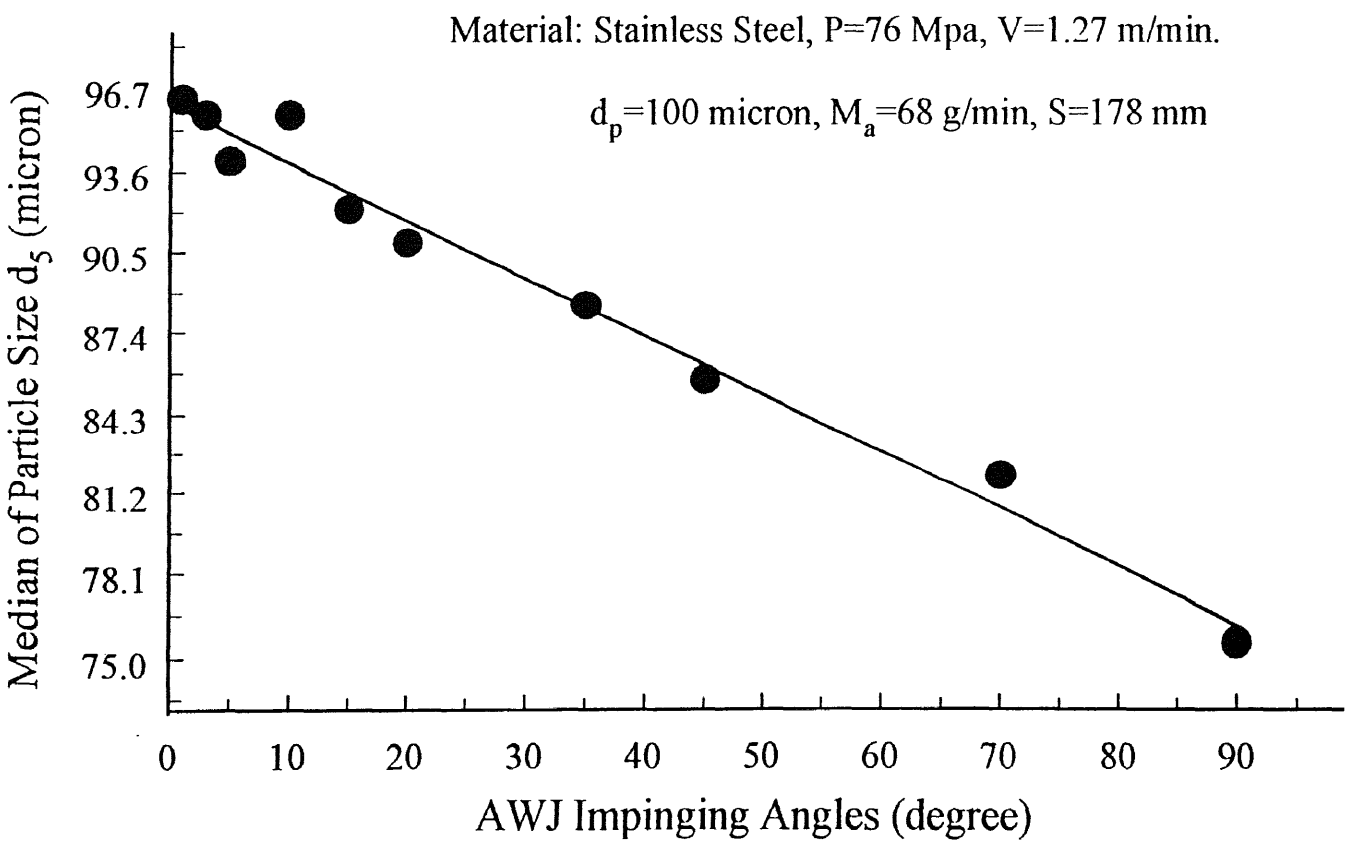

Figure 5.28 Effect of Impinging Angles on Particle Disintegration in Course of AWJ Polishing Processes

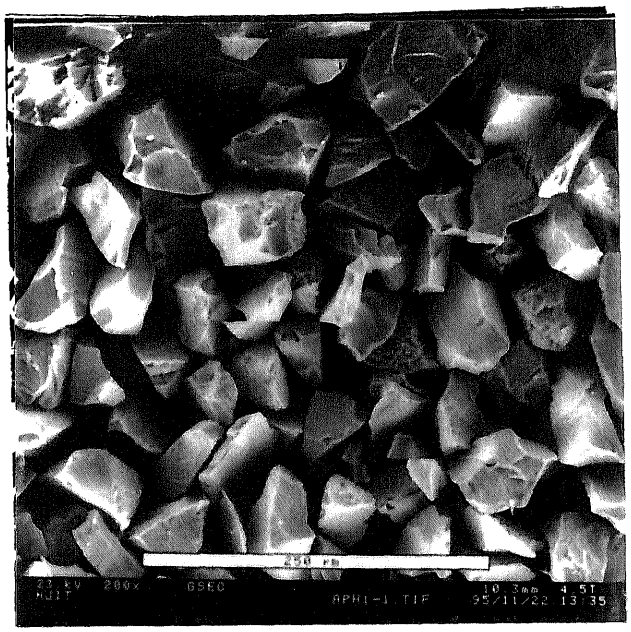

(a) α=3 degree
Note: the Uniform Particle Size and Sharp edge

(b) α=30 degree
Note: Broken Piece of Particles

Figure 5.29 SEM Image of 220 Mesh Garnet Fragment at Various Impinging Angles in the Course of AWJ Polishing

(c) α=90 degree
Notice: Mixing Dimension of Particles

Figure 5.29 (Continued)

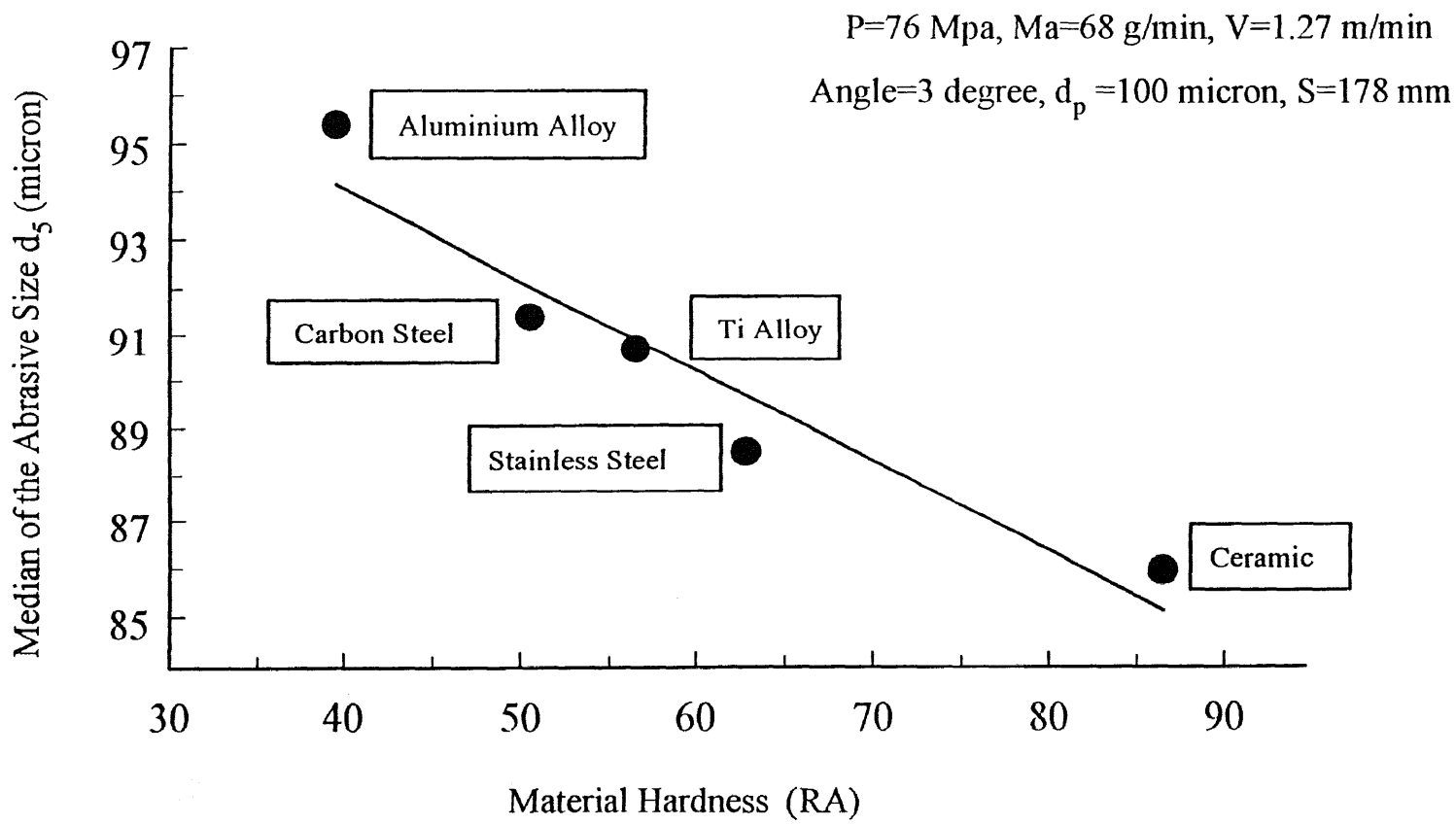

Figure 5.30 Effect of Material Hardness on Abrasive Particle Disintegration in Course of AWJ Polishing Processes

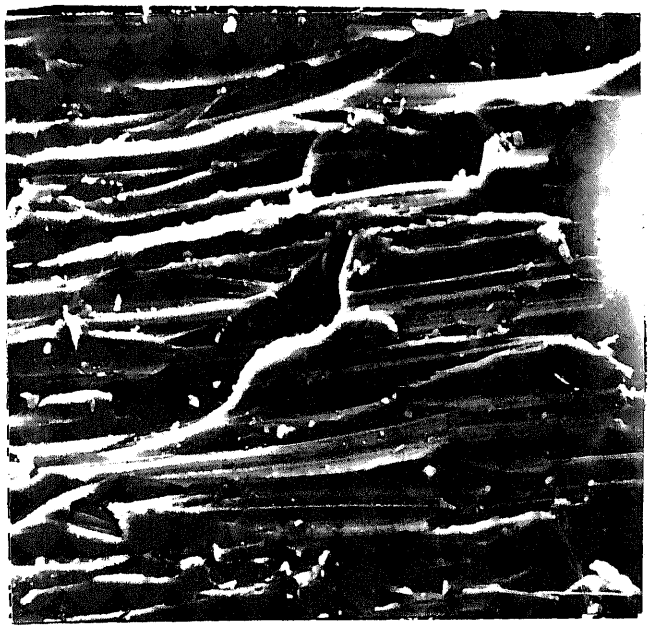

(a) Surface of Aluminum Alloy Sample.
Notice Large Plastic Deformation While Peak are cut.

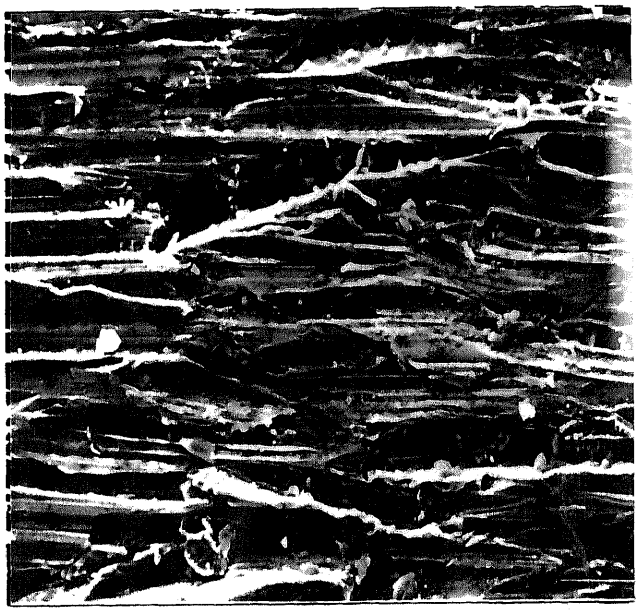

(b) Surface of Carbon Steel Sample

Figure 5.31 SEM Image of an AWJ Polished Surface for Various Materials (x1000)

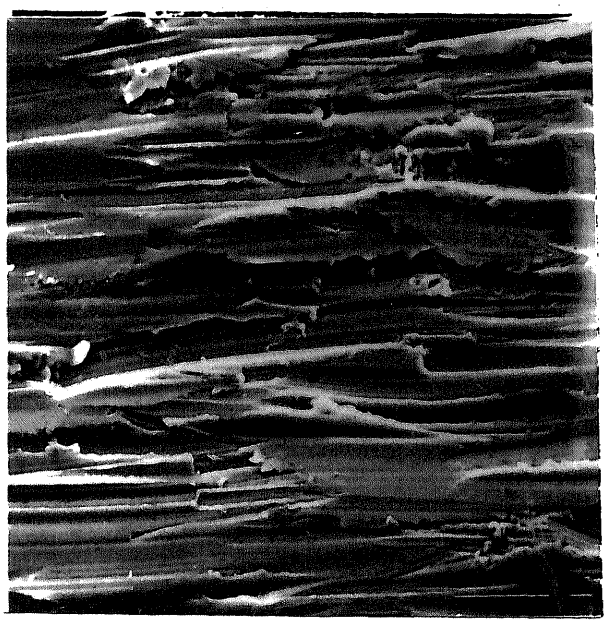

(c) Surface of Titanium Alloy Sample
Notice: Long and shallow grooves created by abrasive particle

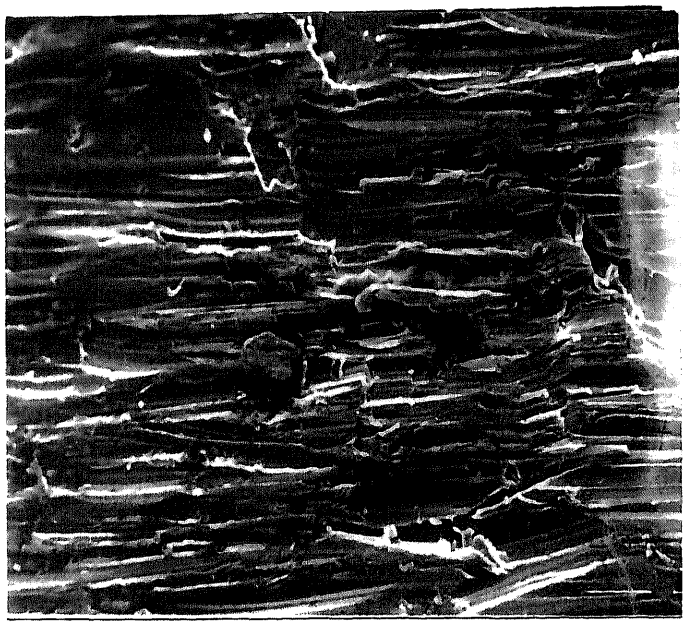

(d) Surface of Stainless Steel Sample
Notice Less Plastic Deformation and Thin and Uniform Grooves

Figure 5.31 (Continued)

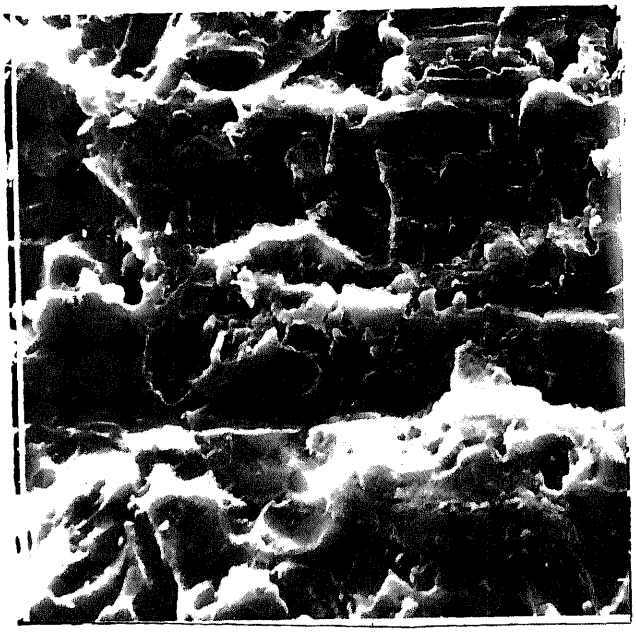

(e) Surface of Glass Sample
Notice Less Plastic Deformation along Grooves and Brittle Chips

(f) Surface of Alumina Ceramic Sample
Note: No plastic deformation and intergranular fracture can be observed

Figure 5.31 (Continued)

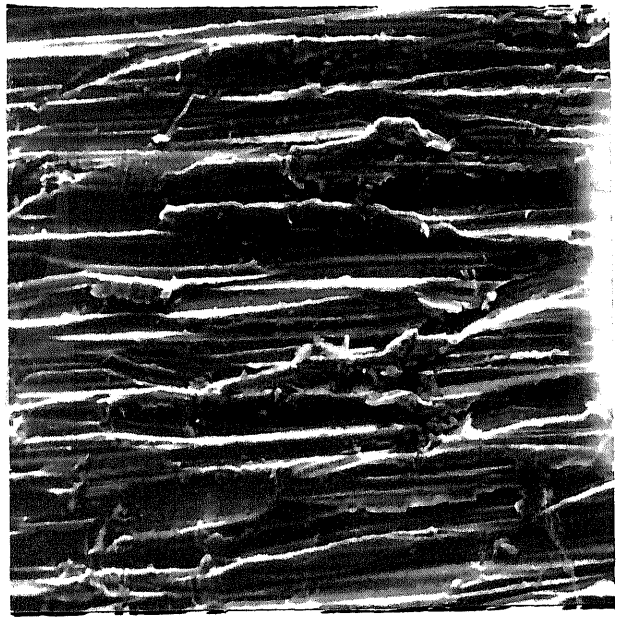

(a) α=3 degree.
Notice: Long and shallow grooves

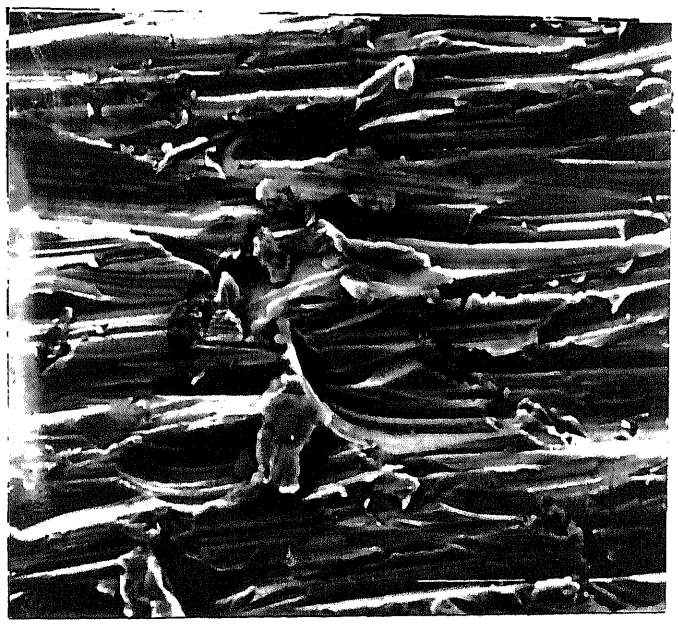

(b) α=10 degree
Note: The groove become short and shallow crater and chip can be found

Figure 5.32 SEM Image of Polished Surface of Stainless Steel Sample by AWJ at Different Impact Angle (x1000)

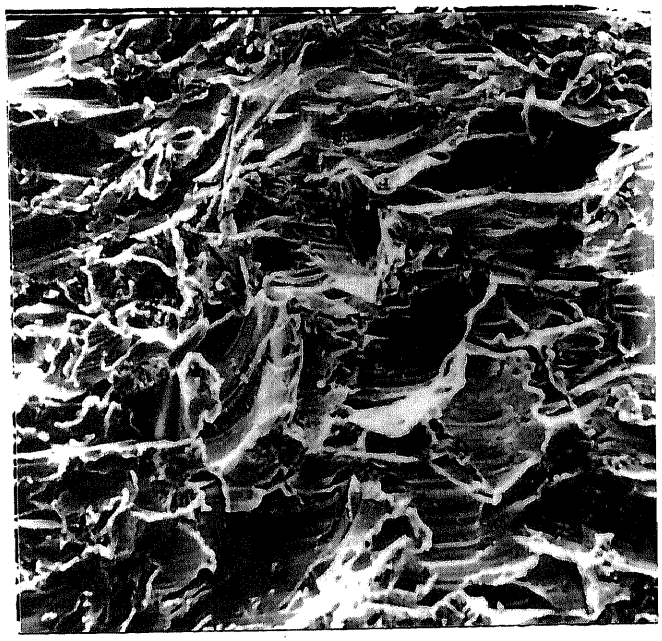

(c) α=30 degree
Note: The crater and short groove are clearly shown at same field examined

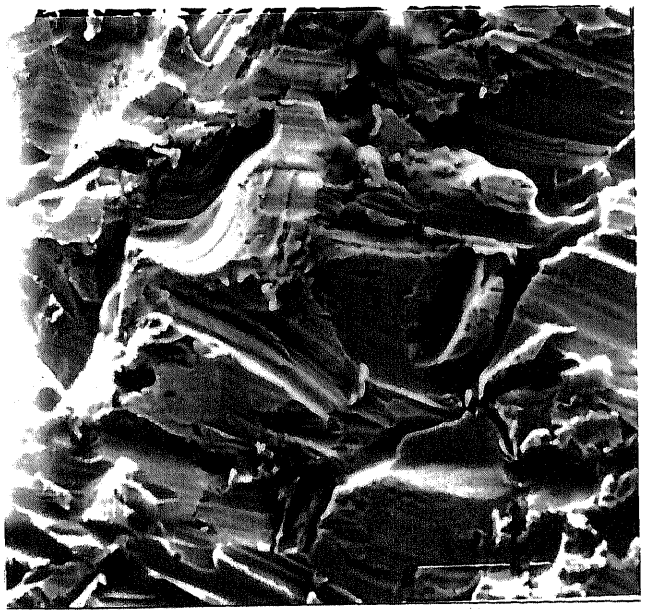

(d) α=70 degree
Note: Large crater and heavier plastic deformation are dominant feature

Figure 5.32 (Continued)

(e)α=90 degree
Notice: Deep crater and uneven surface

Figure 5.32 (Continued)

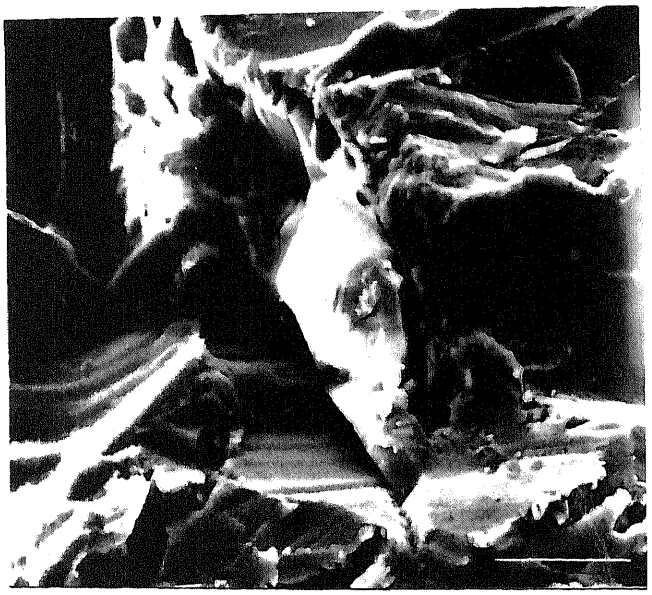

(a))α=90 degree
Note: A particle embedded deeply into the surface at a approximately vertical angle

Figure 5.33 SEM Image of Particle Embedded in Stainless Steel Sample at Various Impinging Angles (x1500)

(b))α=70 degree
Note: A garnet embedded into the surface obliquely with a sharp edge

(c))α=30 degree
Note: A particle plew a deep groove and embedded beneath a chip

Figure 5.33 (Continued)

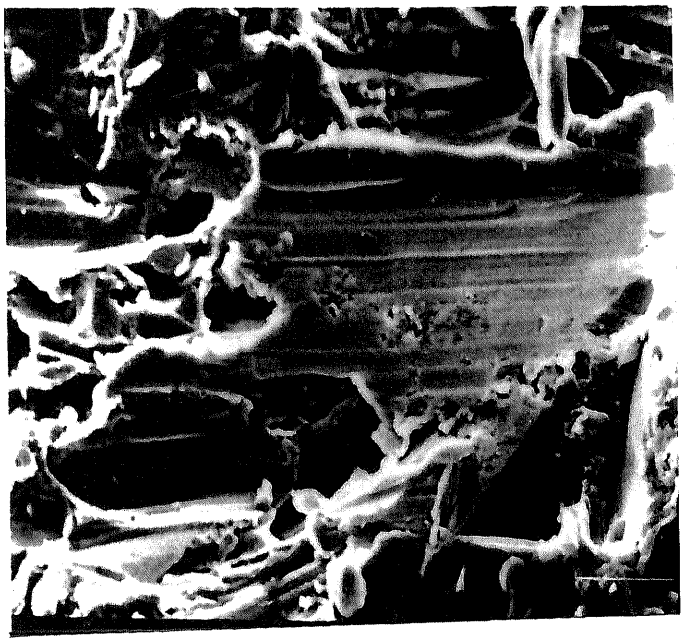

Figure 5.34 SEM Image Clearly Shows that a Peak was Cut off by Garnet at Near-Zero Angle against the Surface for a Stainless Steel Sample (x2000)

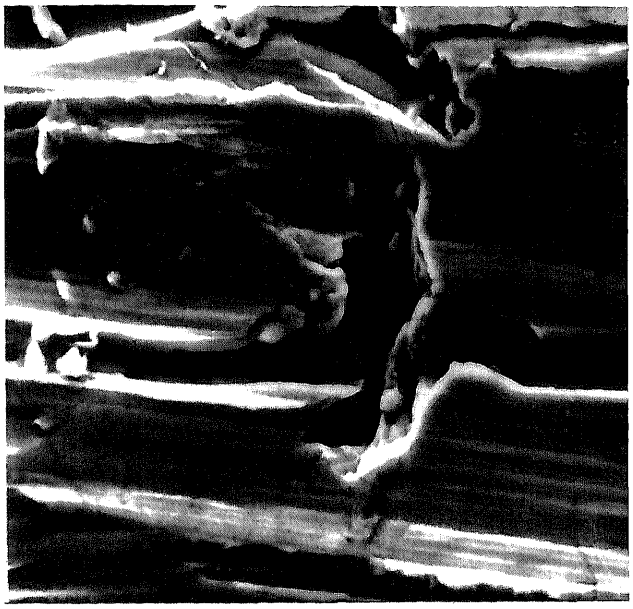

Figure 5.35 SEM Image of the Mark of Peak Cut and Bottom of Valley in the Surface of a Stainless Steel Sample (x2000).

(a) α=3 degree

Note: Thin and long grooves generated in second time Polishing in perpendicular direction with first process

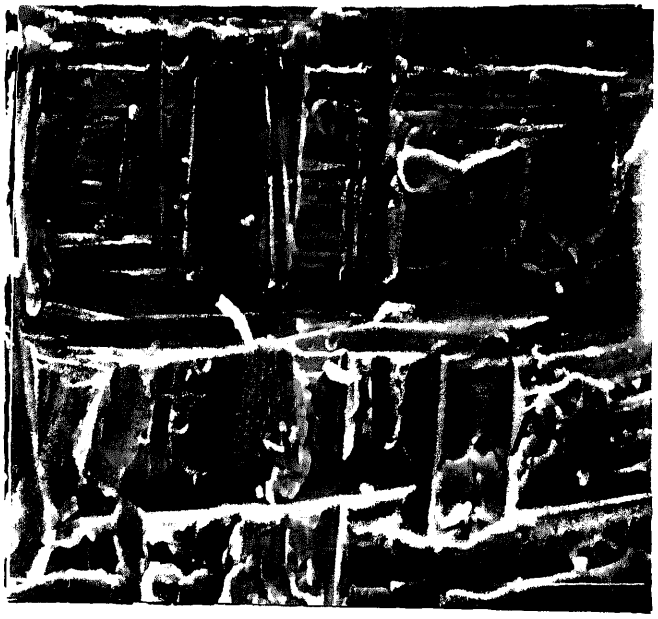

(b) α=5 degree

Note: The higher edges of scratch grooves were improved in second AWJ polishing process with perpendicular jet axial direction

Figure 5.36 SEM Image of the Surface Generated by AWJ with Two Times Processing at the Same Impact Angle (3-5 degree) and wit the Normal Axial Directions each other (x1500).

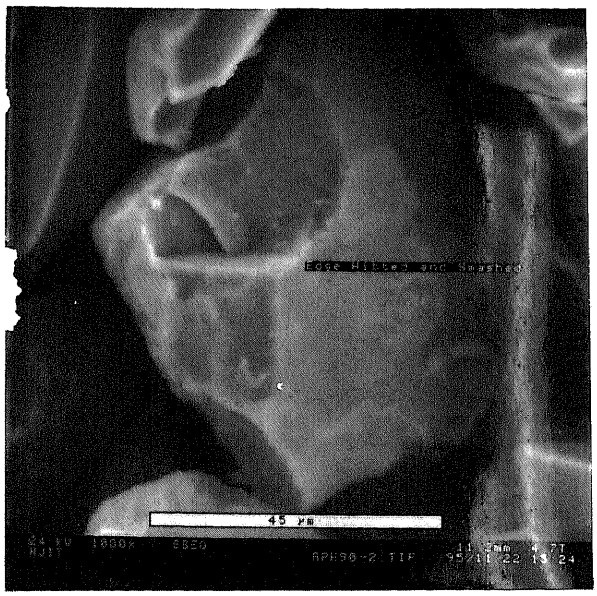

(a) Sharp Edge Hit and Smashed

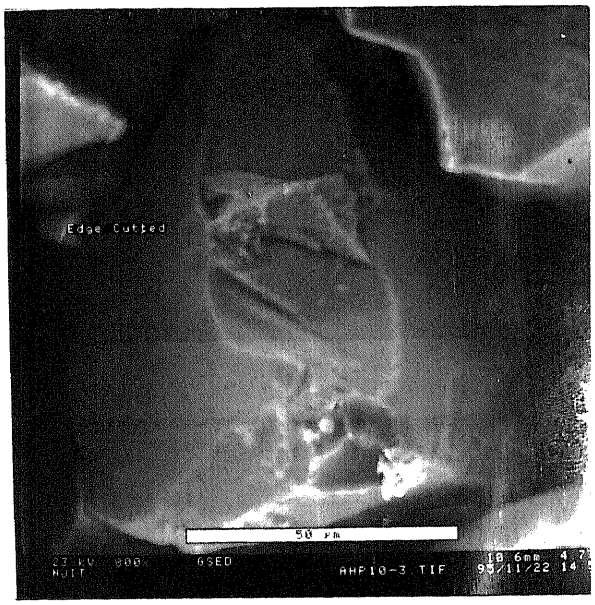

(b) Sharp Edge cut

Figure 5.37 SEM Image of Garnets Collected in Course of AWJ Polishing Process

(c) Broken Edge of a Garnet

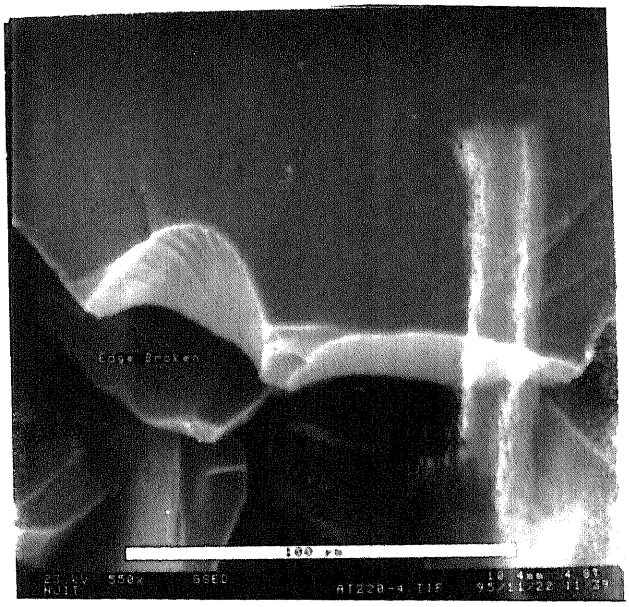

(d) Fracture Surface with Wave Pattern

Figure 5.37 (Continued)

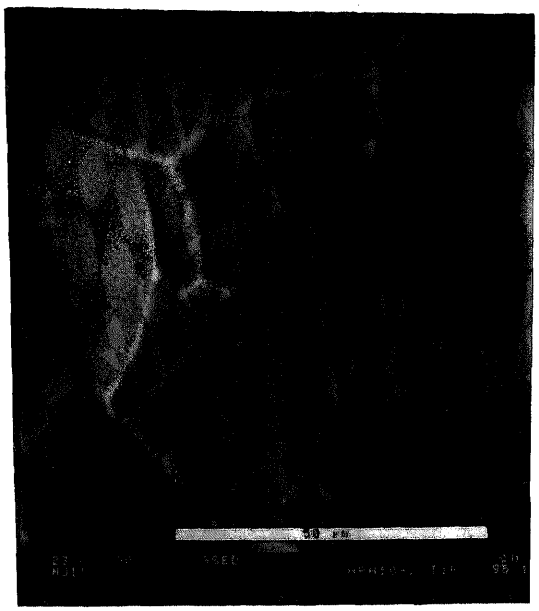

Figure 5.38 SEM Image of Cracks on a Garnet Collected in Course of AWJ Polishing Process

Figure 5.39 SEM Image of a Garnet that was Broken into Several Pieces and Embedded in a Stainless Steel Sample in Course of AWJ Polishing Process

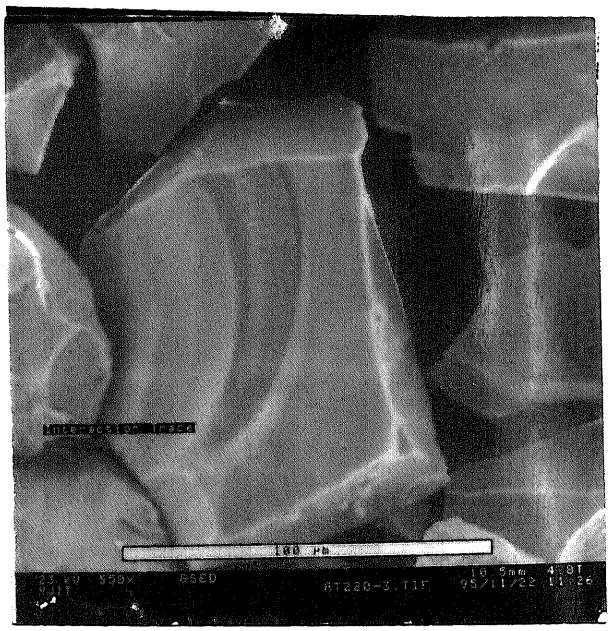

(a)

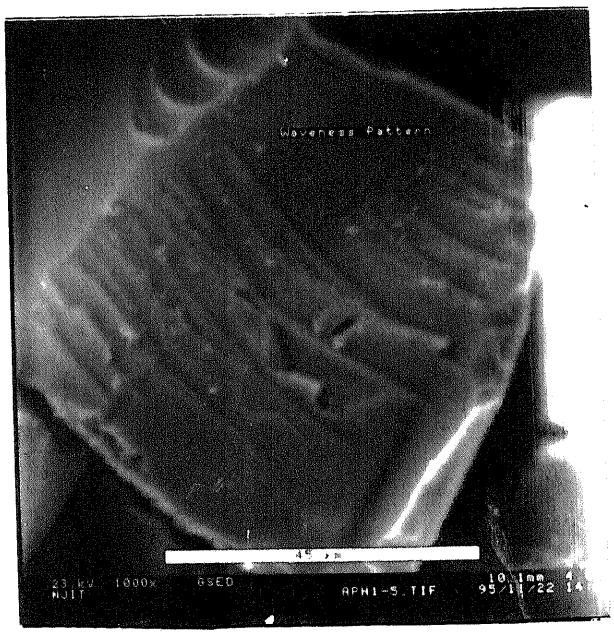

(b)

Figure 5.40 SEM Image of Garnets Collected in Course of AWJ Polishing Process
Notice: The Scratch Mark (a) and Waviness Pattern (b) on the surface

(a)

(b)

Figure 5.41 SEM Image of the Surface Topography of Garnets Collected in Course of AWJ Polishing Process. Notice: the Round Edge (a), Smooth Facet (b) and Wearing Marks (c)and (d) with Target.

(c)

(d)

Figure 5.41 (Continued)

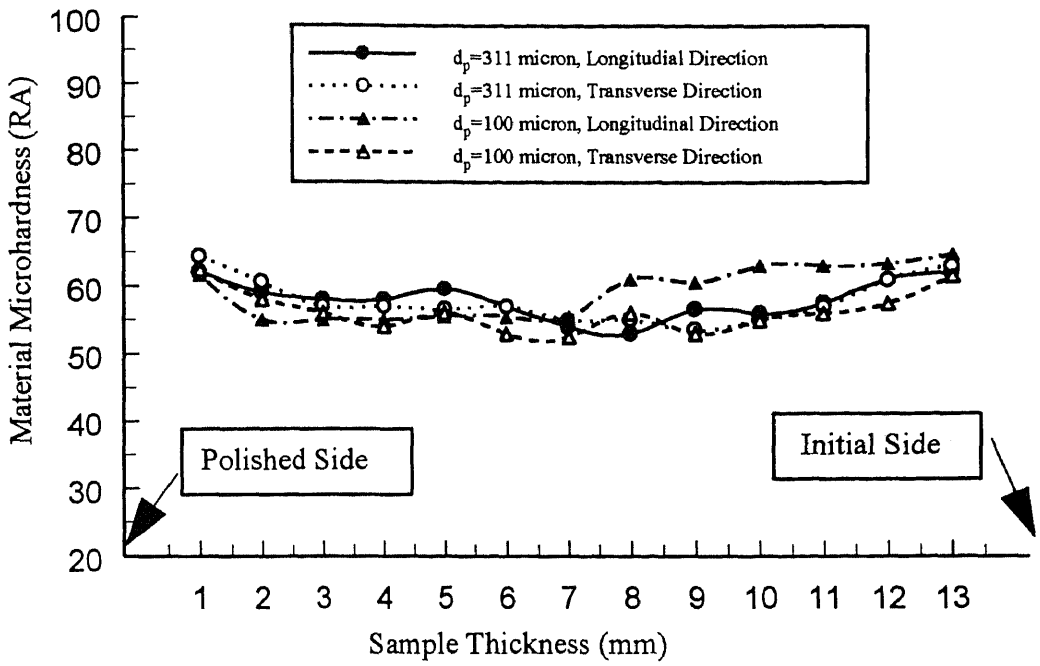

Figure 5.42 Microhardness Measured Through Thickness of Stainless Steel Samples Polished with Different Size of Abrasive Particles

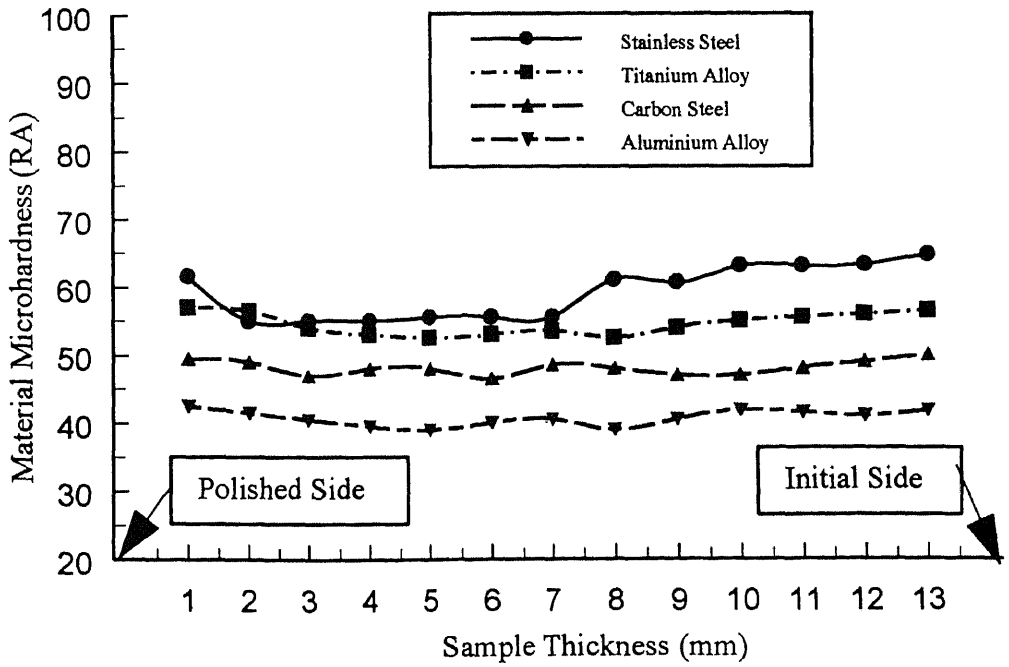

Figure 5.43 Microhardness Measured Through-Thickness of Samples Polished by AWJ for Various Materials

CHAPTER 6

NUMERICAL SIMULATION OF ABRASIVE WATERJET POLISHING

The objective of this study is to predict numerically a two-phase turbulent flow field and abrasive particle trajectory of the abrasive waterjet that impinges on a flat plate in course of AWJ polishing. The fluid dynamics of a free jet impinging on a solid surface are basic to the study of jet machining technology. As advancements are made in the area of analyzing turbulent high velocity free jets, the probabilities increase that a comprehensive model can be constructed. In the long run, the calculation schemes for jets will have to be link to calculation schemes which describe the target material removal dynamics, if a comprehensive jet machining model is to evolve. Turbulence is one of the unsolved problems in the area of physical science. In many areas of fluid mechanics, flows issued from nozzle are almost always turbulent; this means that the jet motion is highly random, unsteady and three dimensional. Therefore, to better understand the jet machining process, it is meaningful to study

6.1 Mathematical Model of the Turbulent Flow

A fully developed turbulent motion is characterized by a large number of three-dimensional entangled eddies (or vortex element) of varying size that involves a wide spectrum of length and time scales. The largest eddies are generated as a result of hydrodynamic instabilities in the mean flow field, i.e., from shearing between two coflowing streams at different velocities, shearing between a stream and a solid boundary.

These large eddies extract kinetic energy from the mean flow and by so doing provide the kinetic energy input which is necessary to maintain turbulent motion. The largest eddies themselves become unstable and break down into progressively smaller eddies and transfer their kinetic energy, which was extracted from the mean flow, to smaller scale of motion. This nonlinear, three dimensional and transient process of eddy breakdown causes vortex-stretching and the associated process of turbulent kinetic energy transfer to progressively smaller scales of motion results in kinetic energy cascade. In cascading down to the fine scales of turbulent motion, the kinetic energy of turbulence is finally 'destroyed' by viscous dissipation. Also, turbulence is a stochastic phenomenon since the exact detailed spatial and temporal evolution of a turbulent flow can never be replicated. Due to these complexities, the turbulent motion and mass transfer phenomena associated with it are extremely difficult to describe and thus predict theoretically for high pressure jet. It is believed that the solution of the time-dependent three dimensional governing equations can describe turbulent flows of waterjet completely. However, even today's supercomputers are not fast enough nor do they have the storage capacity to solve these equations directly for the required range of length and time scales, even for simple flows. The reason is that turbulent motion contains scales which are much smaller than the extent of the flow domain, typically of the order of 10^{-3} times smaller. To resolve the motion on these scales in a numerical procedure would require a mesh discretization far beyond the capabilities of today's computers. Hence, it is of practical importance to describe turbulent motion in terms of time-averaged quantities rather than instantaneous ones.

This approach is based on the modifications of governing equations for case of laminar flow. For the flow involved in this study being steady incompressible, isothermal and chemically homogeneous, these basic conservation laws are expressed by the exact equations as follows:

Mass Conservation: $$u_{i,j} = 0 \tag{6.1}$$

Momentum Conservation: $$\rho u_j \, u_{i,j} = -p_{,i} + [\mu(u_{i,j} + u_{j,i})]_{,j} \tag{6.2}$$

where u_i is velocity, p is pressure, μ is the dynamic viscosity and ρ is density.

Since there was and still is little hope of solving these equations, a statistical approach, first suggested by Osborne Reynolds, is taken and the equations are averaged over a time scale which is long compared with that of the turbulent motion. The resulting equations describe the distribution of mean velocity, pressure and temperature and thus the quantities of prime interest to the engineer. The derivation of these time-averaged equations will now be briefly outlined.

A statistical approach is taken and each of the field variables (velocity u_i and pressure p) is separated into mean and fluctuating quantities. Thus mean values of the field variables will be used to model the large scale flow characteristics. For an arbitrary field variable η, its mean value was defined as,

$$\overline{\eta} = \frac{1}{\Delta t} \int_{t}^{t=\Delta t} \eta \, dt \tag{6.3}$$

where t is a reference point in time and Δt is the averaging time which is long compared with the time scale of the turbulent motion. The variable η is then decomposed as follows:

$$\eta = \overline{\eta} + \hat{\eta} \tag{6.4}$$

where $\hat{\eta}$ reflects the small scale fluctuations associated with turbulence.

In most turbulent flow problems of practical interest, only the overall effect of the turbulent flow field is usually considered. Because of this, an available computational technique is designed for evaluating the average flow characteristics. A mean flow field has a much smoother variation in space and time than the instantaneous flow field, thus significantly coarser meshes can be used for the numerical solution. The mean flow equations, in this case, are obtained from the application of time averaging (6.3) and the decomposition (6.4) to the instantaneous flow governing equations (6.1) and (6.2). For brevity, the overbars indicating averaged values will be dropped from u_i and p from here on. The resulting equations are integrated over the time interval (t, t+Δt) resulting in the following mean field equations:

$$u_{j,j} = 0 \tag{6.5}$$

$$\rho\ u_j u_{i,j} = -p_{,i} + \left[\mu(u_{i,j} + u_{j,i}) - \rho\ \overline{u_i u_j}\right]_{,j} \tag{6.6}$$

These are the equations governing the mean-flow quantities u_i and p. These equations are exact since no assumptions have been introduced in deriving them; but they no longer form a closed set. The term $\overline{u_i u_j}$ is the statistical correlation manifesting the effects of the turbulence (or fluctuating) field on the mean flow process. Due to the nonlinearity of governing equations, the averaging process has introduced unknown correlation between fluctuating velocities. The second moment correlation $\rho\ \overline{u_i u_j}$ appearing in the momentum equation, which is a second order symmetric tensor, may be interpreted as the transport of x_i momentum in the direction of x_j (or vice-versa); it acts

as a stress on fluid and is called the turbulence Reynolds stress tensor, in the mean momentum equation. The Reynolds stress tensor is expanded below in terms of its nine elements in a three dimensional Cartesian framework.

$$\rho\ \overline{u_i u_j} = \rho \begin{bmatrix} \overline{u^2} & \overline{uv} & \overline{uw} \\ \overline{vu} & \overline{v^2} & \overline{vw} \\ \overline{wu} & \overline{wv} & \overline{w^2} \end{bmatrix} \tag{6.7}$$

The diagonal terms, which are the variances of the fluctuating components of the velocity vector multiplied by density, act as normal stresses on the fluid in much the same way as the pressure does. The off-diagonal terms, which are the covariance of the components of a fluctuating velocity field multiplied by density, act as shear stresses in the fluid and produce shearing of the velocity profiles in three principle directions.

6.2 Modeling of the Turbulence

Equations (6.5) and (6.6) can be solved for the mean value of velocity and pressure only when the turbulence correlation can be determined in some way. In fact, the determination of these correlation is the main problem in calculating turbulent flows. A turbulence model must be introduced which approximates these correlation in some manner, typically by expressing them in terms of mean-flow quantities. Such a turbulence model together with the mean flow equations (6.5) and (6.6) form a closed set of equations for the mean values of velocity and pressure. Therefore, turbulent modeling is the task of providing additional equations to describe the temporal and spatial evolution of the turbulent flux $\overline{u_i u_j}$. Thus, the turbulent flux can be solved simultaneously with the mean flow equations to produce a

solution to the mean flow field, if the turbulence model has been described. In general, the more sophisticated the turbulence model is, the more accurate is the prediction. But, it is also true that an increase in the degree of sophistication of a turbulence model often entails a significant increase in the overall computational cost for obtaining a prediction.

The most widely used approach to modeling the Reynolds stresses is Boussinesq's; his eddy-viscosity concept assumes that, in analogy to the viscous stresses in laminar flow, the components of the Reynolds stress tensor are proportional to the mean velocity gradients, i.e.

$$-\rho\ \overline{u_i u_j} = \mu_t (u_{i,j} + u_{j,i}) \tag{6.8}$$

The proportionality parameter μ_t is termed the eddy viscosity and unlike the molecular viscosity μ_0 which is a fluid property, depends on the turbulence of the flow and hence is a function of position. This approximation allows equation (6.6) to be rewritten as equation (6.2) provided the total viscosity is identified with the sum of the laminar and eddy viscosities,

$$\mu = \mu_0 + \mu_t \tag{6.9}$$

The eddy-viscosity concept shifts the problem of turbulence modeling to the determination of the distribution of μ_t; the additional unknowns are limited to the single variable μ_t. The turbulence modeling relates μ_t to the large scale turbulent eddies via the following expression

$$\mu_t \propto \rho u_l \delta_l \tag{6.10}$$

where u_l is characteristic velocity scale and δ_l is characteristic length scale. As u_l and δ_l are physically tangible quantities, it is generally easier to prescribe their variation in a

given flow field than it is to prescribe μ_t. Depending on the number of partial differential equations that are employed to model the scales u_l and δ_l, eddy viscosity models are classified into three groups,

(i) zero-equation models

(ii) one-equation models

(iii) two-equation models

Zero-equation models use only algebraic expressions to solve the equations and get the value of u_l and δ_l. In the one-equation class of models, one additional semi-empirical transport equation is introduced which governs the level of one of the characteristic turbulent scaled u_l and δ_l. Two-equation models introduce two additional semi-empirical transport equations to model the spatial and temporal variation of both turbulent scale u_l and δ_l. These are considerably more universal than zero-and one-equation models and can be applied in complex flow situations with a reasonable degree of confidence.

The most popular two-equation turbulence model in practical use, the so called k-ε turbulent model, has been employed in this simulation. In the k-ε turbulent model the turbulence field is characterized in term of two variables, the turbulent kinetic energy k, which is defined as

$$k = \frac{1}{2}\overline{u_i u_i} \tag{6.11}$$

and the viscous dissipation rate of turbulent kinetic energy ε, which is defined as

$$\varepsilon = \nu \overline{u_{i,j} u_{i,j}} = \nu \frac{1}{\Delta t} \int_{t}^{t+\Delta t} \hat{u}_{i,j} \hat{u}_{i,j} dt \tag{6.12}$$

In the context of the k-ε turbulent model, the characteristic turbulent velocity scale u_l and length scale δ_l are related to the turbulent kinetic energy k and its rate of viscous dissipation ε through the following expressions,

$$u_l \propto k^{1/2} \tag{6.13}$$

$$\delta_l \propto k^{3/2} / \varepsilon \tag{6.14}$$

Substituting equations (6.13) and (6.14) into equation (6.10) leads to the following so called Kolmogorov-Prandtl expression:

$$\mu_t = c_\mu \rho k^2 / \varepsilon \tag{6.15}$$

Thus the turbulent viscosity μ_t is directly related to the turbulent quantities k and ε. Two transport equations for k and ε, respectively can be obtained from the Navier-Stokes equations by a sequence of algebraic manipulations. By simplifying these two equations with application of a number of modeling assumptions the well known equations of turbulent kinetic energy and viscous dissipation of the k-ε model can be obtained (Launder and Spalding, 1972).

6.3 Near-wall Modeling with k-ε Model

When simulating turbulent flows using the k-ε model, it is particularly challenging to use the near-wall modeling methodology to simulate the viscosity affected boundary regions (i.e., regions adjacent to solid boundaries which contain the viscous sublayer). A major reason is that, in order to resolve the sharply varying flow variables in the near-wall

regions, a disproportionately large number of grid points would be required in the immediate vicinity of the solid boundary. For most typical flow scenarios this lead to prohibitively expensive computations. A second difficulty is of a fundamental nature and is directly related to the type of turbulence model employed to model the effect of viscosity on the turbulence field in the viscous sublayer (the so-called low Reynolds number effects on turbulence). The standard k-ε model is of the high Reynolds number type and therefore cannot be used in the near-wall regions. In the near-wall modeling scheme for this study, the computational domain is extended to the physical boundary, and the full set of elliptic mean flow equations is solved all the way to the wall. A one element thick layer of special elements is employed in the near-wall region between the fully turbulent outer flow field and the physical boundary. In these special near-wall elements, specialized shape functions are used to accurately capture the sharp variations of the mean flow variables in the viscosity-affected near-wall region. These specialized shape functions, which are based on universal near-wall profiles, are functions of the characteristic turbulence Reynolds numbers and adjust automatically during the course of computations to accurately resolve the local flow profiles. Since use is still made of the standard high Reynolds number k-ε turbulence model, the k and ε equations are not solved in the layer of special near-wall elements; instead, the variation of the turbulent diffusivities of momentum is modeled using the van Driest's mixing length approach. The variation of the turbulent viscosity μ_t can be defined as:

$$\mu_t = \rho l_m^2 \left[\left(\frac{\partial u_i}{\partial x_j} + \frac{\partial u_j}{\partial x_i} \right) \frac{\partial u_i}{\partial x_j} \right]^{1/2} \tag{6.16}$$

where l_m is the mixing length. For smooth walls l_m is obtained from van Driest's equation

$$l_m = \kappa\delta(1 - \exp(-y^+ / A)). \tag{6.17}$$

Where A is an empirical constant which assumes a value of about 26 for the smooth wall in the equilibrium near-wall layers, κ is a Von Karman constant with a value of 0.41, and y^+ is the dimensionless normal distance from the wall defined in terms of the turbulent kinetic energy at. the top of the element, viz.,

$$y^+ = \frac{\rho(c_\mu^{1/2}k)^{1/2}}{\mu} \tag{6.18}$$

The special element basis (or shape) functions of 3 nodes in the n direction are defined as

$$\begin{aligned} \varphi_1 &= -n(1 - A(n)) \\ \varphi_2 &= 1 + n - 2nA(n) \\ \varphi_3 &= nA(n) \end{aligned} \tag{6.19}$$

where A(n) is the expression based on the universal profiles of semi-empirical form of Reichardt law. For interpolating velocities,

$$A(n) = A_1(n)/A_2 \tag{6.20}$$

where,

$$A_1(n) = (1/\kappa)\ln\left[1 + (\kappa/2)\Delta^+(1+n)\right] + 7.8[1 - \exp(-\Delta^+(1+n)/22) -$$

$$\Delta^+(1+n)\exp(-0.165\Delta^+(1+n)/22)] \tag{6.21}$$

$$A_2 = A_1(n=1) \tag{6.22}$$

where Δ^+ is the dimensionless characteristic height of the element in the n direction, defined by

$$\Delta^+ = \rho(c_\mu^{1/2}k)^{1/2}\Delta/\mu \tag{6.23}$$

where Δ is the actual average dimensional height of the element above the wall and k, the turbulent kinetic energy at the top of the element where n=1. Δ^+ may alternatively be thought of as the characteristic element turbulent Reynolds number. The larger this number, the thinner the viscous sublayer will be with respect to the height of the special element.

In this study, the computational domain for the mean flow equations encompasses the entire flow domain down to the solid boundary whereas the corresponding computation for the k and ε equations of the k-ε turbulence model only extends to the top of the special near-wall elements. The appropriate boundary conditions are applied for k and ε in near-wall methodology which are

$$\frac{\partial k}{\partial n} = 0 \tag{6.24}$$

and

$$\varepsilon = \frac{(c_\mu^{1/2} k)^{1.5}}{\kappa\delta} \tag{6.25}$$

These indicate the equilibrium turbulence conditions in the near-wall regions where k is a constant and the turbulence length scale, defined as $k^{1.5}/\varepsilon$, varies linearly with normal distance from the wall. The above Neuman boundary condition on k plays a pivotal role in the entire near-wall methodology. At the end of each iteration, the value of k is used to arrive at a characteristic turbulence velocity scale of the near-wall region which determines the magnitudes of the local elemental Reynolds/Peclet numbers which in turn control the degree of skewing in the special basis functions for an accurate resolution of the local near-wall flow profiles. In order to use this method properly, it requires that viscous and

transitional sublayers are fully contained within the special near-wall elements. Hence elemental Reynolds number Δ^+ in all special elements must not be significantly less than 30. If it is lower than 30 over significant portions of the computational boundary, then a further simulation must be performed using a coarser grid in the direction normal to the wall.

6.4 Formulation of the Discrete Problem

The objective of the Finite Element Method (FEM) is to reduce the continuum problem (infinite number of degrees of freedom) to a discrete problem (finite number of degrees of freedom) described by a system of algebraic equations.

The finite element procedure begins with the division of the continuum region of interest into a number of simply shaped regions called elements. Within each element, the dependent variables such as u_i and p are interpolated by function of compatible order, in terms of value to be determined at a set of nodal points. For the purpose of developing the equations for these nodal point unknowns, an individual element maybe separated from the assembled system.

Within each element, u, p, k and ε field are approximated by

$$\begin{aligned} u_i(x,t) &= \varphi^T U_i(t) \\ p(x,t) &= \psi^T P(t) \\ k(x,t) &= \varphi^T K(t) \\ \varepsilon(x,t) &= \varphi^T E(t) \end{aligned} \tag{6.26}$$

where U_i, P, K and E are column vectors of element nodal point unknowns and φ and ψ are column vectors of the interpolation functions. Substitution of these approximations into the field equations and boundary conditions yields a set of equations:

$$f_1(\varphi,\psi,U_i,K,E,P) = R_1 \qquad \text{Momentum} \qquad (6.27)$$

$$f_2(\varphi,U_i) = R_2 \qquad \text{Mass conservation} \qquad (6.28)$$

where R_1 and R_2 are the residuals (errors) resulting from the use of the approximations of equation (6.26). The Galerkin form of the Method of Weighted Residuals seeks to reduce these errors to zero, in a weighted sense, by making the residuals orthogonal to the interpolation functions of each element (i.e., φ, ψ).

Of central importance to the development of a finite element program is the choice of the particular element to be included in the element library. Elements for fluid flow are usually categorized by the combination of velocity-pressure approximation used in the element. In this study, the four node quadratic and two dimensional elements are employed. The interpolation (or shape, or basis) function is prescribed by normalized a coordinate r and natural coordinate s. The value of r and s range from -1 to +1. For the four node quadrilateral element, the velocity component u_i is approximately prescribed by bilinear shape function, viz.,

$$\varphi = \begin{bmatrix} 1/4(1-r)(1-s) \\ 1/4(1+r)(1-s) \\ 1/4(1+r)(1+s) \\ 1/4(1-r)(1+s) \end{bmatrix} \qquad (6.29)$$

It is possible to use two types of pressure discretizations with this element: a bilinear continuous approximation with the pressure degree of freedom located at the

nodes on four corners; or a piece wise constant discontinuous pressure approximation where pressure degree of freedom located at the centroid of the element.

6.5 Simulation of Free Jet Flow Impinging on a Flat Target Using k-ε Model

As derived in Art. 6.2 the governing equations employed for the steady two dimensional compressible, isothermal turbulent free jet without consideration of body forces using k-ε turbulence model can be written as follows:

$$u_{i,j} = 0 \tag{6.30}$$

$$\rho u_j u_{i,j} = -p_{,i} + [\mu(u_{i,j} + u_{j,i})]_{,j} \tag{6.31}$$

$$\rho u_j k_{,j} = (\frac{\mu_t}{\sigma_k} k_{,j})_{,j} + \mu_t (u_{i,j} + u_{j,i}) u_{i,j} - \rho\varepsilon \tag{6.32}$$

$$\rho u_j \varepsilon_{,j} = (\frac{\mu_t \varepsilon_{,j}}{\sigma_\varepsilon})_{,j} + \frac{c_1 \varepsilon \mu_t (u_{i,j} + u_{j,i}) u_{i,j}}{k} - \frac{c_2 \rho \varepsilon^2}{k} \tag{6.33}$$

where $\mu = \mu_0 + \mu_t$ and $\mu_t = \rho c_\mu k^2 / \varepsilon$. The above equations contain empirical constants $c_1, c_2, \sigma_k, \sigma_\varepsilon$ and c_μ. Over the years, the k-ε model has been tested, optimized and fine tuned against a wide range of flows of practical interest. For the turbulent free jet in this study, the recommended set of empirical constants has selected as: c_1=1.44, c_2=1.92, σ_k=1.00, σ_ε=1.30 and c_μ=0.055 (Rodi and Spalding, 1983).

The application of Galerkin finite element discretization to the governing equations results in a set of nonlinear algebraic equations which has the matrix form

$$\mathbf{K(X)X=F} \tag{6.34}$$

where **K** is the global system matrix, **X** is the global unknown vectors (i.e., velocities, pressures, etc.) and **F** is a vector of boundary conditions and body forces.

6.5.1 Modeling Two-Phase Flow

The simulation of two-phase flows necessitates a mathematical model which appropriately extends the classical system of equations of the single-phase flow. In this study Lagrangian approach for two-phase flow modeling is used to model AWJ. It has proven to be particularly successful in simulating aerosols, atomizers, spray drying, spray combustion, pollutant dispersion and filtration, and so forth. A major advantage of the lagrangian approach is that it allows the particles of the dispersed phase to be of different sizes. The underlying concept is what is usually called dispersed two-phase flow, or particulate two-phase flow. The conception here is that one of the phases (abrasive) is dispersed throughout the other phase (waterjet), and the latter, roughly speaking, acts as the "carrier" of the former. At the same time, strong coupling occurs between the phases. The Lagrangian model represents the dispersed phase by a continuous stream of particles moving through the carrier phase at a certain mass flow rate and coexisting with it. The conservation equations for the carrier phase are described by the standard Eulerian equations, while the motion of the particle is described in a Lagrangian frame of reference. The information transfer between phases is accounted for by the momentum along the particle paths. The motion of the particles is determined by local force; the particles have enough time to respond to these forces before colliding with other particles. This, in turn,

means that information between phases is carried along trajectories rather than by pressure waves.

6.5.2 Theoretical Model of Dispersed Phase

The motion of each particle of the dispersed phase is governed by an equation that balances the mass-acceleration of the particles with the forces acting on it. For a particle of density ρ_p and diameter D_p the relevant governing equation is

$$\rho_p \frac{du_i^p}{dt} = \frac{1}{\tau}(u_i - u_i^p) + (\rho_p - \rho)g_i + \rho_p f_i^p \tag{6.35}$$

where u_i^p is the particle velocity, u_i is the velocity of the fluid (i.e., the carrier phase), f_i^p is the combination of forces acting on the particle, and τ is the particle relaxation time, defined by

$$\tau = \frac{4\rho_p D_p^2}{3\mu C_D \operatorname{Re}^p} \tag{6.36}$$

where μ is the viscosity of the fluid, Re^p is the particle Reynolds number defined by

$$\operatorname{Re}^p = \frac{D_p \left| u_i - u_i^p \right| \rho}{\mu} \tag{6.37}$$

and C_D is the drag coefficient. The first term on the right hand side of (6.35) is a generalization of the classical Strokes drag on a particle. A number of models have been proposed on the literature, mostly empirically based. Among the more commonly used models are the polynomial model:

$$C_D \operatorname{Re}^p = 24(a + b\operatorname{Re}^p + c(\operatorname{Re}^p)^2 + d / \operatorname{Re}^p) \tag{6.38}$$

where a, b, c, and d are constants.

The second term on the right of (6.35) is important in simulating sedimentation of solid particles in liquid. The force that appears as the third term on the right of (6.35) may be a combination of several force that appear in particulate motion in fluid.

As regards the particulate phase, there is also the kinematics equation, namely

$$\frac{dx_i^p}{dt} = u_i^p \tag{6.39}$$

where x_i^p is the position coordinate of the particle at time t. A particle trajectory is obtained by the solution of the particle momentum equation (6.35) coupled with the equation (6.39).Each distinct solution of the pair of equations (6.35) and (6.39), i.e., each set of initial conditions, each different size of particle, defines a distinct trajectory.

6.5.3 Turbulence Model of Particle Trajectories

A stochastic model based on the works of Gosman and Ioannides (1981) was used to model the influence of, turbulent fluctuation on particle trajectories. The instantaneous velocities U_∞ in the carrier phase are used to solve the particle velocities. These instantaneous characteristics are computed by adding random fluctuations to the mean flow solutions $\overline{U}$ obtained from a k-ε simulation. These instantaneous characteristics are computed as follows:

$$U_\infty = \overline{U} + \lambda u' \tag{6.40}$$

and

$$u' = (\frac{2}{3}k)^{1/2} \tag{6.41}$$

where λ is a random number between -1 and 1 sampled from a normal distribution. The motion of each particle is traced as it interacts with a succession of turbulent eddies. The interaction time with one fluid eddy is limited by the eddy life time T_e, or the time needed for the particle to traverse the eddy T_t. After each interaction, a new fluctuation is assumed to act on the particle which means that the particle enters a new eddy. In this model, the eddy life and the transit time are computed by:

$$T_e = \frac{L_e}{\sqrt{(\frac{2}{3}k)}} \tag{6.42}$$

and

$$T_t = -2\ln\left[1 - \frac{L_e}{\tau\left|u_\infty - u_p\right|}\right] \tag{6.43}$$

where L_e is the eddy characteristic size $L_e = \frac{c_\mu^{3/4} k^{3/2}}{\varepsilon}$.

It is recognized now that the presence of the particulate phase affects the continuum phase by transfer of momentum from the former to the latter.This momentum transfer is due to the relative drag between the phases. This is quantified by means of the Particle Source in Cell (PSIC) method: the computed trajectories of the particles are combined into source terms for momentum, which are then inserted into the right-hand sides of the continuum equations (6.31) as following:

$$\rho u_j u_{i,j} = p_{,i} + [\mu(u_{i,j} + u_{j,i}) \ - \rho \ \overline{u_i u_j}]_{,j} + \Phi_i^M \tag{6.44}$$

where $\Phi_i^M(E)$ is source term. For each element E it is defined as

$$\Phi_i^M(E) = \frac{1}{V_E}\sum_{j=1}^{n_E}\eta_j\int_{\delta t_j^E}\frac{3\mu C_D \operatorname{Re}^p V_p}{4D_p^2}(u_i - u_i^p)dt \tag{6.45}$$

where V_E is the volume of the element and V_p is the volume of the particle, η_j is the number of particles per unit time traversing the jth trajectory and δt_j^E is the time that a particle on the jth trajectory takes to pass through element E.

6.6 Solution Procedures

At present, there are mainly two different solution methodologies utilized for solving the nonlinear equation system. The first approach solves all conservation equations in a simultaneous coupled manner, while the second approach solves each equation separately in a sequential segregated manner. Here, a segregated algorithm with implicit time integration is used in the numerical solution of the discretized equations which result from the application of the Galerkin finite element scheme to the flow governing equations. In this approach, the global matrix system is never directly constructed. Instead, the discretized implicit equations associated with each primary flow variables are assembled in smaller sub-matrices. It uses mixed velocity-pressure formulation. At the beginning of an iteration, an approximation to the pressure is obtained from the solution of the Poison type pressure matrix using latest available values of the field variables. The various components of the momentum equations and any other conservation equations presented in the flow problem are then solved in a sequential manner using the most recent field variables. Finally, at the end of each iteration the velocity field is mass adjusted via an irrotational projection onto a divergence free sub-space. This last step involves the solution of a

further Poisson type matrix equation for a pressure corresponding vector Δp. The implicit segregated algorithm employed in this numerical simulation needs a relaxation factor of 0.5 for the equations of mean velocities, k and ε.

The density of the computational domain is varied to make the solution grid independent. The density of the mesh is reasonably re-adjusted to avoid "wiggle" if spurious spatial oscillations exists in the flow variable because of the large grid Renolds number. Numerical techniques of streamline upwinding and clipping are used to supress solution instabilities.

The solution procedure used in the Lagrangain two-phase flow model is an iterative one. First, a solution to the governing continuum equation (6.44) with source term set equal to zero for the carrier phase is obtained. The solution u_i of the equation is then inserted into the Lagrangain equations (6.35) which is then integrated together with the trajectory equation (6.39). From these solutions the source terms are compiled from the formulas (6.45) and the values are then substituted back into (6.44). The procedure is repeated until convergence is attained.

6.7 Convergence Criteria

Since the segregated algorithm is used in solving the equations, an appropriate convergence criteria is employed to terminate the iteration. Two important variables for use in designing termination criteria are the solution vector $\mathbf{u}_i$ (at iteration i) and the residual vector $R(\mathbf{u}_i)$. It is of course desired that $\mathbf{u}_{i-1}$ be within a given tolerance, ε_u, of the

accurate solution vector u at the end of each iteration. Hence, a realistic convergence criterion, depended on relative error, is defined as

$$\frac{\|\Delta u_i\|}{\|u\|} \leq \varepsilon_u \tag{6.46}$$

where $\Delta \mathbf{u}_i = \mathbf{u}_i - \mathbf{u}$, and $\|\bullet\|$ is an appropriate norm. Since u is not known at first, this value must be approximated, and the obvious selection is $\|u\|$ replaced by $\|u_i\|$ in above equation and u by $\mathbf{u}_{i-1}$ in the expression of $\Delta \mathbf{u}_i = \mathbf{u}_i - \mathbf{u}_{i-1}$.

Another more suitable convergence criterion which depends on the residual vector and tends to zero with $\mathbf{u}_{i-1}$ tending to u, is also employed in this numerical solution. Such a criterion is defined as

$$\frac{\|R(u_i)\|}{\|R_0\|} \leq \varepsilon_f \tag{6.47}$$

where $R_0 = R(u_0)$, is a reference vector.

Both of these two checks are used in the involved numerical solutions which provides an effective overall convergence criterion for all possible situations, since both $\Delta \mathbf{u}_i$ and $R(\mathbf{u}_i)$ tend to zero near the solution. In this study, the solution is considered to be convergent if the normalized residuals are smaller than 0.001.

6.8 Problem Description

In order to simplify the study, the following assumptions are made:

- Round waterjet is a two-phase, steady, incompressible and isothermal turbulent flow.
- All particles are assumed to be spherical.

- There is no transfer of mass and heat between the two phases.
- The dispersed phase is sufficiently dilute, and thus, particle-particle interactions are neglected.
- The interfacial force between the two phases is negligible.

6.8.1 Computational Domain

In general, the computational domain of the two-dimensional obliquely impinging jet flow field involves the following three regions (Chuang and Wei 1991): the free jet region in which the flow is essentially the same as that of a jet issuing into an unbounded region; the impingement region in which the flow changes direction with a large pressure gradient; and the wall-jet region in which the flow traverses the target surface.

In theoretical analysis of the structure of the high-speed waterjet in air Yanaida and Ohashi (1978) suggested that the radius of the waterjet is related to the standoff distance x, as follows

$$r=Cx \tag{6.48}$$

where C is the spreading coefficient and measured as 0.06. The computational domain was approximately determined by the above equation. When jet fans out on the target, a complicated three-dimensional flow pattern is formed. The problem can be approximately treated as the description of the behavior of a two-dimensional. Due to the dominant effect of the jet axial velocity on impingement conditions, the motion in Z-direction can be disregarded (Naib et al, 1988 and Chuang et al, 1991). The computational domain, the

boundary conditions and corresponding typical numerical grid used for description of the flow generated by the jet impinging on a flat plate at a small angle is shown

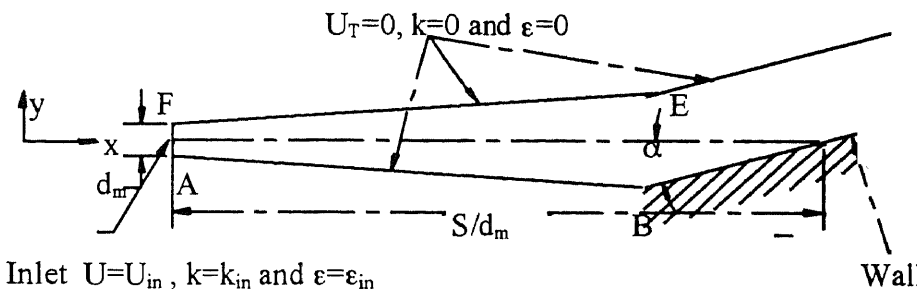

(a) Computation Model , Domain and Boundary Condition

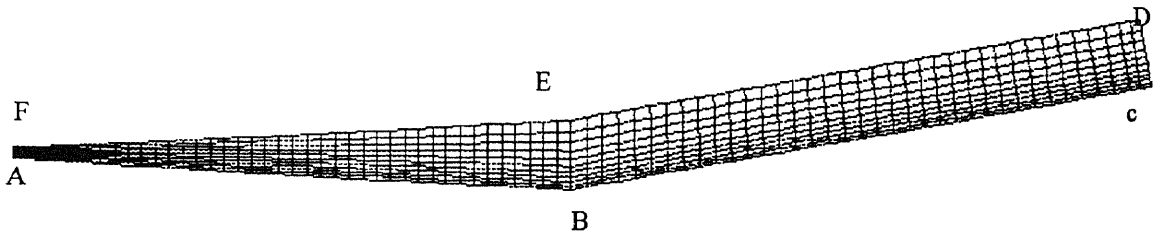

(b) Typical Numerical Mesh

Figure 6.1 Domain, boundary Conditions and Numerical Grid for the Simulation

6.8.2 Mesh Development and Boundary Conditions

The typical computational mesh comprises of 2760 4-node element; 69 along the axial of the jet and 15 across the jet width. The mesh has been selectively graded towards the wall of the target. In this way, finer grids near the wall are obtained for a better resolution of the sharp flow gradients in these critical region. The condition at the jet discharge AF where the flow is fully developed is important in predicting the centerline velocity and shear stress. The velocity profile at the nozzle exit is affected by the nozzle design. Based on our measurement, we found that the nozzle exit velocity has a power profile. In this study, therefore, the nozzle velocity profile is assumed to be the 5.5 power velocity profile which is a result of experimental measurements (Bradshow and Love, 1959), expressed as

$$U = U_0[1 - 0.3412(\frac{y}{r_N})^{5.5}] \tag{6.49}$$

where U is the stream wise velocity component in the x-direction at inlet plane, U_0 is velocity measured at the center of the inlet plane.

Boundary condition for k and ε are calculated as follows:

$$k=iu^2 \tag{6.50}$$

$$\varepsilon=2k^{3/2}/\lambda d_m \tag{6.51}$$

where, i is the turbulence intensity, λ is the length-scale constant, and d_m is the diameter of the mixing tube.

Outflow boundary CD is located fifteen diameters d_m of striking point downstream so as to allow the development of the flow in the downstream direction. At outlet plane no velocity boundary conditions are explicitly imposed, but Neumann (i. e. zero normal and tangential stresses and zero flux) boundary conditionat are specified on the outflow

boundary. Similarly, the turbulent kinetic energy k and dissipation ε are not specified at the outflow resulting in zero flux boundary conditions for both quantities.

The boundaries AB, DE and EF are external free boundary. The free boundary is defined as the position where the mean velocity starts to deviate from the velocity far away from the jet (Rodi and Spalding 1983). The average shear stress is zero at this point. This boundary does not coincide with the average position of the interface. At boundaries considered, the velocity of the liquid outside the boundary is, if we neglect the very small entrainment velocity, zero. Turbulence energy, k, and eddy viscosity, μ_t must therefore vanish at the boundary; so U and k are taken at theses boundaries equal to zero. Therefore the conditions on the boundaries are given as

$$U=0,\ k=0,\ \varepsilon=0 \tag{6.52}$$

At the target wall BC, no-slip and impermeable boundary conditions are imposed, thus we can assume that the velocity components have a zero value at the wall. Because the k-ε turbulence model is not valid for the description of the viscosity affected regions close to the wall, the wall shear stress and values of k and ε in the close proximity of the solid walls are modeled by the near-wall modeling approach.

6.8.3 Initial Condition

Non-zero initial guess for u, k and ε improves the convergence characteristic. In general the constant values of u, k, and ε which have been obtained from the above equations are used for the further computations. For profiles, the intermediate values are used as the initial guess.

6.8.4 Particle Characteristics

Each particle is injected with an initial velocity equal to the fluid phase velocity at the nodes of nozzle exit. The optimal value of the particles mass flow rate equal to 1.13e-3 kg/s (68 g/min.) is used for computations. Each set of particles is composed of 10 particles with diameters sampled from a Gaussian distribution obtained by Laser Scanning Sizer.

Particles are allowed to rebound on the target surface with an angle equal to the incidence angle or get trapped on it. And they may escape through other bounders.

6.9 Presentation and Discussion of Results

The numerical solutions of the equations representing the impinging annular jet are obtained in terms of the velocity u, the pressure p, the turbulent kinematics energy k and dissipation ε. The Reynolds number is defined by $U_0 d_m \rho / 2\mu$, where U_0 is jet centerline velocity at the nozzle inlet and d_m is diameter of the mixing tube.

In order to evaluate the accuracy of the developed computational technique, we determine the water velocity at the exit of the nozzle and compare the computed value with those determined experimentally by the use of the Laser Transitional Anemometer (Figure 6.2). The results of the comparison, depicted in Fig. 6.2 demonstrate a sufficient accuracy of the numerical technique used in this research. Our previous studies also show that the Bernoulli equation closely predicts water velocity at the nozzle exit as shown in Figure 6.2. The accuracy of the LTA was also demonstrated.

In order to understand the features of the flow field, it is expedient to present the contour plots of stream function and pressure. Figures 6.3 to 6.6 show the streamline flow

pattern and contour of pressure of two-phase jet at the impact angles of 3, 5, 10, 15 and 20 degree and dimensionless standoff distances S/d_m of 30, 50, 70 and 90 separately. It can be observed that streamline completely parallel the target surface at near-zero angle (a), while streamline at very beginning of jet impacting the target become curve. The pressure contour at various impinging angles (Figure 6.4) shows that the pressure along the surface of the target is up with an increase in the angle. Comparison of the patterns of streamline of WJ (Figure 6.7 and 6.8) and AWJ (Figures 6.3 and 6.4) shows that there is no visible difference in streamline and pressure contour for both flows.

Figure 6.9 shows the decay of the axial centerline velocity as a function of distance along the jet. Note agreement within 5% between the computed axial centerline velocity and the experimental results. Figure 6.10 shows radial velocity against radial distance and compares the numerical and experimental results with experiments. The compliance between numerical and experimental data is reasonably good. The agreement between the values of the forces exerted on the substrate surface determined numerically and experimentally is shown on Figure 6.11. The presented results show feasibility to predict velocity and forces in the impingement zone and control impact conditions.

The trajectories of individual particles impacting the substrate and moving along the target are very complicated, and depend on impact conditions (velocity, angle, site). In order to assess and design an intelligent process of polishing, it is necessary to predict the details of impact (force, post impact trajectory etc.) for individual particles. This information, will enable us to understand mechanism of erosion and to optimize process conditions.

In the final analysis the process of polishing is carried out by particles which flow along the substrate surface at the distance which is less than the height of peaks. Figure 6.12 to 6.14 shows the simulation results of particle trajectories at impinging angles of 3, 10 and 20 degree and S/d_m=70 and describes the abrasive erosion pattern at different impinging angles, which take place in the course AWJ polishing processes. Generally particles move following the stream line of the carried fluid due to the drag force specified in the model and the effect the flow field on the particle trajectories are obvious. As a result, x-component of the vector velocity is equal to that of the main flow. It can be also observed that particle trajectories are of fluctuation due to feature of turbulent flow and these trajectories are relatively independent. With the reduction of jet impinging angle against the target plate, more particles move along the surface parallel or at a small angle.

As it is shown in Figs 6.12 to 6.14, there are five modes of particles motion after the jet impingement. (1) A particle can move along surface at the very close distance (Figure 6.12 a, b and c and Figure 6.13 g and h). These particles actually perform polishing. (2) A particle can for some times move at a distance from the substrate, but eventually enter subsurface layer(Figure 6.12 d and e and Figure 6.13 h). These particles also carry out polishing although not so intensively as the former. (3) A particle can be embedded into the substrate at the impingement site (Figure 6.13 a and b and Figure 6.14 a) or rebounded from the surface with a large strike angle (Figure 6.14 d and 6.13 d, i and j). This phenomena however occurs only at a comparatively large impact angle. The particles which are embedded at the impingement site increase the surface roughness and might induce a surface defect. (4) Particles can move along the surface at the distance

exceeding the heights of the peaks (Figure 6.13 a , c and d and Figure 6.14 a, b and). These particles have no effect, positive or negative, on the surface roughness. Finally, (5) a particle can move at the distance from the surface and eventually reenter the sub-surface layer and be embedded into the material (Figure 6.13 e and f and Figure 6.14 c). These particles also increase the surface roughness.

It is obvious that at a low impact angle a number of particles moving in close vicinity of the surface is much larger than that of the large impact angle, while number of embedded particles increases with the increase of this angle.

In addition to particles the water flow along the surface also results in the destruction of the peaks. The shear stress developed at the flow-substrate boundary characterize the wear of the surface due to water flow which brings about wear destruction of peaks. The value of tangential forces can be evaluated by the skin friction coefficients at jet-workpiece interphase. As shown in Fig. 6.15, the skin friction coefficient are maximal for α=3 degree., while the minimal friction is developed at α=20 degree. At the impact angle of 10 degrees the value of the skin friction coefficient has an intermediate value. These results show, because water flow has some contribution to the peaks destruction, the optimal polishing conditions are attained at a non-zero impact angle. Probably the optimal value of α, accounting for both water and particles effect is 3 degrees.

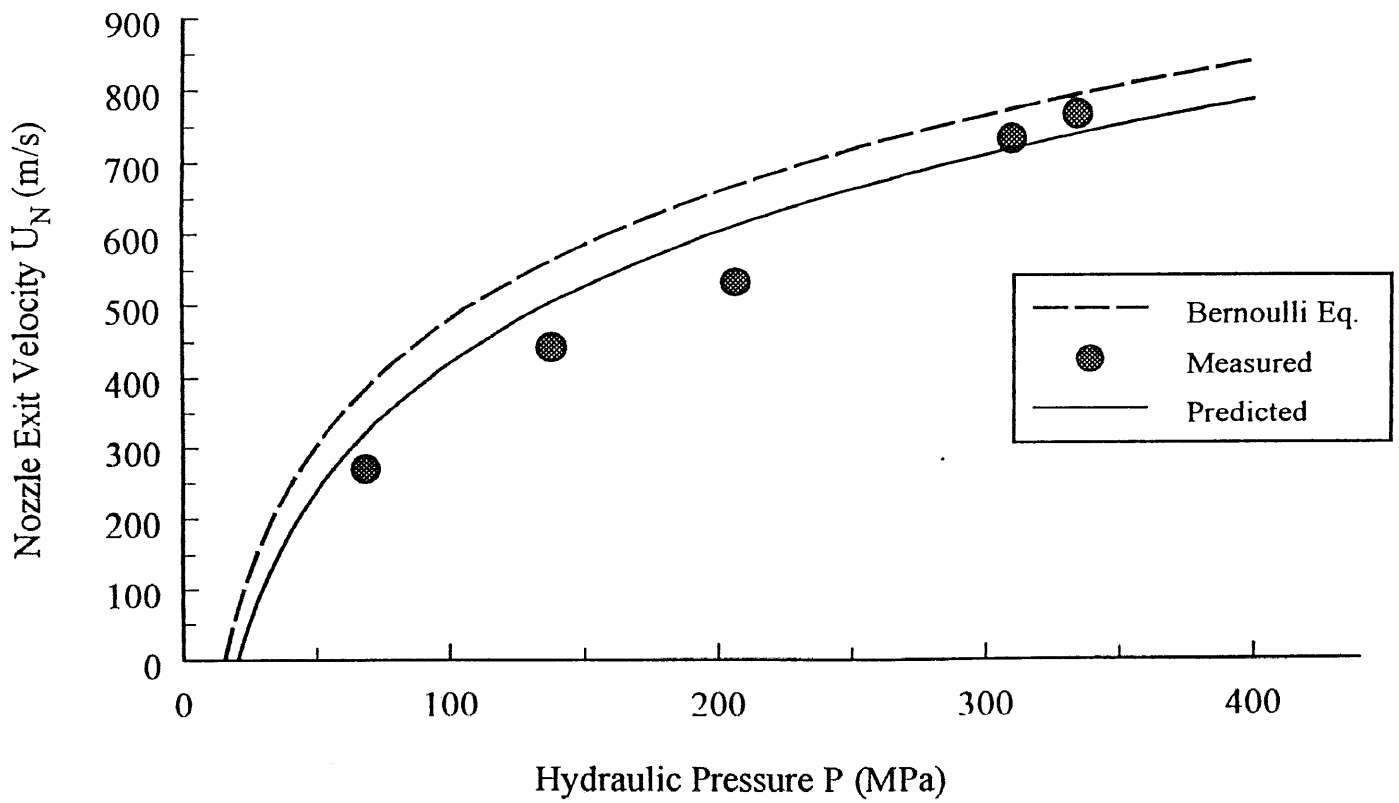

Figure 6.2 Calculated and Measured Nozzle Exit Velocity as a Function of Hydraulic Pressure

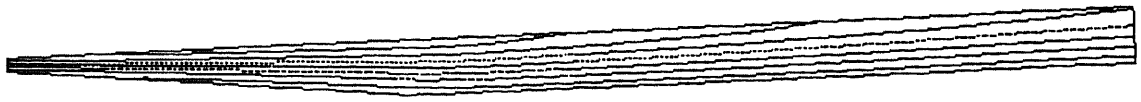

(a) α=3

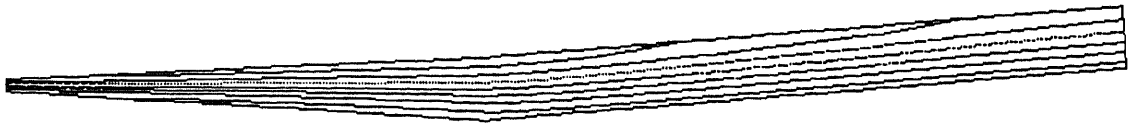

(b) α=5

(c) α=10

(d) α=15

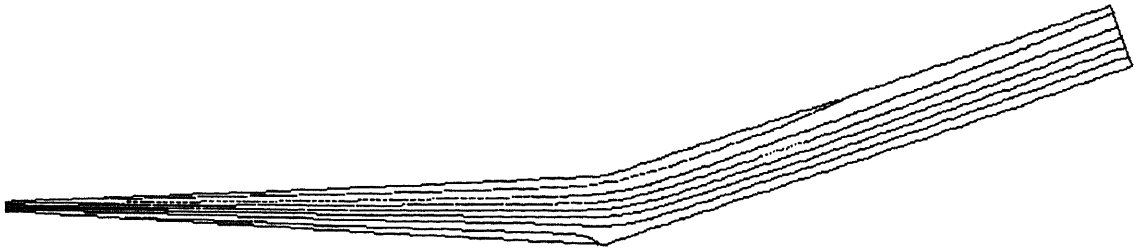

(e) α=20

Figure 6.3 Streamline Flow Pattern for Various Impinging Angles in Course of AWJ Polishing Processes ($S/d_m = 70$)

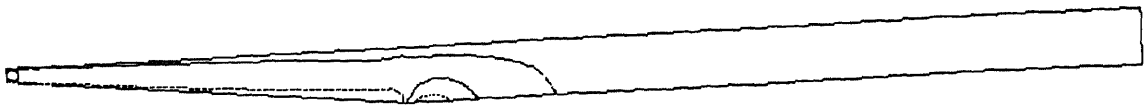

(a) $\alpha = 3$

(b) $\alpha = 5$

(c) $\alpha = 10$

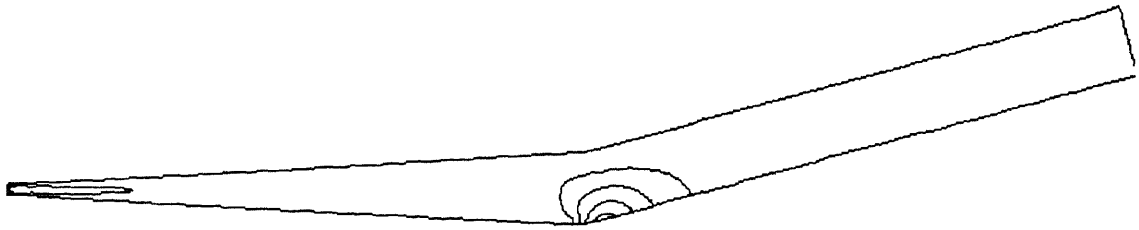

(d) $\alpha = 15$

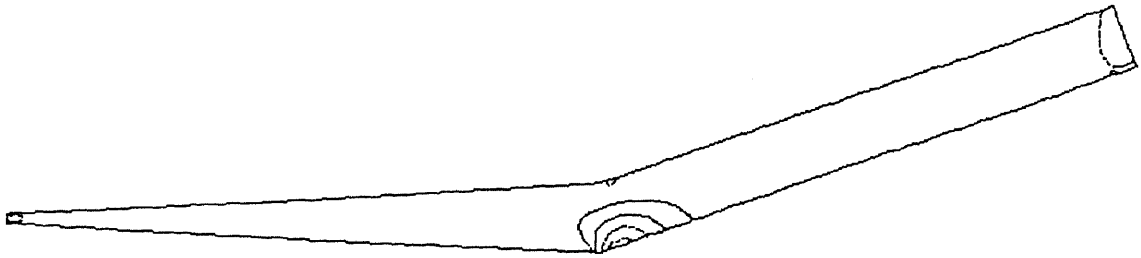

(e) $\alpha = 20$

Figure 6.4 Pressure Contour for Various Impinging Angles in Course of AWJ Polishing Processes ($S/d_m = 70$)

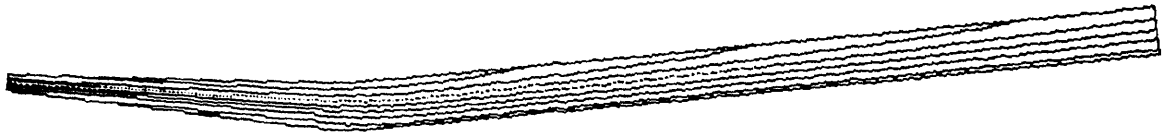

(a) $S/d_m = 30$

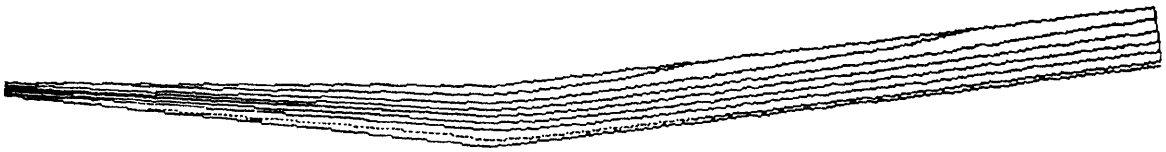

(b) $S/d_m = 50$

(c) $S/d_m = 70$

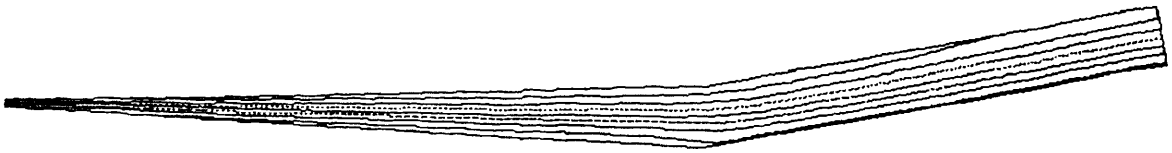

(d) $S/d_m = 100$

Figure 6.5 Streamline Flow Pattern for Various Stand-off Distance in Course of AWJ Polishing Processes (α=10 degree)

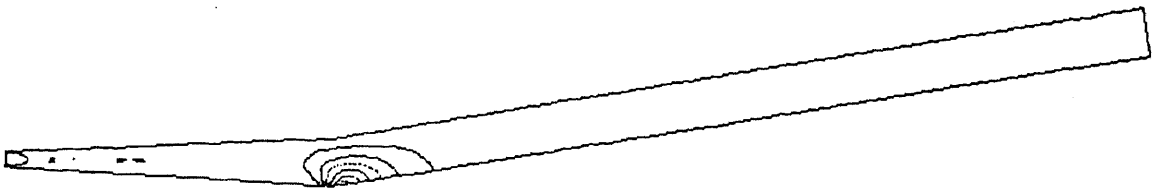

(a) $S/d_m = 30$

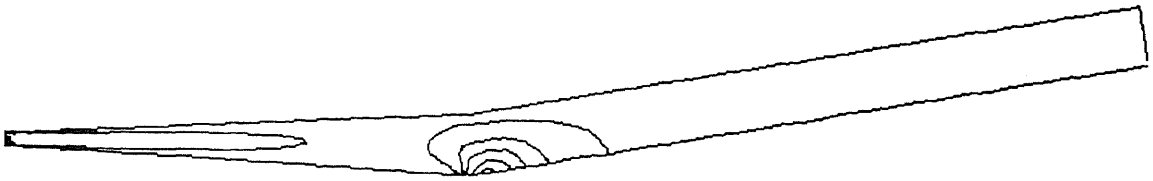

(b) $S/d_m = 50$

(c) $S/d_m = 70$

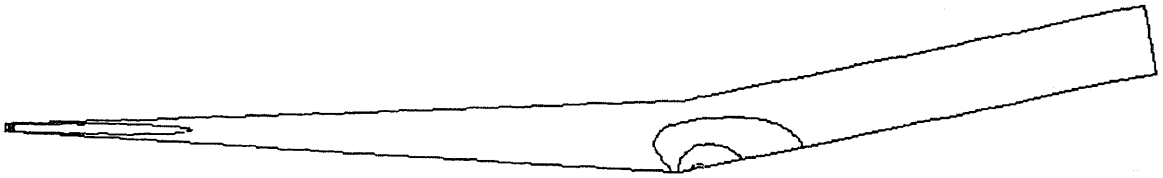

(d) $S/d_m = 100$

(e) $S/d_m = 130$

Figure 6.6 Pressure Contour for Various Stand-off Distance in Course of AWJ Polishing Processes (α=10 degree)

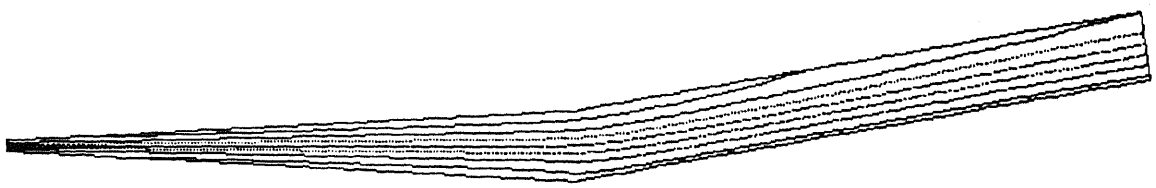

α=10

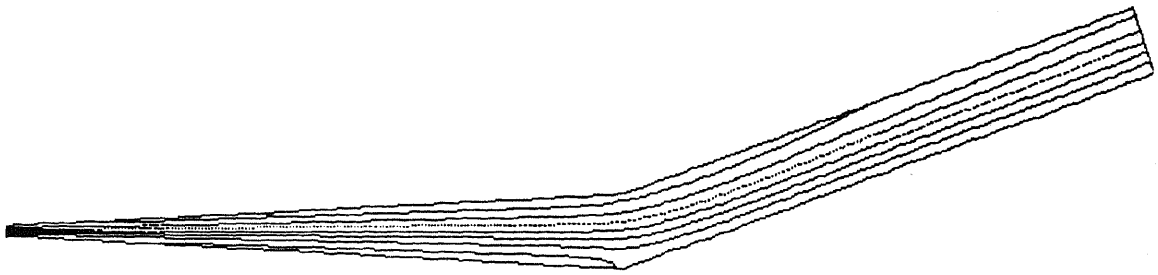

α=20

Figure 6.7 Streamline Flow Pattern of Waterjet at Various Impinging Angles (S/d_m = 70)

α=10

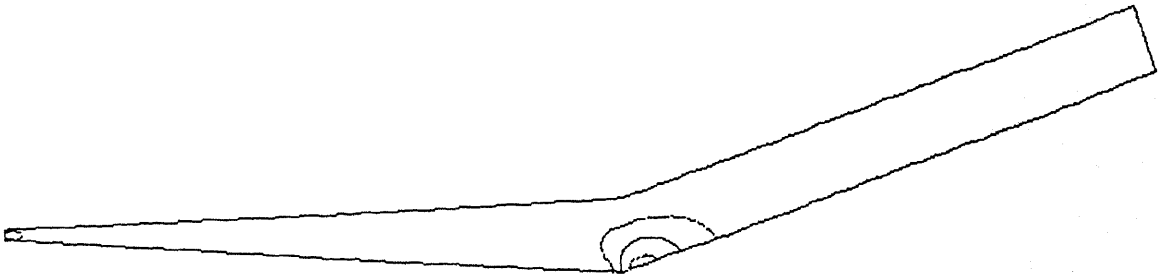

α=20

Figure 6.8 Pressure Contour of Waterjet at Various Impinging Angles (S/d_m = 70)

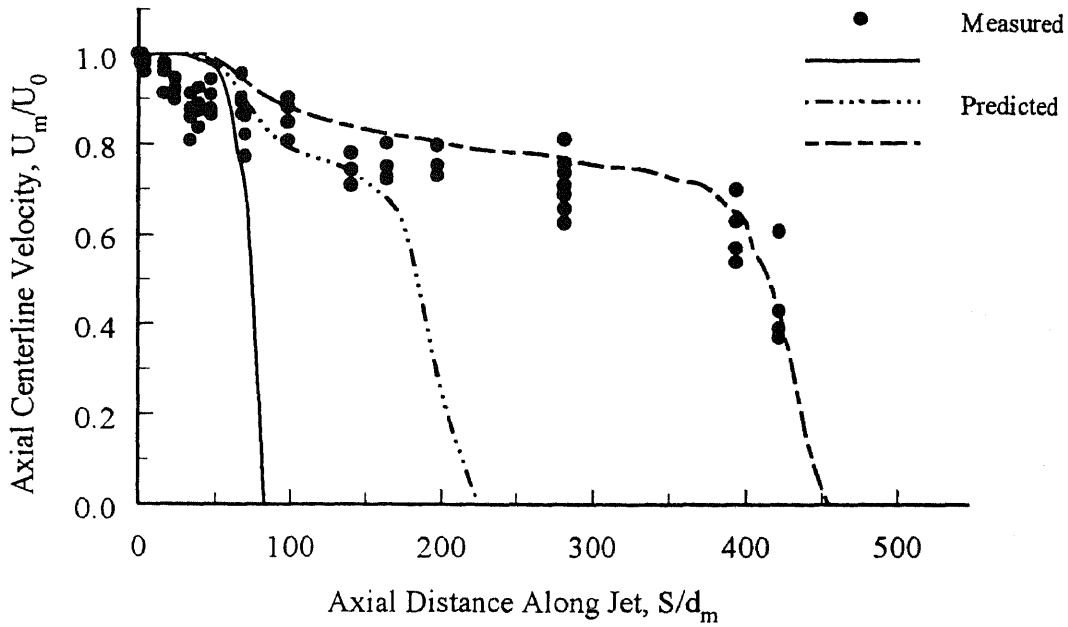

Figure 6.9 Decay of Axial Centerline Velocity for An Jet impinging on a Flat Plate U_m=Axial Centerline Velocity, U_0=Axial Velocity at Exit of Nozzle, S=Stand-off Distance and d_m=Diameter of Mixing Tube

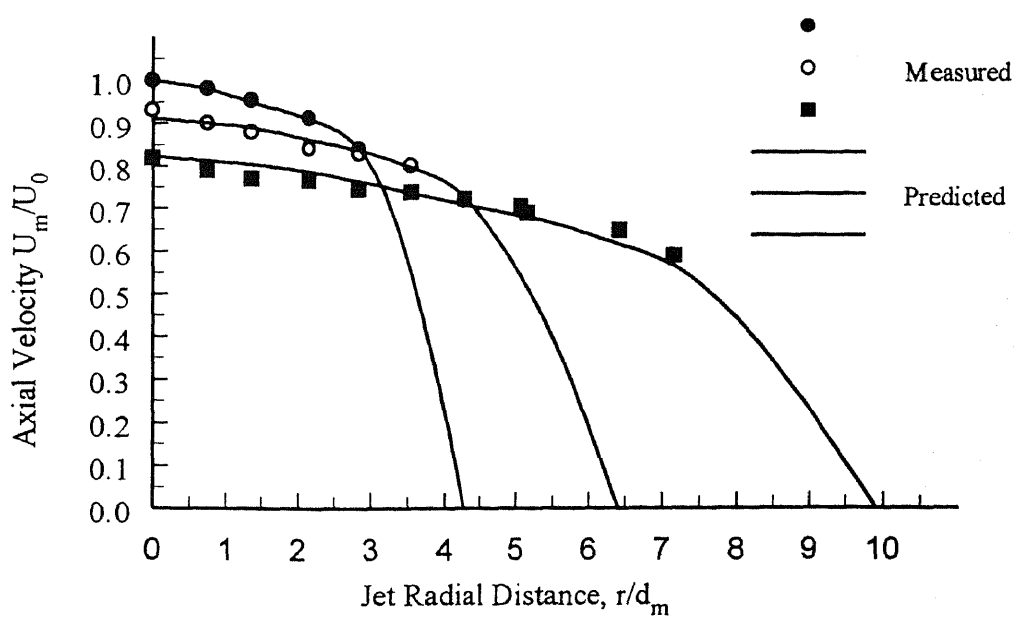

Figure 6.10 Axial Velocity Distribution Along Radial Distance
U_m=Axial Centerline Velocity, U_0=Axial Velocity at Exit of Nozzle, S=Stand-off Distance d_m=Diameter of Mixing Tube and r=jet radial Distance

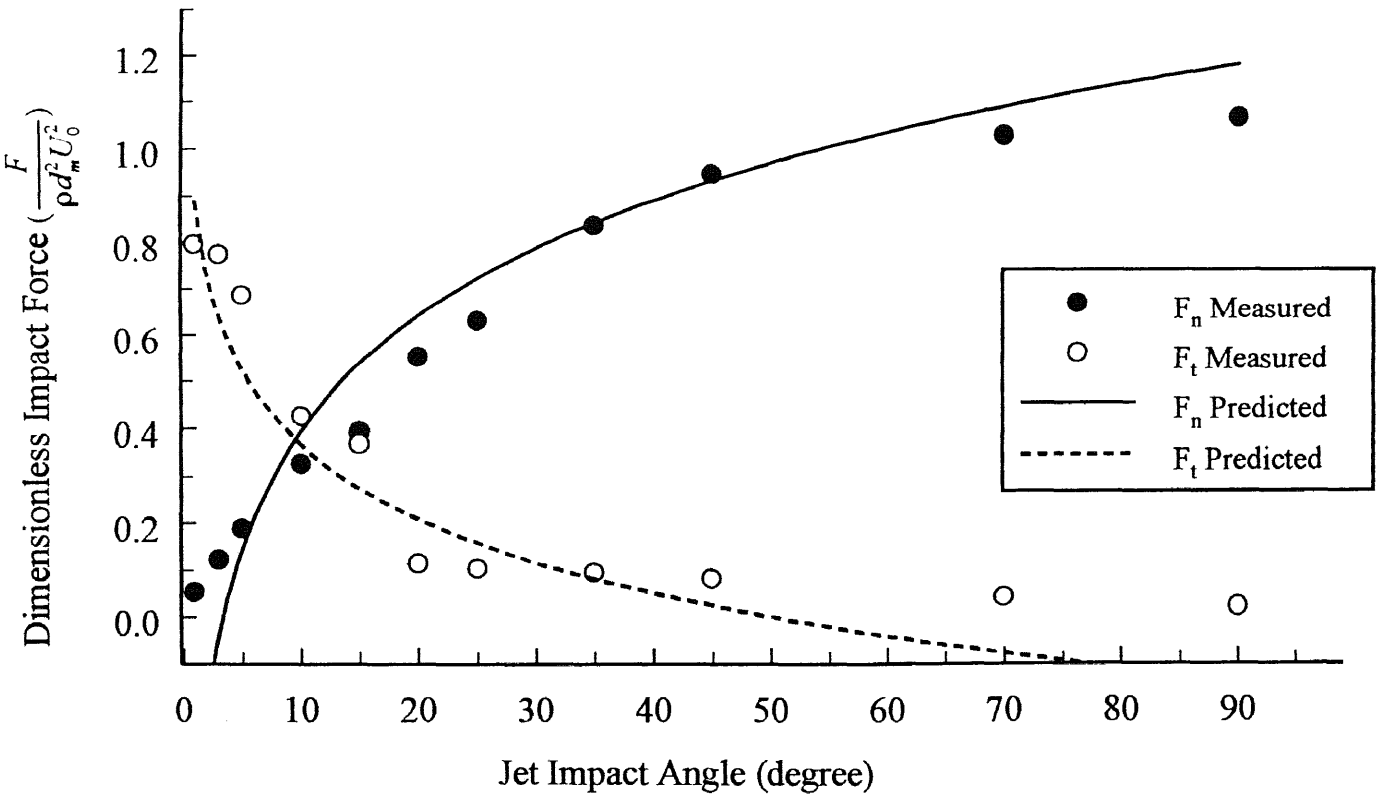

Figure 6.11 Numerical Prediction of Tangential (F_t) and Normal (F_n) Force Developed on the Target Surface by AWJ at Various Impact Angles

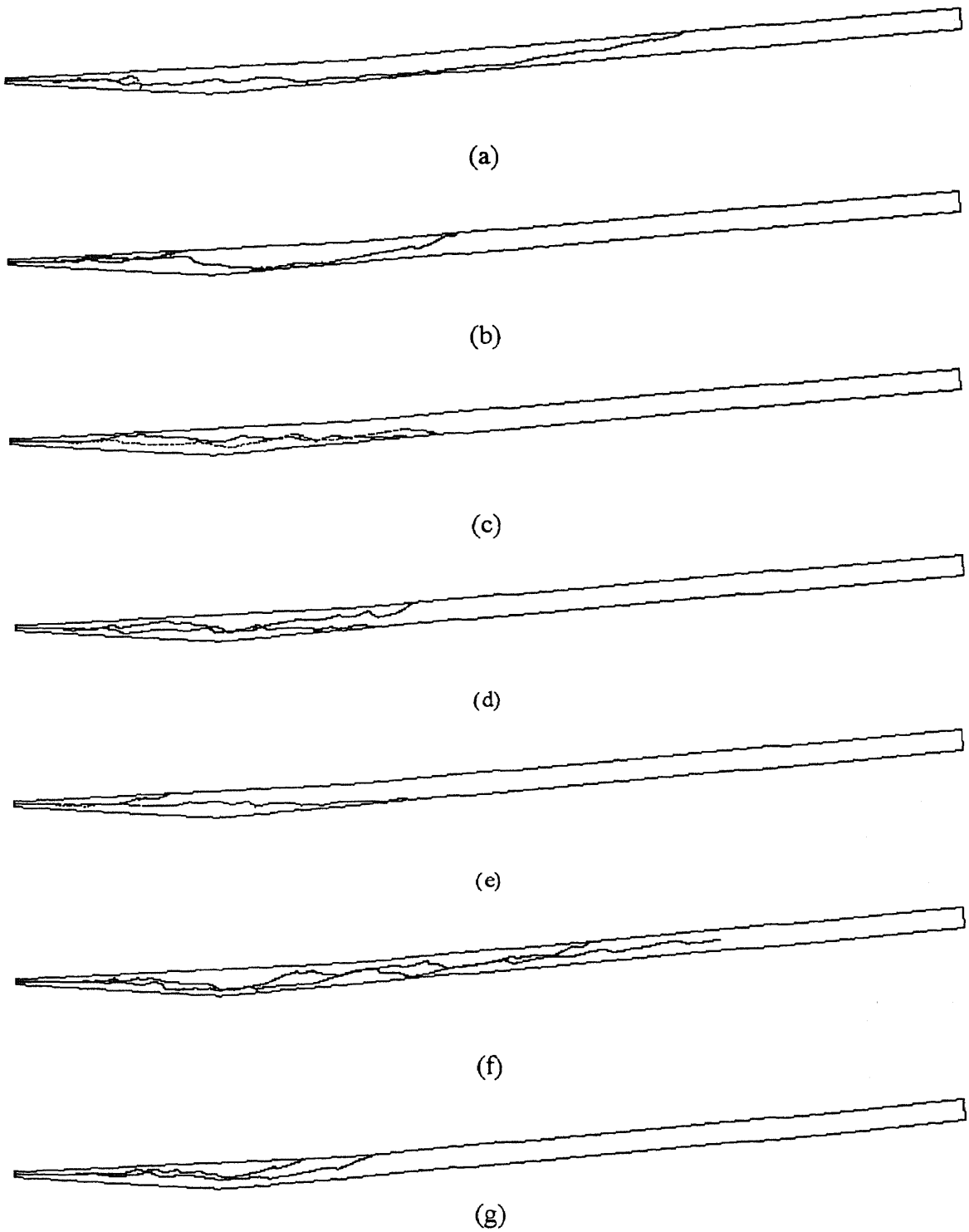

Figure 6.12 Particle Trajectories for Jet Impinging Angle of 3 degree in Course of AWJ Polishing Processes with d_p=100 micron, P=76 MPa, M_a=68 g/min. and S=178 mm

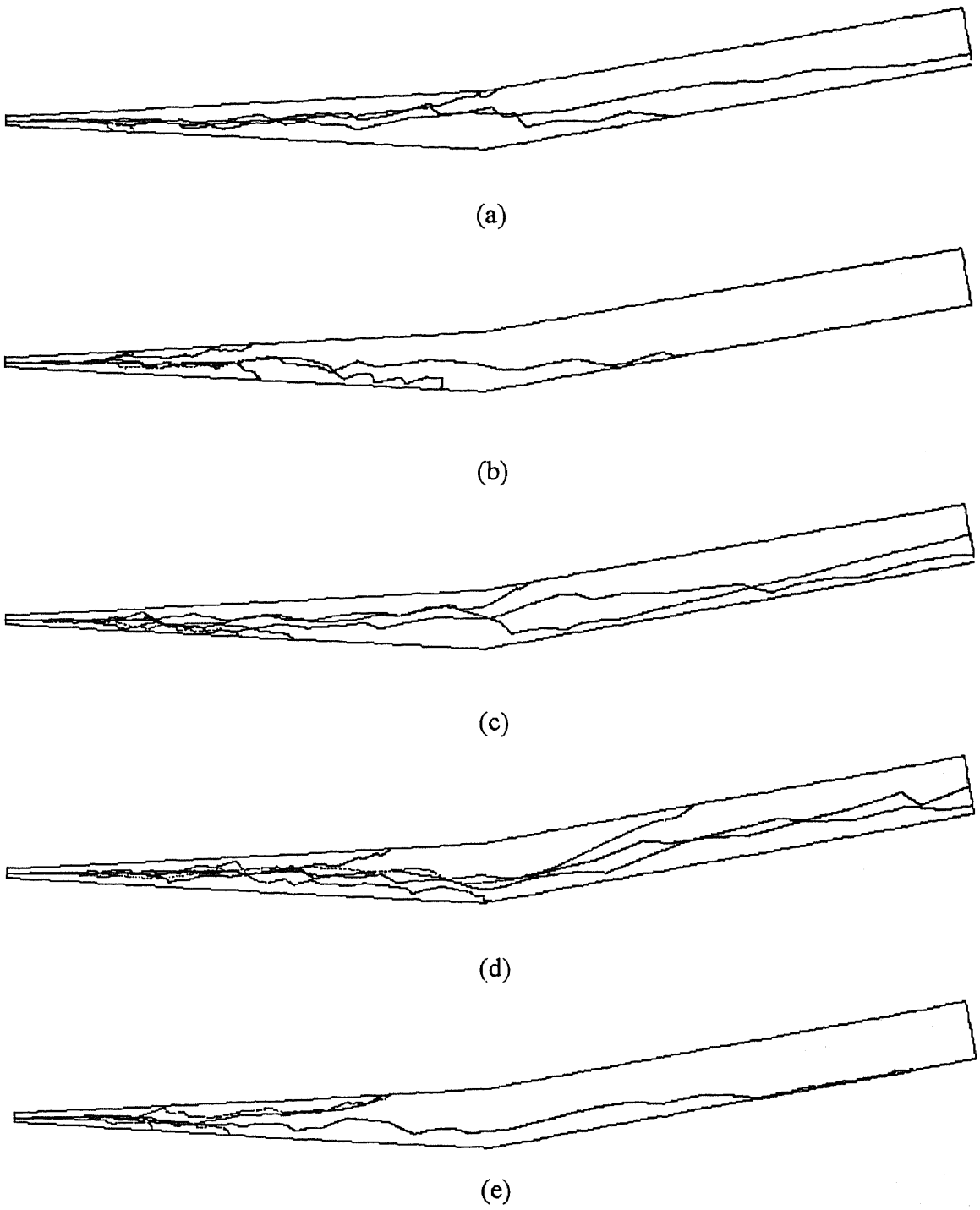

Figure 6.13 Particle Trajectories for Jet Impinging Angle of 10 degree in Course of AWJ Polishing Processes with d_p=100 micron, P=76 MPa, M_a=68 g/min. and S=178 mm

(f)

(g)

(h)

(i)

(j)

Figure 6.13 (Continued)

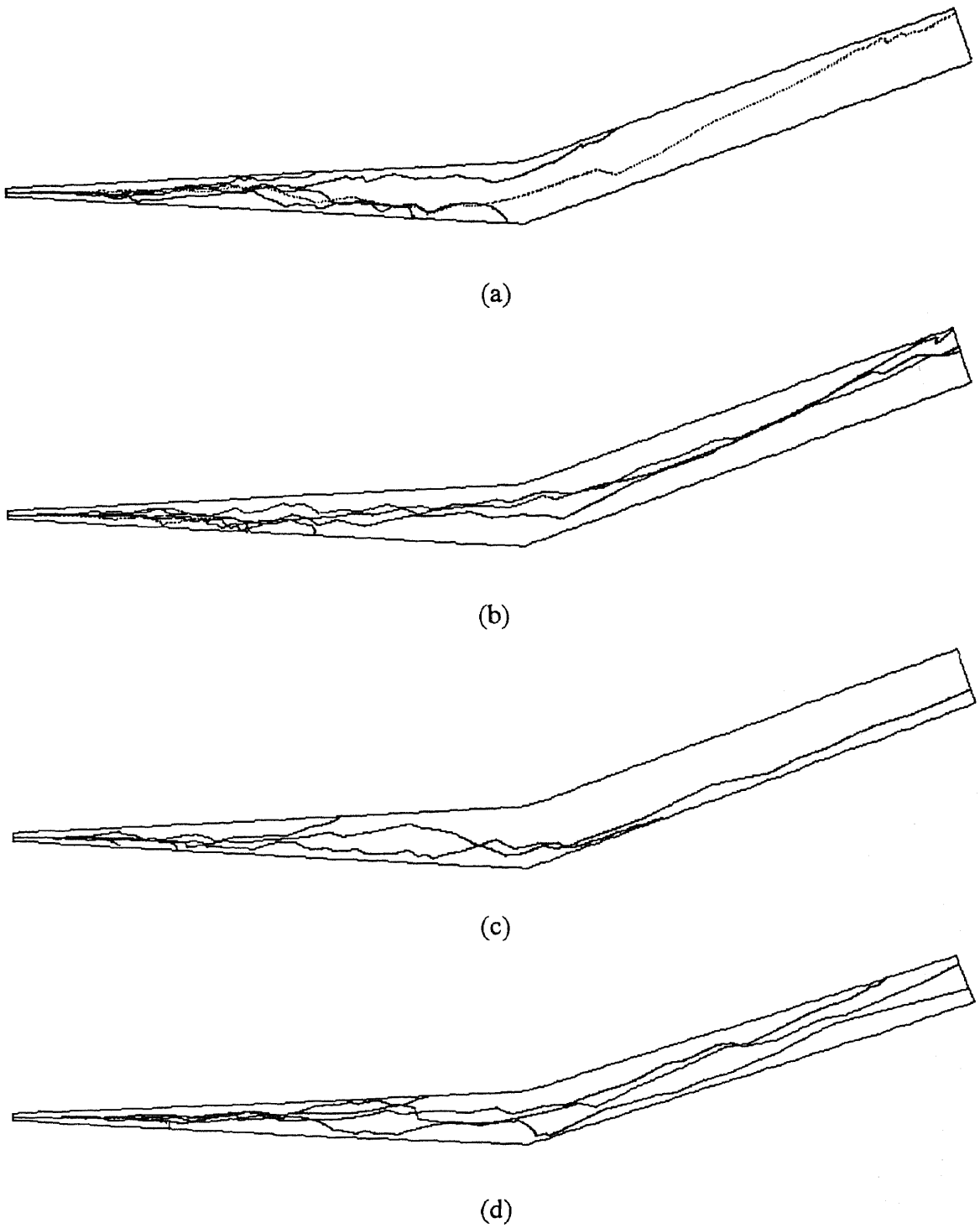

Figure 6.14 Particle Trajectories for Jet Impinging Angle of 20 degree in Course of AWJ Polishing Processes with d_p=100 micron, P=76 MPa, M_a=68 g/min. and S=178 mm

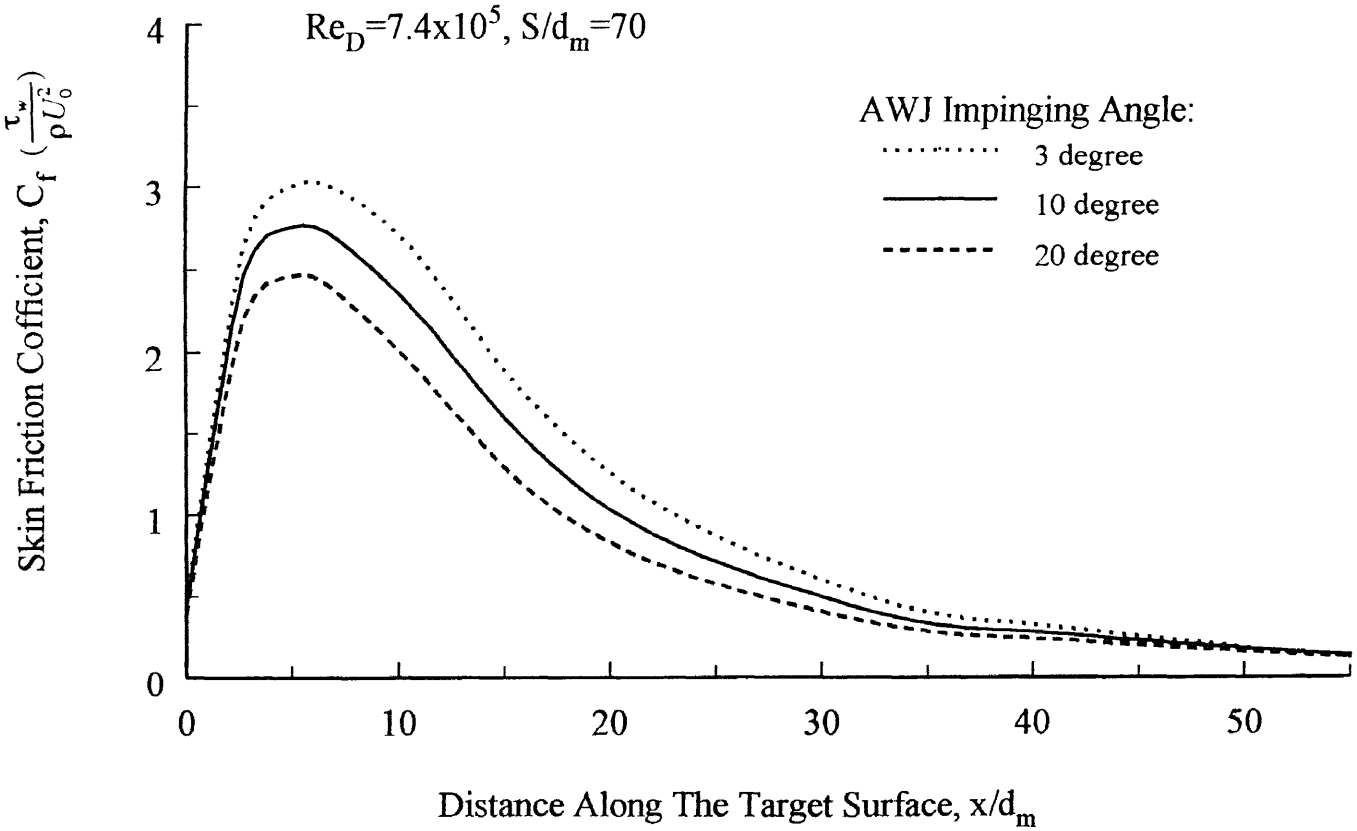

Figure 6.15 Calculated Skin Friction Along an Target Surface in Course of AWJ Polishing

CHAPTER 7

CONCLUSION AND RECOMMENDATIONS

7.1 Conclusion

The following conclusions can be drawn based on the experimental and numerical results found in this work:

7.1.1. General

1. This pioneered the use of AWJ as a polishing tool. Although the feasibility of such a technology was suggested earlier, the first experimental validation of the technology feasibility was done by this study.

2. The principal features of AWJ polishing has been identified.

3. This work pioneered the use of computational packages based on the laws of conventional turbulent systems for evaluation of the behavior of ultrahigh speed two phase flows. The flow of free, impacting and post impacting jets were examined. The results of numerical analysis were validated by the experimental data. This demonstrates the feasibility of the use of a variety of turbulence based commercial packages for investigation of high speed single and multiphase jets.

4. The samples obtained by the use of the developed technology have been demonstrated to the industrial companies. Extremely positive response was obtained.

7.1.2 Polishing Technology

1. Abrasive-waterjet can be used to polish hard-to-machine materials such as ceramics, stainless steel and alloys. The surface roughness of. 0.3-micron was attained in the course of AWJ polishing at a reasonable rate using 500 mesh garnet abrasive.

2. Finish of the material surface generated in the course of AWJ polishing is strongly correlated with AWJ impinging angles and abrasive particles size. The former determines the feasibility of AWJ polishing and the later limits the extent of improvement of the surface topography. The effect of other process parameters (water pressure, abrasive flow rate, nozzle and focusing tube geometry, standoff distance, the topography of the original surface etc.) is less substantial.

3. Integrity of surfaces machined by AWJ polishing do not show any defects induced. Through-thickness microhardness survey test of cross section of polished samples shows no changed of the subsurface hardness. Also, no micro-defects was observed in the course of SEM examination

4. The abrasive-waterjet polishing technique is sensitive to the type of material being machined. This behavior was confirmed by SEM examination of topography of sample surface and abrasive particle collected after polishing.

5. It was determined that particles disintegration mostly occurs during mixing. During particles-materials interaction material wear results in the formation of almost identical mating surface.

7.1.3 Numerical Simulation

1. A computational technique is applied to simulate and analyze abrasive particle trajectories in a two-dimensional two phase turbulent free jet impinging obliquely on a flat surface in course of AWJ polishing process using finite element code FIDAP. The calculations show that the flow field structure of the jet impinging obliquely on a flat surface is strongly affected by the oblique impingement angle. It is validated by experiments in this investigation.

2. The waterjet velocity in the axial and traverse direction and force developed on target surface by AWJ are obtained by experimental measurement and numerical simulation. The numerical prediction of velocity and impact force complies well with the measured results. The flow fields deeply depend on the standoff distance and jet spreading. The change in components of normal and tangential forces with the AWJ impinging angle can be predicted numerically.

3. The simulation of particles trajectories reveals existence of five distinctive patterns of particles motion which determine the surface topography.

7.2 Recommendation

1. Full technical analysis and comparative studies with other techniques need to be conducted for a full assessment. The results of this preliminary investigation, however, have been very encouraging.

2. A system with equipment such as fine abrasive feed device and rotating table needs to be established for more precision control of material removal.

3. Further theoretical investigation is necessary to set up a comprehension model to predict the surface topography in course of AWJ polishing processes.

BIBLIOGRAPHY

Ahmadi, G. And Ounis, H., "Dispersion of Small Rigid Spheres in a Turbulent Flow Field," *Proceedings of International Conference on Mechanics of Two-Phase Flow*, June, 1989.

Ansari, A. I. and Hashish, M., "Effect of Abrasive Waterjet Parameters on Volume Removal Trends in Turning," *ASME Journal of Engineering for Industry*, Vol. 117, pp. 475-484, 1995.

Ansari, A., "A Study on Turning with Abrasive Waterjets," *Ph.D. Thesis*, Michigan Technological University, Houghton, MI, 1990.

Beilby, S. G., *Aggregation and Flow of Solids*, MacMillan, London, 1921.

Barklow, R. H., Goebel, J. A., and Pettit, F. S., "Erosion-Corrosion of Coatings and Superalloys in High-Velocity Hot Gases," *Erosion: Prevention and Useful Application, ASTM STP 664*, pp. 163-192, 1979.

Bellows, G., "Nontraditional Machining Guide," *Machining Hard Materials, SME*, pp. 3-12, 1982.

Benchaita, M. T., Griffith, P. And Rabinowicz, E., "Erosion of Metallic Plate by Solid Particles Entrained in a Liquid Jet," *Journal of Engineering for Industry*, vol. 215, pp. 215-222, Aug., 1883.

Bitter, J. G. A., "A Study of Erosion Phenomena - Part I," *Wear*, Vol. 6, pp. 5-21, 1963 a.

Bitter, J. G. A., "A Study of Erosion Phenomena - Part II," *Wear*, Vol. 6 pp. 169-190, 1963 b.

Blau, P. J., "Report on the Planning Workshop on Cost-effective Ceramic Machining," *Oak Ridge National Laboratory Report ORNL/M-1745*, 1991.

Blickwedel, H., Guo, N. S., Haferkamp, H., and Louis, H., "Prediction of Abrasive Jet Cutting Performance and Quality," *Proceeding of the 9th International Symposium on Jet Cutting Technology*, pp. 163-179, 1990.

Bradshaw, P. and Love, E. M., "The Normal Impingement of a Circular Air Jet on a Flat Surface," *ARCR. and M., No. 3205*, 1959.

Brown, N. J., "Some Speculations on the Mechanisms of Abrasive Grinding and Polishing," *Precision Engineering*, Vol. 9, pp. 129-138, 1987.

BIBLIOGRAPHY
(Continued)

Budinski, Kenneth G., *Surface Engineering for Wear Resistance*, Prentice-Hall, Inc., Englewood Cliffs, NJ, 1988.

Chao, J., Geskin, E. S. and Chung, Y., "Investigations of the Dynamics of the Surface Topography Formation during Abrasive Waterjet Machining," *Proceeding of the 11th International Symposium on Jet Cutting Technology*, pp. 593-603, 1992.

Chuang, S. H., and Wei, C. Y., "Numerical Simulation of an Impinging Jet on a Flat Plate,' *Int. J. Numer. Methods Fluid*, 9, 1413-1420, 1989.

Curhan, J., Reuber, M. and Kim, T. J., "Force Control of Surface Finish in Abrasive Waterjet," *The winter Annual Meeting of the ASME*, pp. 31-36, San Francisco, CA, Dec., 1989.

Danon, H., Wolfshtein, M. and Hetsroni, G., "Numerical Calculation of Two-Phase Turbulent Round Jet," *Int. J. Multiphase Flow*, Vol. 3, pp. 223-234, 1977.

Doyle, E. D., and Aghan, R. L., "Mechanism of Metal Removal in the Polishing and Fine Grinding of Hard Metals," *Metallurgical Transactions B*, vol. 6B, pp. 143-147, March 1975.

Farago, F. T., *Abrasive Methods Engineering*, Industrial Press, New York, NY, 1980.

Fekaier, A., Guinot, J. C., Schmitt, A. and Houssaye, G., "Optimization of the Abrasive Jet Cutting surface Quality by the Workpiece reaction Force Analysis," *Proceeding of the 12th International Symposium on Jet Cutting Technology*, pp. 127-138, 1994.

Field, M., and kahles, J. F., "Review of Surface Integrity of Machined Components", *Annals of the CIRP*, Vol. 20, No. 2, 1971.

Field, M., Kahles, J. F., and Koster, W. P., "Surface Finish and Surface Integrity", *Metal Handbook*, Vol. 16, pp. 19-36, 1989.

Finnie, I. "Erosion of Surfaces by Solid Particles," *Wear*. Vol. 3, pp. 87-103, 1960.

Finnie, I., "Erosion by Solid Particle in a Fluid Stream," *ASTM STP 307*, pp., 70-82, 1962.

Finnie, I., "Erosion by Solid Particle in a Fluid Stream," *ASTM Technical Publication 309*, 1961.

BIBLIOGRAPHY
(Continued)

Finnie, I., "The mechanism of Erosion of Ductile Metals," *Proceeding of the 3rd National Congress of Applied Mechanics*, pp. 527-532, 1958.

Finnie, I., levy, A., and Fandden, D. H., "Fundamental Mechanisms and the Erosive Wear of Ductile Metals by Solid Particles," *Erosion: Prevention and Useful Applications, ASTM Publication No. 664*, pp. 36-58, 1977.

Finnie, I., Wolak, J., and Kabil, Y., *J Materials*, Vol. 2, No. 3, pp. 682-700, 1967.

Geskin, E.S., "Feasibility Study of Abrasive Waterjet Machining for Manufacturing Precision Optical Components," *Oak Ridge National Laboratory, Report ORNL/Sub/91-SE192/1*,.1991.

Geskin, E.S., "Waterjet Machining and Manufacturing Processes for Year 2000 and Beyond," *Proceeding of 10th Japanese Conference on Waterjet Technology*, pp. 1-10, Invited Lecture, Tokyo, Japan, 1993.

Givler, R. C. And Mikatarian, R. R.,, "Numerical Simulation of Fluid-Particle Flows: Geothermal Drilling Applications," *Journal of Fluids Engineering*, Vol. 109, pp. 324-331, 1987.

Gosman, A., D. And Loannides, E., "Aspects of Computer Simulation of Liquid-Fuelled Combustors," *AIAA 19th Aerospace Science Mtg.*, Paper No. 81-0323, St. Louis, MO,1981.

Guo, N. S., Louis, H. and Meier, G., "Surface Structure and Kerf Geometry in Abrasive Water Jet Cutting: Formation and Optimization," *Proceedings of the 7th American Water Jet Conference*, pp. 1-25, 1993.

Hashish, M., "A Modeling Study of Metal Cutting with Abrasive Waterjets," *Journal of Engineering for Industry*, Vol. 106, pp. 88-100, 1984 a.

Hashish, M., "Characteristics of Surfaces Machined with Abrasive-Waterjets," *Journal of Engineering for Industry*, Vol. 113, pp. 354-362, 1991.

Hashish, M., "Characteristics of Surface Machined with Abrasive-Waterjet," *In: Machining Characteristics of Advanced Materials*, pp. 23-32, Presented at Winter Annual Meeting of ASME, San Francisco, CA,1989.

Hashish, M., "Milling with Abrasive-Waterjets: A Preliminary Investigation," *Proceedings of the 4th American Water Jet Conference*, pp. 1-10, Berkeley, CA, 1987 b.

BIBLIOGRAPHY
(Continued)

Hashish, M., "On the Modeling of Abrasive-Waterjet Cutting ," *Proceeding of the 7th International Symposium on Jet Cutting Technology*, pp. 249-265, 1984 b.

Hashish, M., "On the Modeling of Surface Waviness Produced by Abrasive-Waterjet," *Proceeding of the 11th International Symposium on Jet Cutting Technology*, pp. 17-34, 1992 b.

Hashish, M., "Optimum and Critical Traverse Rate in Jet Cutting," *First US Waterjet Symposium*, Golden, CO, Apr. 1981.

Hashish, M., "Pressure Effects in AWJ Machining," *ASME Journal of Engineering Materials and Technology*, Vol. 111, pp. 221-228. 1989.

Hashish, M., "Three Dimensional Machining with Abrasive-Waterjet," *11th International Symposium on Jet Cutting Technology*, pp. 609-620, Scotland, Sept. 8-10, 1992.

Hashish, M., "Turning with Abrasive-Waterjets - A First Investigation," *ASME Journal of Engineering for Industry*, Vol. 109, pp. 281-296, 1987 a.

Hashish, M., "Turning, Milling and Drilling with Abrasive-Waterjets," *Proceeding of the 9th International Symposium on Jet Cutting Technology*, pp. 113-131, 1988 a.

Hashish, M., "An Improves Model of Erosion by Solid Particle Impact," *Proc. 7th Int. Conf. on Erosion by Liquid and Solid Impact*, pp. 66-1 to 66-9. 1987 c.

Hashish. M., "Drilling of Small-diameter Holes in Sensitive Materials," *Proceeding of the 13th International Symposium on Jet Cutting Technology*, pp. 409-424, 1994.

Hinze, J. O., *Turbulence*, McGraw-Hill Book Company, Inc., New York, NY, 1959.

Hjelmfelt, A. T., Jr. And Mockros, L. F., "Motion of Discrete Particles in a Turbulent Fluid," *Appl. Sci. Res.*, 1965.

Hunt, D. C., "Surface Finish Optimization for Abrasive Waterjet Cutting," *Proceeding of the 9th International Symposium on Jet Cutting Technology*, pp. 99-112, 1988.

Hutchings, I. M., and Winter, R. E., "Deformation of Metal Surface by the Oblique Impact of Square Plates," *International Journal Mechanical Science*, Vol. 19, pp. 45-52, 1977.

BIBLIOGRAPHY
(Continued)

Hutchings, I. M., and Winter, R. E., "Mechanism of the Erosion of Metals by Solid Particles," *Erosion: Prevention and Useful Application, ASTM STP 664*, pp. 59-76, 1979.

Ives, L. K., and Ruff, A. W., "Electron Microscopy Study of Erosion Damage in Copper," *Erosion: Prevention and Useful Application, ASTM STP 664*, pp. 5-35, 1979.

Johnson, L. F., "Ion beam Microstructure Fabrication in Optical, Magnetic and Surface Acoustical Technologies," *Ion Bombardment Modification of Surfaces: Fundamental and Applications*, Elsevier Science Publishing Inc., pp. 361-383, 1984.

Kalpakjian, S., *Manufacturing Processes for Engineering Materials*, Addison-Wesley, NY, pp. 562-578, 1984.

Koepke, B. G. and Strokes, R. J., "Grinding Damage In Ceramics," *Machining Hard Materials, SME*, pp. 145-153, 1982.

Kovacevic, R., "Surface Texture in Abrasive Waterjet Cutting," *Journal of Manufacturing System*, Vol. 10, No. 1, pp. 32-40, 1991.

Lansdown, A. R. and Price, A. L., *Materials to Resist Wear*, Pregamon Press, New York, NY, 1986.

Launder, B. E. and Spalding, D. B., *Lectures in Mathematical Models of Turbulence*, Academic Press, Watertown, MA, 1972.

Li, H. Y., Geskin, E. S. and Chen, W. L., "Investigation of Force Exerted by An Abrasive Waterjet on a Workpiece," *Proceedings of the 5th American Water Jet Conference*, pp. 69-77, 1989.

Loveless, T. R., Williams, R. E. and Rajurkar, K. P., "A Study of the Effect of Abrasive-Flow Finishing on Various Machined Surfaces," *Journal of Materials Processing Technology*, Vol. 47, pp. 133-151, 1994.

Maji, J., and Sheldon, G. L., "Mechanism of Erosion of a Ductile Material by Solid Particle," *Erosion: Prevention and Useful Application, ASTM STP 664*, pp. 136-147, 1979.

BIBLIOGRAPHY
(Continued)

Matsui, S., Matsumura, H., Ikemoto, Y., Tsujita, K. And Shimizu, H., "High Precision Cutting Method for Metallic Materials by Abrasive Waterjet." *Proceeding of the 10th International Symposium on Jet Cutting Technology, Paper No. G3*, 1990.

Maxey, M. R. and Riley, J. J., "Equation of Motion for a Small Rigid Sphere in a Nonuniform Flow," *Phys. Fluids*, Vol. 4, pp. 26, 1983.

Melville, W. K. and Bray, K. N. C., "A Model of the Two-Phase Turbulent Jet," *Int. J. Heat Mass Transfer*, Vol. 22, 1979.

Mori, Y and Yamauchi, K., "Elastic Emission Machining," *Proc. of Int. Precision Engineering Seminar*, 1987.

Morrison, C. T. and Scattergood, R. O., "Erosion of 304 Stainless Steel," *Wear*, Vol. 111, pp. 1-13, 1986.

Naib, S. K. Al. Rasiah, V and Sanders, J. E., "Oblique and Vertical Jet Dispersion in Confined Spaces," *9th International Symposium on Jet Cutting Technology*, pp. 173-188, Oct., 1988.

Namba, Y., "Float Polishing and Defects of Fused Silica." *Laser Induced Damage in Optical Materials*, Boulder, Colorado, NBS Special Publication 669, pp. 130, 1980.

Namba, Y., Tsuwa, H., "Float Polishing of Mn-Zn Ferrite and Characteristics of Finished Surfaces." *Proceedings of the 4th International Conference on Production Engineering, Tokyo*, Japan, pp. 1017-1022, 1980.

Namba, Y., Tsuwa, H., "Mechanism and Some Applications of Ultra-fine Finishing." *Annals of the CIRP, 27(I)*, pp. 511-516, 1978,

Namba, Y., Tsuwa, H., "Surface Properties of Polished Stainless Steel." *Annals of the CIRP, 29(I)*,1980.

Namba, Y., Tsuwa, H., "Ultra fine Finishing of Ceramics and Metals by Float Polishing." *Laser Induced Damage in Optical Materials*, Boulder, CO, NBS Special Publication 620, pp. 171, 1980.

Neilson, J. H. And Gilchrist, A. "Erosion by a Stream of Solid Particles," *Wear* II, 1968.

BIBLIOGRAPHY
(Continued)

Ojmertz, K. M. C., "Abrasive Waterjet Milling: An Experimental Investigation," *Proceedings of the 7th American Water Jet Conference*, pp. 777-791, Seattle, WA, August, 1993.

Pandey, P. C., and Shan, H. S., *Modern Machining Processes*, McGraw-Hill Book Company, New York, NY, 1980.

Phiillips, K., Crimes, G. M. and Wilshaw, T. R., "On the Mechanism of Material Removal by Free Abrasive Grinding of Glass and Fused Silica," *Wear*, Vol. 41, pp. 327-350, 1977.

Preece, C., ed., "Treatise on Materials Science and Technology,' *Erosion*, Vol. 16, Academic Press, New York, 1979.

Rabinowicz, E. C., "Polishing", *Journal* of *Scientific American*, Vol. 218, pp. 91-99,. 1968.

Rodi, W. and Spalding, D. B., "A Two-Parameter Model of Turbulence, and its Application to Free Jets," *Numerical Prediction of Flow, Heat Transfer, Turbulence and Combustion*, Pergamon Press Ltd., New York, NY, 1983

Samuels, L. E., *Metallographic Polishing by Mechanical Methods*, American Society for Metals, 1982.

Schodl, R., "A Laser Dual-beam Method for Flow Measurements in Turbomachines", *ASME paper No. 74-GT-157*, 1982.

Sheldon, G. L," Effect of Surface Hardness and Other Material Properties on Erosion Wear of Metals by Solid Particles," *ASME Journal of Engineering Materials and Technology*, vol. 99, pp. 133-137, 1977.

Sheldon, G. L. and Finnie, I., "On the Brittle Behavior of Nominally Brittle Materials During Erosive Cutting," *ASME Journal of Engineering for Industry*, Vol. 88, pp. 387-392, 1966 a.

Sheldon, G. L. And Finnie, I., "The Mechanism of Material Removal in the Erosive Cutting of Brittle Material," *Journal of Engineering for Industry*, Vol. 88, pp. 393-400, 1966 b.

Sheldon, G. L., and Kanhere, A., "An Investigation of Impingement Erosion Using Single Particles," *Wear*, Vol. 21, pp. 195-207, 1972.

BIBLIOGRAPHY
(Continued)

Sheng, P. S. and Liu, Ko-Wang, "Development of A Laser-Based Tool for Secondary Finishing," *Japan-USA Symposium on Flexible Automation*, Kobe, Japan, pp. 1409-1416, July, 1994.

Sheridan, M. D., Kim, T. J., and Taggart, D., "Screw Thread Machining of Composite Materials Using Abrasive Waterjet Cutting," *International Mechanical Engineering Symposium on Nontraditional Manufacturing Process in the 1990's*, 1994.

Simpson, M., 1990, "Abrasive Particle Study in High Pressure Waterjet Cutting," *Int. J. of Waterjet Technology*, Vol. 1, No. 1, pp. 17-28.

Singh, P. J., Chen, W. L. and Munoz, J., "Comprehensive Evaluation of Abrasive Waterjet Cut Surface Quality," *Proceedings of the 6th American Water Jet Conference*, pp. 139-161, St. Louis, MO, 1991.

Situ, M. and Schetz, J. A., "Numerical Calculations of the Breakup of Highly Loaded Slurry Jets," *Journal of Fluids Engineering*, Vol. 109, pp. 332-336, 1987.

Soo, S. L., *Fluid Dynamics of Multiphase System*, Blaisdell Pub. Co., Waltham, MA., 1967.

Tan, D. K. M., "A Model for the Surface Finish in Abrasive-Waterjet Cutting," *Proceeding of the 8th International Symposium on Jet Cutting Technology*, pp. 309-313, 1986.

Tilly, G. P, " A Two Stages Mechanism of Ductile Erosion," *Wear*, Vol. 23, pp. 87-96, 1973.

Tilly, G. P, "Erosion Caused by Airborne Particles," *Wear*, Vol. 14, pp. 63-79, 1969 b.

Tilly, G. P, *Wear*, Vol. 14, pp. 241-248, 1969 a.

Tilly, G. Pand Sage, W., *Wear*, Vol. 16. pp. 447-465, 1970.

Wernick, S. and Pinner, R., *The Surface Treatment and Finishing of Aluminum and its Alloys*, Robert Draper LTD, 1972.

Winter, R. E., and Hutchings, I. M., " Solid Particle Erosion Studies Using Single Anglular Particle," *Wear*, Vol. 29, pp. 181-194, 1974.

Winter, R. E., and Hutchings, I. M., "The Role of Adiabatic Shear on Solid Particle Erosion," *Wear*, Vol. 34, pp. 141-148, 1975.

Yanaida, K and Ohashi, A., "Flow Characteristic of Water Jets in Air," *4th International Symposium on Jet Cutting Technology,* Paper A3, pp. 39-54, 1978.

Yanta, W. J, Gates, D. F. and Brown, F. W., "The Use of a Laser Doppler Velocimeter in Supersonic Flow", *AIAA paper No. 71-287,* 1971.